Fabrication and Structural Performance of Random Wetlay Composite Sandwich Panels

by

Christopher Edward Glenn

Thesis submitted to the Faculty of the Virginia Polytechnic Institute and State University
in partial fulfillment of the requirements for the degree of

Master of Science
in
Engineering Mechanics

M. W. Hyer, Chairman
L. G. Kraige
S. Thangjitham

June 6, 2003
Blacksburg, Virginia

Key Words: low-cost composite, random wetlay, sandwich beam,
sandwich plate, flatwise tension, shadow moiré

Fabrication and Structural Performance of Random Wetlay Composite Sandwich Panels

by

Christopher Edward Glenn

M. W. Hyer, Chairman

(Abstract)

The random wetlay process is used to make fiber-reinforced thermoplastic sheets that can be compression molded into composite panels at little cost. By utilizing these composite panels as the facesheets of honeycomb sandwich structures, it is possible to greatly increase the bending stiffness of the composite without adding significant weight. The random wetlay composite facesheets used in this research consisted of 25% E-glass fibers and 75% PET by weight. The thickness uniformity of the facesheets was difficult to control. The core of the sandwich structure was HexWeb™ EM. Three low-cost adhesives were examined for secondarily bonding the facesheets to the core: polyurethane glue; epoxy paste; and 3M Scotch-Grip™ plastic adhesive. The polyurethane glue mixed with Cab-O-Sil filler was easiest to apply and provided the largest flatwise tensile strength. Mathematical models were developed to predict the static behavior of sandwich beams and plates in bending. Three-point bend tests were performed on a sandwich beam in accordance with ASTM C 393. A sandwich plate simply supported along two opposite edges and free along the other two edges was subjected to a line-load using weights and a wiffle tree arrangement. An effective facesheet modulus and Poisson's ratio were found by comparing the measured displacements to the sandwich plate theory. The shadow moiré technique was used to visualize the displacement of the line-loaded sandwich plate. The overall shape of the displacement was very similar to the shape predicted by the sandwich plate theory.

Acknowledgments

First and foremost, I would like to thank my committee chairman, Professor M. W. Hyer, for taking the time to work with me on this research over the past two years. I would also like to thank Professors L. G. Kraige and S. Thangjitham for serving on my graduate committee. This research has been made possible through the financial support of the Center for High Performance Manufacturing in the Grado Department of Industrial and Systems Engineering and the Department of Engineering Science and Mechanics. Material donations have been made by DuPont, Hexcel, and 3M. Also, Tom Owen from Hexcel provided material data and manufacturing advice.

I greatly appreciate the assistance of fellow graduate students Marc Shultz, Gabriela Wolford, Majed Majeed, and Sontipee Aimmanee. Thanks to David Simmons and Darrell Link in the ESM machine shop for not only machining high quality parts, but also providing countless pieces of practical advice. Much of the compression molding was done with the assistance of Joe Price-O'Brien and Danny Reed. Flatwise tension tests were performed in the Materials Testing Laboratory under the supervision of Bob Simonds and George Lough. Shadow moiré experiments were accomplished with the guidance of Professor Dan Post.

Lastly, I would like to thank my parents and my brother, Luke, for all of their love and encouragement while I've been away at school for the past seven years.

Table of Contents

List of Figures

List of Tables

Chapter 1 Introduction

Composite materials have many advantages over traditional isotropic materials. They generally have high specific strength and stiffness, factors which can create significant weight savings in aerospace and automotive applications. The makeup of a composite structure can often be tailored to provide different properties in various directions. Composites also provide excellent durability and corrosion resistance. Despite all the advantages, one of the major factors limiting the use of composite materials is cost. Due to their complex nature, composites are more difficult to manufacture and analyze than traditional materials. Also, some composite materials have a lower stiffness than traditional isotropic materials such as steel and aluminum. By incorporating composite materials into sandwich structures, it is possible to greatly increase the bending stiffness of the composite construction without adding significant weight.

A typical sandwich structure consists of two stiff facesheets bonded to a lightweight core. Composite materials are ideally suited for the facesheets. The purpose of the core is to separate the facesheets to increase the bending stiffness and strength of the sandwich structure. The core can be made out of any lightweight material such as wood, foam, or aluminum honeycomb. Figure 1.1 shows a typical honeycomb sandwich panel.

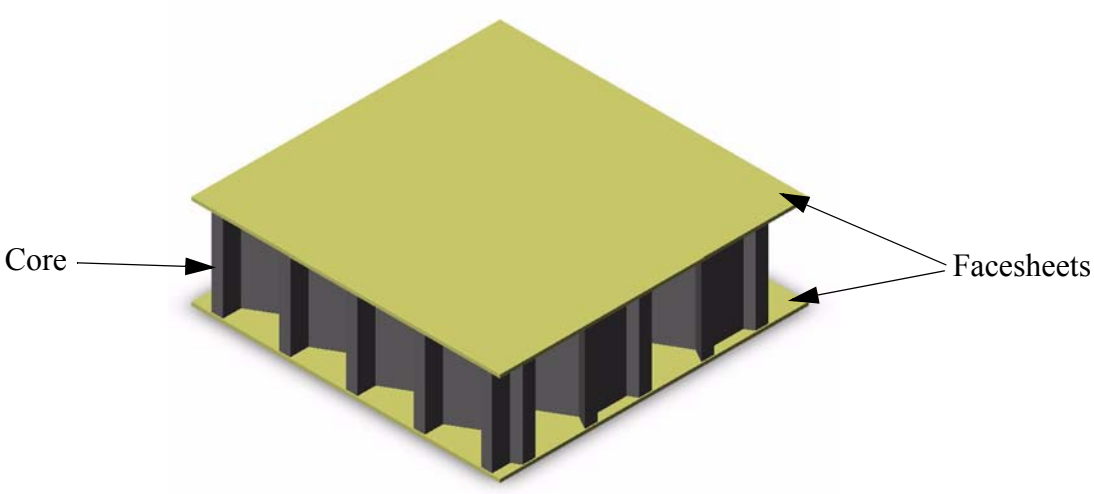

Figure 1.1: Typical honeycomb sandwich structure

A relatively new and inexpensive process for manufacturing composite parts is compression molding of fiber-reinforced thermoplastic sheets. These sheets consist of chopped fibers randomly distributed in a thermoplastic matrix. One method for making these sheets is known as random wetlay. Common fibers are made of E-glass or carbon, and common matrix materials are polyethylene terephthalate (PET) or polypropylene. Typical fiber amounts range from 25% to 40% by weight. The research discussed herein considers the use of these random wetlay composites for use as facesheets in a honeycomb sandwich structure.

The goals of this research are five-fold: 1) develop mathematical models to predict the static behavior of sandwich panels, 2) construct sandwich panels using random wetlay composite facesheets and HexWeb™ EM honeycomb core, 3) measure the flatwise tensile strength of the constructed sandwich panels, 4) test the sandwich panels under static loading, and 5) compare the results of the static tests with predictions from the theory.

There is a great deal of research available concerning the modeling of composite sandwich beams and plates. The research spans a number of decades. However, in the more recent literature Dugundji [1] presents a sandwich beam model that allows for the transverse shear deformations of the core. Transverse flexibility of the core, in shear, extension, or both, has been studied by many authors, including Sokolinsky and Frostig [2], Whitney [3], and Swanson [4]. Gdoutos et al. [5] consider both material and geometric nonlinearities of a sandwich beam in three-point bend. Sandwich beams with mid-plane asymmetry have been considered by Satapathy and Vinson [6]. Thomsen and Vinson [7] present an analysis of sandwich beams and plates with variable core thickness. The effective elasticity tensor for a cellular core is discussed by Hohe and Becker [8]. Nonlinear sandwich plate theories including dynamic and temperature effects are given by Librescu et al. [9] and Ebcioglu [10]. All of these various sandwich theories are considered viable theories and advance the state of the art. However, for the work here to develop predictive mathematical models, the sandwich beam theory presented by Dugundji is verified and then extended to sandwich plates. This theory is selected because it uses simple kinematics, reasonable assumptions regarding the mechanical behavior of materials in the context of the beams and plates to be tested, and reasonable assumptions regarding the relative importance of the various stress and displacement components within the sandwich construction.

Chapters 2 and 3 will present the mathematical models of sandwich beams and plates based on Dugundji's work. Variational and energy methods will be used to derive the governing equations and boundary conditions. The predicted responses to various loading and boundary conditions will be discussed. Sandwich beams will be initially studied to serve as a foundation for sandwich plates. Chapter 4 will then discuss the compression molding technique for making the facesheets and the various adhesives used to bond the facesheets to the core. The specific materials considered in this study, and the quality of the facesheets both in terms of mass loss during processing and thickness variations will be described. Chapter 5 will discuss the flatwise tension tests designed to measure the quality of the bond between the facesheets and the core, and will describe the experimental set-up for loading beams and plates and measuring deflections. Deflection measurements, both from dial gauges and from the shadow moiré technique, will be compared with the mathematical models. The final chapter will give conclusions and recommendations for future work.

Chapter 2 Sandwich Beam Theory

2.1 Introduction

In a standard Euler beam formulation, it is assumed that lines perpendicular to the midsurface of the beam before deformation remain perpendicular after deformation. This assumption is not accurate for sandwich beams because the transverse shear modulus of the core is often much less than that of the stiffer facesheets, as is the case here. Like a Timoshenko beam formulation, an independent rotation angle $\alpha(x)$ is specified, in addition to the midsurface deflection $w(x)$.

Dugundji [1] presents an interesting solution for finding the displacement and stresses of an end-loaded cantilever sandwich beam in which the facesheets are treated as Euler beams. This solution will be discussed and then extended to include a simply-supported sandwich beam with a point load in the center using energy and variational methods. Comparisons to other beam theories, including ASTM C 393 [11], will be given.

2.2 Cantilever Sandwich Beam

An end-loaded cantilever sandwich beam as discussed by Dugundji is shown in Figure 2.1. Deformations in the figure have been greatly exaggerated. The total width of the beam (dimension into the page) is b. The top and bottom facesheets are assumed to behave as isotropic Euler beams with uniform thickness t and extensional modulus E. The interior core has thickness c and transverse shear modulus G_{xz} in the x-z plane, which will simply be denoted as G. The extensional modulus of the core in the x-direction is assumed to be negligible compared to that of the facesheets. The core is also assumed to be infinitely stiff through the thickness, i.e., in the z-direction.

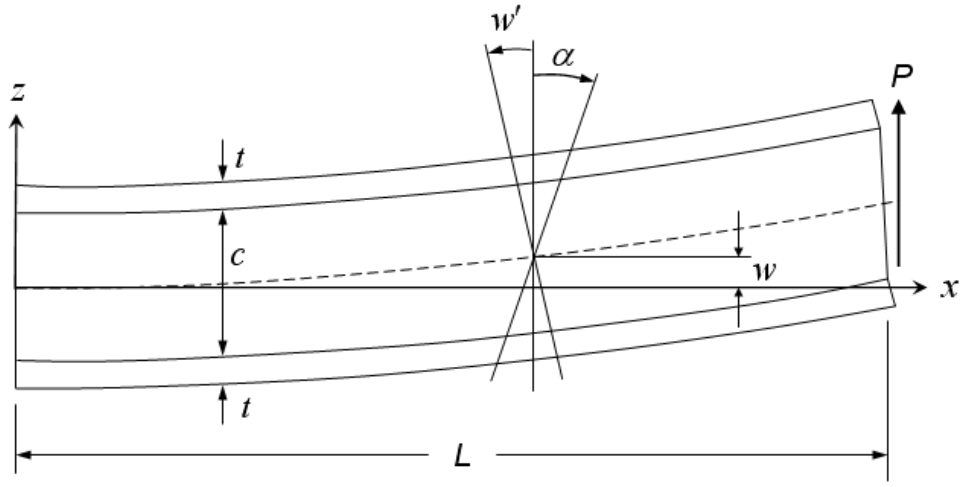

Figure 2.1: Cantilever sandwich beam deformations

In keeping with the infinite rigidity of the core in the z-direction and the Euler beam behavior of the facesheets, the deflection in the z-direction is given by

$$w_T(x,z) = w_C(x,z) = w_B(x,z) = w(x) \tag{2.1}$$

where the subscripts T, C, and B represent the top facesheet, core, and bottom facesheet, respectively. The slope of the beam is the slope of the dashed line in Figure 2.1 given by $w'(x)$. The cross-section rotation of the core is denoted by $\alpha(x)$. The displacements in the x-direction for the top (u_T), core (u_C), and bottom (u_B) consistent with Figure 2.1 are

$$u_T(x,z) = \left(\frac{c}{2}\right)\alpha(x) - \left(z - \frac{c}{2}\right)w'(x) \tag{2.2}$$

$$u_C(x,z) = z\alpha(x) \tag{2.3}$$

$$u_B(x,z) = -\left(\frac{c}{2}\right)\alpha(x) - \left(z + \frac{c}{2}\right)w'(x) \tag{2.4}$$

where z is the vertical position above the midsurface and $' = d/dx$. The normal strain in the x-direction of the top and bottom facesheets is defined as

$$\varepsilon_x = \frac{\partial u}{\partial x} \tag{2.5}$$

and the through thickness shear strain in the core is defined as

$$\gamma_{xz} = \frac{\partial u}{\partial z} + \frac{\partial w}{\partial x} \tag{2.6}$$

The constitutive behavior is assumed to be linearly elastic. Thus, the nonzero stresses are given by

$$\left(\sigma_x\right)_T = E\left(\varepsilon_x\right)_T = E\left[\frac{c}{2}\left(\alpha' + w''\right) - zw''\right] \tag{2.7}$$

$$\left(\tau_{xz}\right)_C = G\gamma_{xz} = G\left(\alpha + w'\right) \tag{2.8}$$

$$\left(\sigma_x\right)_B = E\left(\varepsilon_x\right)_B = E\left[-\frac{c}{2}\left(\alpha' + w''\right) - zw''\right] \tag{2.9}$$

The equations and boundary conditions governing the displacement and rotation of the sandwich beam are found directly through the use of energy and variational principles. The strain energy of any solid body is defined as

$$U = \frac{1}{2}\int_V \sigma_{ij}\varepsilon_{ij}dV = \frac{1}{2}\int_V (\sigma_x\varepsilon_x + \sigma_y\varepsilon_y + \sigma_z\varepsilon_z + \tau_{xy}\gamma_{xy} + \tau_{xz}\gamma_{xz} + \tau_{yz}\gamma_{yz})dV \tag{2.10}$$

For the sandwich beam in Figure 2.1, the above integral is separated into three parts for the two facesheets and the core. Since the facesheets are assumed to behave as Euler beams, they exhibit only extensional strains. As stated earlier, the extensional modulus of the core is negligible, so the only remaining term is from the transverse shear. The strain energy of the sandwich beam reduces to

$$U = \frac{1}{2}\int_0^L \int_{-(c/2+t)}^{-c/2} (b\sigma_x\varepsilon_x)_B dzdx + \frac{1}{2}\int_0^L \int_{-c/2}^{c/2} (b\tau_{xz}\gamma_{xz})_C dzdx + \frac{1}{2}\int_0^L \int_{c/2}^{c/2+t} (b\sigma_x\varepsilon_x)_T dzdx \tag{2.11}$$

Upon substitution of the stress and strain relationships given previously, and integration through the thickness, the strain energy is given by

$$U = \frac{1}{2}\int_0^L \left[B_3(w'')^2 - 2B_2w''\alpha' + B_1(\alpha')^2 + GA(w' + \alpha)^2 \right]dx \tag{2.12}$$

where

$$B_1 = \frac{1}{2} Ebc^2 t \tag{2.13}$$

$$B_2 = \frac{1}{2} Ebct^2 \tag{2.14}$$

$$B_3 = \frac{2}{3} Ebt^3 \tag{2.15}$$

$$A = bc \tag{2.16}$$

The flexural rigidity of the sandwich beam can be expressed as

$$EI = B_1 + 2B_2 + B_3 \tag{2.17}$$

The total potential energy of the beam, Π, is the strain energy minus the work done by the external forces. For a cantilever beam loaded with force P at its tip, $x = L$, the work done is

$$W = Pw(L) \tag{2.18}$$

The total potential energy is thus given by

$$\Pi = U - W = \frac{1}{2}\int_0^L \left[B_3 (w'')^2 - 2B_2 w''\alpha' + B_1(\alpha')^2 + GA(w' + \alpha)^2 \right] dx - Pw(L) \tag{2.19}$$

For the sandwich beam to be in equilibrium, the first variation of the total potential energy must equal zero. After much algebra and several integrations by parts, the first variation is given by

$$\begin{aligned} \delta^{(1)}\Pi = \int_0^L \left\{ \left[B_3 w^{IV} - B_2\alpha''' - GA(w'' + \alpha') \right] \delta w + \left[B_2 w''' - B_1\alpha'' + GA(w' + \alpha) \right] \delta\alpha \right\} dx \\ + \left(B_3 w'' - B_2\alpha' \right) \delta w' \Big]_0^L + \left[-B_3 w''' + B_2\alpha'' + GA(w' + \alpha) \right] \delta w \Big]_0^L \\ + \left(-B_2 w'' + B_1\alpha' \right) \delta\alpha \Big]_0^L - P\delta w(L) = 0 \end{aligned} \tag{2.20}$$

Each grouping of terms in the above equation must equal zero for the first variation to be zero. The two Euler-Lagrange equations are

$$B_3 w^{IV} - B_2\alpha''' - GA(w'' + \alpha') = 0 \tag{2.21}$$

$$B_2 w''' - B_1 \alpha'' + GA(w' + \alpha) = 0 \tag{2.22}$$

In addition, there are three sets of boundary conditions given by the remaining boundary terms in the first variation. For the first boundary term to be zero, the following two boundary conditions must apply at the ends of the beam:

$$B_3 w''(0) - B_2 \alpha'(0) = 0 \quad \text{OR} \quad w'(0) \text{ must be specified} \tag{2.23}$$

AND

$$B_3 w''(L) - B_2 \alpha'(L) = 0 \quad \text{OR} \quad w'(L) \text{ must be specified} \tag{2.24}$$

The force P must be included with the second boundary term because it is associated with $\delta w(L)$. Thus, for the second boundary term to be zero,

$$-B_3 w'''(0) + B_2 \alpha''(0) + GA\big(w'(0) + \alpha(0)\big) = 0 \quad \text{OR} \quad w(0) \text{ must be specified} \tag{2.25}$$

AND

$$-B_3 w'''(L) + B_2 \alpha''(L) + GA\big(w'(L) + \alpha(L)\big) = P \quad \text{OR} \quad w(L) \text{ must be specified} \tag{2.26}$$

Similarly, for the third boundary term to be zero,

$$-B_2 w''(0) + B_1 \alpha'(0) = 0 \quad \text{OR} \quad \alpha(0) \text{ must be specified} \tag{2.27}$$

AND

$$-B_2 w''(L) + B_1 \alpha'(L) = 0 \quad \text{OR} \quad \alpha(L) \text{ must be specified} \tag{2.28}$$

For the cantilever sandwich beam, the displacement, slope, and core rotation are known to be zero at the clamped end. Therefore, the boundary conditions at $x = 0$ are

$$w(0) = 0 \tag{2.29}$$

$$w'(0) = 0 \tag{2.30}$$

$$\alpha(0) = 0 \tag{2.31}$$

The boundary conditions at the free end of the cantilever beam ($x = L$) are not as obvious. The displacement, slope, and core rotation are not prescribed, so the following boundary conditions must apply:

$$-B_3 w'''(L) + B_2 \alpha''(L) + GA\left[w'(L) + \alpha(L)\right] = P \tag{2.32}$$

$$B_3 w''(L) - B_2 \alpha'(L) = 0 \tag{2.33}$$

$$-B_2 w''(L) + B_1 \alpha'(L) = 0 \tag{2.34}$$

The last two equations form a set of homogeneous equations in $w''(L)$ and $\alpha'(L)$. The determinant of the coefficients is not zero, so these two boundary conditions can be written

$$w''(L) = 0 \tag{2.35}$$

$$\alpha'(L) = 0 \tag{2.36}$$

The assumed solutions for the governing homogeneous linear differential equations in $w(x)$ and $\alpha(x)$ are

$$w(x) = Ce^{\lambda x} \tag{2.37}$$

$$\alpha(x) = De^{\lambda x} \tag{2.38}$$

where C, D, and λ, are unknown constants. Substitution of these solutions into the differential equations given by Eqs. (2.21) and (2.22) yields the following homogeneous algebraic equations:

$$\left(B_3\lambda^4 - GA\lambda^2\right)C + \left(-B_2\lambda^3 - GA\lambda\right)D = 0 \tag{2.39}$$

$$\left(B_2\lambda^3 + GA\lambda\right)C + \left(-B_1\lambda^2 + GA\right)D = 0 \tag{2.40}$$

The determinant of the coefficients of C and D results in a sixth-order characteristic equation with roots $\lambda = +\beta, -\beta, 0, 0, 0, 0$, where

$$\beta = \sqrt{\frac{GA(B_1 + 2B_2 + B_3)}{B_1 B_3 - B_2^2}} \tag{2.41}$$

The solutions for $w(x)$ and $\alpha(x)$ with the given roots are

$$w(x) = C_1 e^{\beta x} + C_2 e^{-\beta x} + C_3 + C_4 x + C_5 x^2 + C_6 x^3 \tag{2.42}$$

$$\alpha(x) = D_1 e^{\beta x} + D_2 e^{-\beta x} + D_3 + D_4 x + D_5 x^2 + D_6 x^3 \tag{2.43}$$

The relationships between C_i and D_i are found by substituting the above solutions into the second differential equation given in Eq. (2.22) and setting the coefficients of $e^{\beta x}$, $e^{-\beta x}$, x^3, x^2, x and the constant equal to zero. Expressing D_i in terms of C_i gives

$$\mathrm{D}_1 = \left(-\frac{GA\beta + B_2\beta^3}{GA - B_1\beta^2} \right) C_1 \tag{2.44}$$

$$D_2 = \left(\frac{GA\beta + B_2\beta^3}{GA - B_1\beta^2} \right) C_2 \tag{2.45}$$

$$D_3 = -C_4 - \left[\frac{6(B_1 + B_2)}{GA} \right] C_6 \tag{2.46}$$

$$D_4 = -2C_5 \tag{2.47}$$

$$D_5 = -3C_6 \tag{2.48}$$

$$D_6 = 0 \tag{2.49}$$

The coefficients C_1 through C_6 are found from the six boundary conditions given by Eqs. (2.29) through (2.36). A closed-form solution found using *Mathematica* [12] is

$$\mathrm{C}_1 = \frac{P(GA - B_1\beta^2)}{GA\beta^3(B_1 + 2B_2 + B_3)(e^{L\beta} - 1)^2 + 2\beta^5(B_1 B_3 - B_2^2)e^{L\beta}} \tag{2.50}$$

$$C_2 = -\frac{P(GA - B_1\beta^2)e^{2L\beta}}{GA\beta^3(B_1 + 2B_2 + B_3)(e^{L\beta} - 1)^2 + 2\beta^5(B_1B_3 - B_2^2)e^{L\beta}} \tag{2.51}$$

$$C_3 = \frac{P(GA - B_1\beta^2)(e^{2L\beta} - 1)}{GA\beta^3(B_1 + 2B_2 + B_3)(e^{L\beta} - 1)^2 + 2\beta^5(B_1B_3 - B_2^2)e^{L\beta}} \tag{2.52}$$

$$C_4 = -\frac{P(GA - B_1\beta^2)(e^{2L\beta} + 1)}{GA\beta^2(B_1 + 2B_2 + B_3)(e^{L\beta} - 1)^2 + 2\beta^4(B_1B_3 - B_2^2)e^{L\beta}} \tag{2.53}$$

$$C_5 = \frac{PGAL(e^{2L\beta} + 1)}{2GA(B_1 + 2B_2 + B_3)(e^{L\beta} - 1)^2 + 4\beta^2(B_1B_3 - B_2^2)e^{L\beta}} \tag{2.54}$$

$$C_6 = -\frac{PGA(e^{2L\beta} + 1)}{6GA(B_1 + 2B_2 + B_3)(e^{L\beta} - 1)^2 + 12\beta^2(B_1B_3 - B_2^2)e^{L\beta}} \tag{2.55}$$

The remaining coefficients D_1 through D_5 found from Eqs. (2.44) through (2.48) are

$$\mathrm{D}_1 = -\frac{P(GA + B_2\beta^2)}{GA\beta^2(B_1 + 2B_2 + B_3)(e^{L\beta} - 1)^2 + 2\beta^4(B_1B_3 - B_2^2)e^{L\beta}} \tag{2.56}$$

$$D_2 = -\frac{P(GA + B_2\beta^2)e^{2L\beta}}{GA\beta^2(B_1 + 2B_2 + B_3)(e^{L\beta} - 1)^2 + 2\beta^4(B_1B_3 - B_2^2)e^{L\beta}} \tag{2.57}$$

$$D_3 = \frac{P(GA + B_2\beta^2)(e^{2L\beta} + 1)}{GA\beta^2(B_1 + 2B_2 + B_3)(e^{L\beta} - 1)^2 + 2\beta^4(B_1B_3 - B_2^2)e^{L\beta}} \tag{2.58}$$

$$D_4 = -\frac{PGAL(e^{2L\beta} + 1)}{GA(B_1 + 2B_2 + B_3)(e^{L\beta} - 1)^2 + 2\beta^2(B_1B_3 - B_2^2)e^{L\beta}} \tag{2.59}$$

$$D_5 = \frac{PGA(e^{2L\beta} + 1)}{2GA(B_1 + 2B_2 + B_3)(e^{L\beta} - 1)^2 + 4\beta^2(B_1B_3 - B_2^2)e^{L\beta}} \tag{2.60}$$

If the material properties, geometry, and force are specified, numerical results can be directly obtained. Dugundji examines the effect of nondimensional material parameters on displacement, rotation, and stresses for an end-loaded cantilever sandwich beam.

2.3 Simply-Supported Sandwich Beam

The technique used for a cantilever sandwich beam can be extended and applied to a simply-supported sandwich beam. Figure 2.2 shows a sandwich beam of length L that is simply supported on both ends with a point load P applied in the middle. The coordinate axis is placed in the middle of the beam with the z-axis pointing down. As before, the facesheets are isotropic with uniform thickness t and the core has a thickness c.

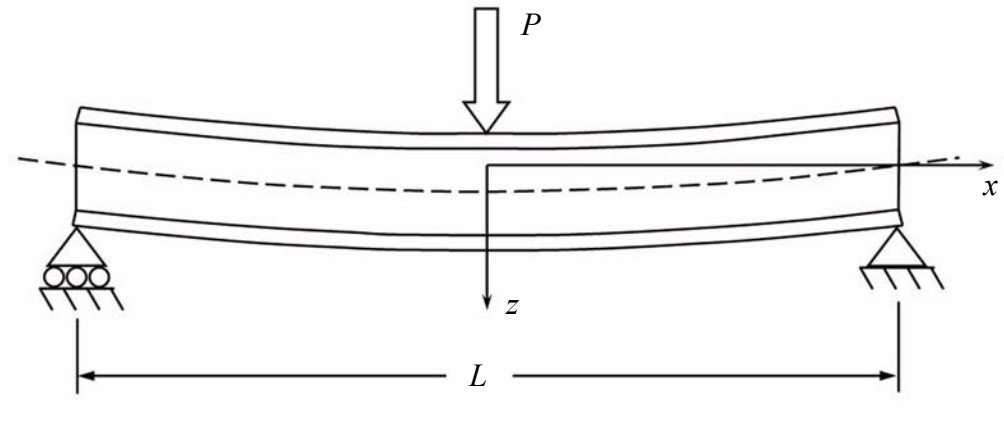

Figure 2.2: Simply-supported sandwich beam

To find the displacements and rotations, it necessary to divide the beam into left (w_L, α_L) and right (w_R, α_R) halves. Proceeding in exactly the same manner as for the cantilever sandwich beam, the total potential energy is, in analogy to Eq. (2.19),

$$\begin{aligned}\Pi = U - W = \frac{1}{2}\int_{-L/2}^{0}\left[B_3(w_L'')^2 - 2B_2 w_L''\alpha_L' + B_1(\alpha_L')^2 + GA(w_L' + \alpha_L)^2\right]dx \\ + \frac{1}{2}\int_{0}^{L/2}\left[B_3(w_R'')^2 - 2B_2 w_R''\alpha_R' + B_1(\alpha_R')^2 + GA(w_R' + \alpha_R)^2\right]dx - Pw(0)\end{aligned} \tag{2.61}$$

The subscript has been left off the displacement in the work done by the external load because the displacement at the center of the beam is continuous, and thus $w_L(0) = w_R(0) = w(0)$. After much algebra and several integrations by parts, the first variation is given by

$$\begin{aligned}\delta^{(1)}\Pi = &\int_{-L/2}^{0}\left\{\left[B_3 w_L^{IV} - B_2\alpha_L''' - GA(w_L'' + \alpha_L')\right]\delta w_L + \left[B_2 w_L''' - B_1\alpha_L'' + GA(w_L' + \alpha_L)\right]\delta\alpha_L\right\}dx \\ &+\int_{0}^{L/2}\left\{\left[B_3 w_R^{IV} - B_2\alpha_R''' - GA(w_R'' + \alpha_R')\right]\delta w_R + \left[B_2 w_R''' - B_1\alpha_R'' + GA(w_R' + \alpha_R)\right]\delta\alpha_R\right\}dx \\ &+\left[-B_3 w_L''' + B_2\alpha_L'' + GA(w_L' + \alpha_L)\right]\delta w_L\Big]_{-L/2}^{0} + \left(B_3 w_L'' - B_2\alpha_L'\right)\delta w_L'\Big]_{-L/2}^{0} \\ &+\left(-B_2 w_L'' + B_1\alpha_L'\right)\delta\alpha_L\Big]_{-L/2}^{0} + \left[-B_3 w_R''' + B_2\alpha_R'' + GA(w_R' + \alpha_R)\right]\delta w_R\Big]_{0}^{L/2} \\ &+\left(B_3 w_R'' - B_2\alpha_R'\right)\delta w_R'\Big]_{0}^{L/2} + \left(-B_2 w_R'' + B_1\alpha_R'\right)\delta\alpha_R\Big]_{0}^{L/2} - P\delta w(0) = 0\end{aligned} \tag{2.62}$$

This equation yields the following four homogeneous differential equations, which are the Euler-Lagrange equations for this beam:

$$B_3 w_L^{IV} - B_2\alpha_L''' - GA(w_L'' + \alpha_L') = 0 \tag{2.63}$$

$$B_2 w_L''' - B_1\alpha_L'' + GA(w_L' + \alpha_L) = 0 \tag{2.64}$$

$$B_3 w_R^{IV} - B_2\alpha_R''' - GA(w_R'' + \alpha_R') = 0 \tag{2.65}$$

$$B_2 w_R''' - B_1\alpha_R'' + GA(w_R' + \alpha_R) = 0 \tag{2.66}$$

The boundary conditions at the ends of the beam are found from the boundary terms evaluated at $x = L/2$ and $x = -L/2$. The displacements are known to be zero but the slope and rotation are unknown, so the boundary conditions are

$$w_L(-L/2) = 0 \tag{2.67}$$

$$w_R(L/2) = 0 \tag{2.68}$$

$$B_3 w_L''(-L/2) - B_2\alpha_L'(-L/2) = 0 \tag{2.69}$$

$$-B_2 w_L''(-L/2) + B_1\alpha_L'(-L/2) = 0 \tag{2.70}$$

$$B_3 w_R''(L/2) - B_2 \alpha_R'(L/2) = 0 \tag{2.71}$$

$$-B_2 w_R''(L/2) + B_1 \alpha_R'(L/2) = 0 \tag{2.72}$$

As in the case of the cantilever beam, the determinant of the coefficients of w'' and α' is not zero, so the last four boundary conditions reduce to

$$w_L''(-L/2) = 0 \tag{2.73}$$

$$\alpha_L'(-L/2) = 0 \tag{2.74}$$

$$w_R''(L/2) = 0 \tag{2.75}$$

$$\alpha_R'(L/2) = 0 \tag{2.76}$$

The boundary terms in Eq. (2.62) evaluated at $x = 0$ produce center conditions that relate the solutions for the left and right sides of the beam. The displacement, slope, and rotation are all continuous, but unknown, at the center of the beam, so the following six conditions must be satisfied at this point:

$$w_L(0) = w_R(0) \tag{2.77}$$

$$w_L'(0) = w_R'(0) \tag{2.78}$$

$$\alpha_L(0) = \alpha_R(0) \tag{2.79}$$

$$\left[B_3 w_L''(0) - B_2 \alpha_L'(0)\right] - \left[B_3 w_R''(0) - B_2 \alpha_R'(0)\right] = 0 \tag{2.80}$$

$$\left[-B_2 w_L''(0) + B_1 \alpha_L'(0)\right] - \left[-B_2 w_R''(0) + B_1 \alpha_R'(0)\right] = 0 \tag{2.81}$$

$$\begin{aligned} &\left\{-B_3 w_L'''(0) + B_2 \alpha_L''(0) + GA\left[w_L'(0) + \alpha_L(0)\right]\right\} \\ &\qquad - \left\{-B_3 w_R'''(0) + B_2 \alpha_R''(0) + GA\left[w_R'(0) + \alpha_R(0)\right]\right\} = P \end{aligned} \tag{2.82}$$

Once again, the coefficient matrix is not zero, so Eqs. (2.80) and (2.81) reduce to

$$w_L''(0) = w_R''(0) \tag{2.83}$$

$$\alpha_L'(0) = \alpha_R'(0) \tag{2.84}$$

The last condition simplifies to become

$$B_2\left[\alpha_L''(0) - \alpha_R''(0)\right] - B_3\left[w_L'''(0) - w_R'''(0)\right] = P \tag{2.85}$$

To ease the solution of the problem, the following relationships between the left and right sides of the beam can be assumed due to symmetry considerations:

$$w_R(x) = w_L(-x) \tag{2.86}$$

$$\alpha_R(x) = -\alpha_L(-x) \tag{2.87}$$

The differential equations for each side of the simply-supported beam take the exact same form as the differential equations for the cantilever beam. Therefore, if the displacement and rotation for the left side of the beam take the same form as Eqs. (2.42) and (2.43), then the displacements and rotations for both halves of the beam are

$$w_L(x) = C_1 e^{\beta x} + C_2 e^{-\beta x} + C_3 + C_4 x + C_5 x^2 + C_6 x^3 \tag{2.88}$$

$$\alpha_L(x) = D_1 e^{\beta x} + D_2 e^{-\beta x} + D_3 + D_4 x + D_5 x^2 + D_6 x^3 \tag{2.89}$$

$$w_R(x) = C_1 e^{-\beta x} + C_2 e^{\beta x} + C_3 - C_4 x + C_5 x^2 - C_6 x^3 \tag{2.90}$$

$$\alpha_R(x) = -D_1 e^{-\beta x} - D_2 e^{\beta x} - D_3 + D_4 x - D_5 x^2 + D_6 x^3 \tag{2.91}$$

where β has been defined by Eq. (2.41). The relationships between C_i and D_i are the same as those given by Eqs. (2.44) through (2.49).

By considering only the left half of the beam in Figure 2.2, only the three boundary conditions at $x = -L/2$ in Eqs. (2.67), (2.73), and (2.74) must be satisfied. Three of the six conditions at

the center of the beam given by Eqs. (2.77), (2.80), and (2.81) are identically satisfied by using the solutions given in Eqs. (2.88) through (2.91). The coefficients C_1 through C_6 found from these three boundary conditions and the three remaining conditions in the center of the beam are

$$C_1 = \frac{P(GA - B_1\beta^2)e^{L\beta}}{2\beta^5(B_1B_3 - B_2^2)(e^{L\beta}+1)} \tag{2.92}$$

$$C_2 = -\frac{P(GA - B_1\beta^2)}{2\beta^5(B_1B_3 - B_2^2)(e^{L\beta}+1)} \tag{2.93}$$

$$C_3 = \frac{PL\left[12B_1\beta^2 + GA(L^2\beta^2 - 12)\right]}{48\beta^4(B_1B_3 - B_2^2)} \tag{2.94}$$

$$C_4 = -\frac{P(GA - B_1\beta^2)}{2\beta^4(B_1B_3 - B_2^2)} \tag{2.95}$$

$$C_5 = -\frac{PGAL}{8\beta^2(B_1B_3 - B_2^2)} \tag{2.96}$$

$$C_6 = -\frac{PGA}{12\beta^2(B_1B_3 - B_2^2)} \tag{2.97}$$

The remaining coefficients D_1 through D_6 obtained using Eqs. (2.44) through (2.49) are

$$D_1 = -\frac{P(GA + B_2\beta^2)e^{L\beta}}{2\beta^4(B_1B_3 - B_2^2)(e^{L\beta}+1)} \tag{2.98}$$

$$D_2 = -\frac{P(GA + B_2\beta^2)}{2\beta^4(B_1B_3 - B_2^2)(e^{L\beta}+1)} \tag{2.99}$$

$$D_3 = \frac{P(GA + B_2\beta^2)}{2\beta^4(B_1B_3 - B_2^2)} \tag{2.100}$$

$$D_4 = \frac{PGAL}{4\beta^2(B_1B_3 - B_2^2)} \tag{2.101}$$

$$D_5 = \frac{PGA}{4\beta^2(B_1B_3 - B_2^2)} \tag{2.102}$$

$$D_6 = 0 \tag{2.103}$$

2.4 Approximate Solution for Simply-Supported Sandwich Beam

Due to the complexities of having different solutions valid over the left and right halves of the beam, it may be desirable to find an approximate solution to the simply-supported sandwich beam such that the displacement and rotation can each be represented by one continuous function along the length of the beam. Finding an approximate solution based on the Rayleigh-Ritz technique is one approach. In the Rayleigh-Ritz method, the approximate solutions for displacement and rotation should satisfy as many boundary conditions as possible, but in principle, only the kinematic boundary conditions need to be satisfied. For a simply-supported beam with the origin in the middle, approximation functions of the form

$$w_{app}(x) = \sum_{i=1,3,5...}^{\infty} W_i \cos\left(\frac{i\pi x}{L}\right) \tag{2.104}$$

$$\alpha_{app}(x) = \sum_{i=1,3,5...}^{\infty} \Omega_i \sin\left(\frac{i\pi x}{L}\right) \tag{2.105}$$

satisfy all of the boundary conditions given by Eqs. (2.67), (2.68), and (2.73) through (2.76). These trigonometric functions also exhibit the same symmetry characteristics as the displacement and rotation. The unknown constants W_i and Ω_i are determined by minimizing the total potential energy of the beam.

Use of the approximate functions in the total potential energy of Eq. (2.61), when now only a single integral is necessary, gives the approximate total potential energy as

$$\Pi = \frac{1}{2}\int_{-L/2}^{L/2}\left[B_3(w''_{app})^2 - 2B_2 w''_{app}\alpha'_{app} + B_1(\alpha'_{app})^2 + GA(w'_{app} + \alpha_{app})^2\right]dx - Pw_{app}(0) \tag{2.106}$$

Consideration of only the first two terms (i = 1,3) in each of the infinite series of Eqs. (2.104) and (2.105) reveals the total potential energy to be

$$\begin{aligned}\Pi = \frac{1}{4L^3}\Big(& AGL^2\left(\Omega_1^2L^2 - 2L\pi\Omega_1W_1 + \pi^2W_1^2 + \Omega_3^2L^2 - 6L\pi\Omega_3W_3 + 9\pi^2W_3^2\right) \\ & + \pi^2\left(B_1L^2\Omega_1^2 + 2B_2L\pi\Omega_1W_1 + B_3\pi^2W_1 + 9B_1L^2\Omega_3^2 + 54B_2L\pi\Omega_3W_3 + 81B_3\pi^2W_3\right)\Big) \\ & - P(W_1 + W_3)\end{aligned} \tag{2.107}$$

To minimize this expression it is necessary that the partial derivatives of the expression with respect to W_1, W_3, Ω_1, Ω_3 each be zero. Solving the resulting four equations yields

$$W_1 = \frac{2PL^3(AGL^2 + B_1\pi^2)}{\pi^4(AGL^2B_1 + 2AGL^2B_2 + AGL^2B_3 + B_1B_3\pi^2 - B_2^2\pi^2)} \tag{2.108}$$

$$W_3 = \frac{2PL^3(AGL^2 + 9B_1\pi^2)}{81\pi^4(AGL^2B_1 + 2AGL^2B_2 + AGL^2B_3 + 9B_1B_3\pi^2 - 9B_2^2\pi^2)} \tag{2.109}$$

$$\Omega_1 = \frac{2PL^2(AGL^2 - B_2\pi^2)}{\pi^3(AGL^2B_1 + 2AGL^2B_2 + AGL^2B_3 + B_1B_3\pi^2 - B_2^2\pi^2)} \tag{2.110}$$

$$\Omega_3 = \frac{2PL^2(AGL^2 - 9B_2\pi^2)}{27\pi^3(AGL^2B_1 + 2AGL^2B_2 + AGL^2B_3 + 9B_1B_3\pi^2 - 9B_2^2\pi^2)} \tag{2.111}$$

Careful examination of these coefficients reveals similarities between W_1 and W_3 as well as Ω_1 and Ω_3. If more terms are included in the infinite series, it is found that

$$W_i = \frac{2PL^3(AGL^2 + i^2B_1\pi^2)}{i^4\pi^4(AGL^2B_1 + 2AGL^2B_2 + AGL^2B_3 + i^2B_1B_3\pi^2 - i^2B_2^2\pi^2)} \tag{2.112}$$

$$\Omega_i = \frac{2PL^2(AGL^2 - i^2B_2\pi^2)}{i^3\pi^3(AGL^2B_1 + 2AGL^2B_2 + AGL^2B_3 + i^2B_1B_3\pi^2 - i^2B_2^2\pi^2)} \tag{2.113}$$

As more terms are added to the approximate solutions, the potential energy given by Eq. (2.106) becomes very computationally intensive, so the above relationships in Eqs. (2.112) and (2.113) give a much more efficient method of including many terms in the infinite series.

To compare the exact and approximate solutions, the variables are nondimensionalized by the following scheme suggested by Dugundji:

$$W(x) = \frac{w(x)}{L} \tag{2.114}$$

$$\xi = \frac{x}{L} \tag{2.115}$$

$$g = \frac{GAL^2}{EI} \tag{2.116}$$

$$\overline{P} = \frac{PL^2}{EI} \tag{2.117}$$

$$\eta = \frac{t}{c} \tag{2.118}$$

$$\overline{B}_1 = \frac{B_1}{EI} = \frac{\frac{1}{2}}{\frac{1}{2} + \eta + \frac{2}{3}\eta^2} \tag{2.119}$$

$$\overline{B}_2 = \frac{B_2}{EI} = \frac{\frac{1}{2}\eta}{\frac{1}{2} + \eta + \frac{2}{3}\eta^2} \tag{2.120}$$

$$\overline{B}_3 = \frac{B_3}{EI} = \frac{\frac{2}{3}\eta^2}{\frac{1}{2} + \eta + \frac{2}{3}\eta^2} \tag{2.121}$$

After much algebra, the nondimensional displacement $W(\xi)$ is found to be a function of the nondimensional load $\overline{P}$, the facesheet to core thickness ratio η, and the shear parameter g. Figure 2.3 shows the exact displacement solution and four approximate displacement solutions normalized with the exact displacement at the center of the beam, $W(0)$. As the number of terms in the approximate solution increases, the approximate solution approaches that of the exact solution from below. For this particular plot, numerical values of $\eta = 0.04$ and $g = 10$ were used. The These values are representative of the sandwich beams to be tested in Chapter 5.

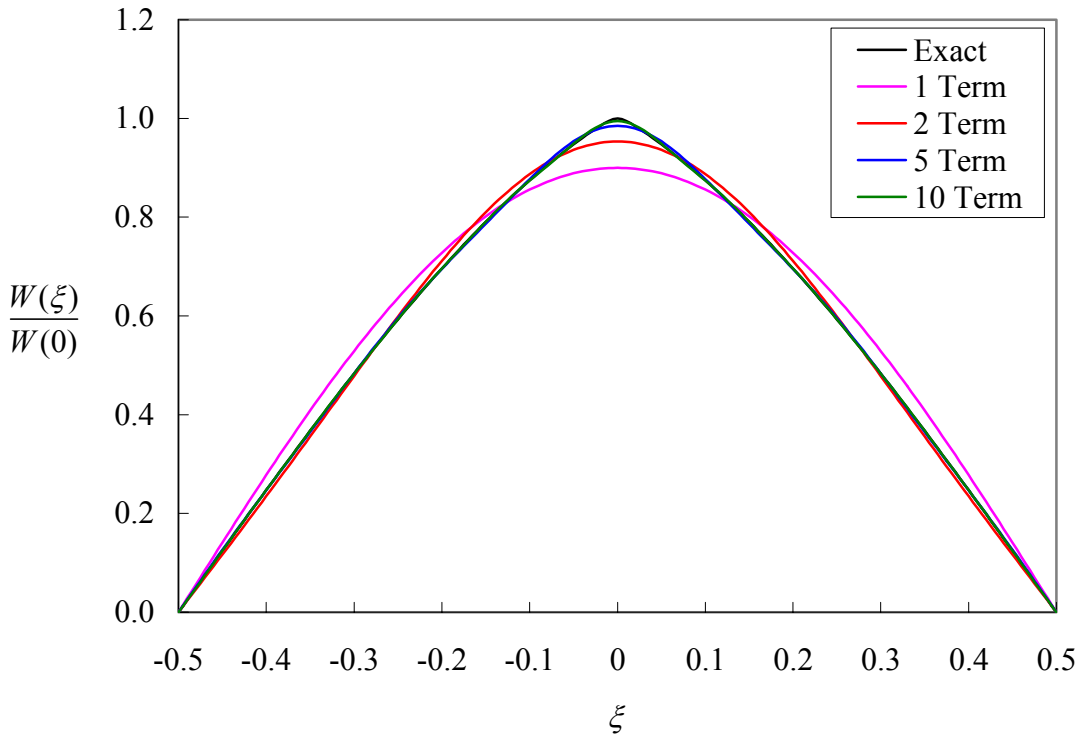

Figure 2.3: Exact and approximate solutions for displacement of simply-supported sandwich beam

2.5 Shear Plus Bending Theory

Another theory to describe the deflection of a simply-supported sandwich beam with a point load in the center is given by Allen [13]. The total deflection can be assumed to be a sum of deflection due to pure bending and deflection due to pure shear, as shown in Figure 2.4. In pure bending, the sandwich beam is treated as an Euler beam with flexural rigidity *EI* defined by Eq. (2.17). The displacement of such a beam given in any standard mechanics of materials book is

$$w_L^1(x) = -\frac{P}{12EI}x^3 - \frac{PL}{8EI}x^2 + \frac{PL^3}{48EI} \tag{2.122}$$

$$w_R^1(x) = \frac{P}{12EI}x^3 - \frac{PL}{8EI}x^2 + \frac{PL^3}{48EI} \tag{2.123}$$

where the superscript 1 represents the bending solution, and the subscripts *L* and *R* represent the left and right halves of the beam, respectively.

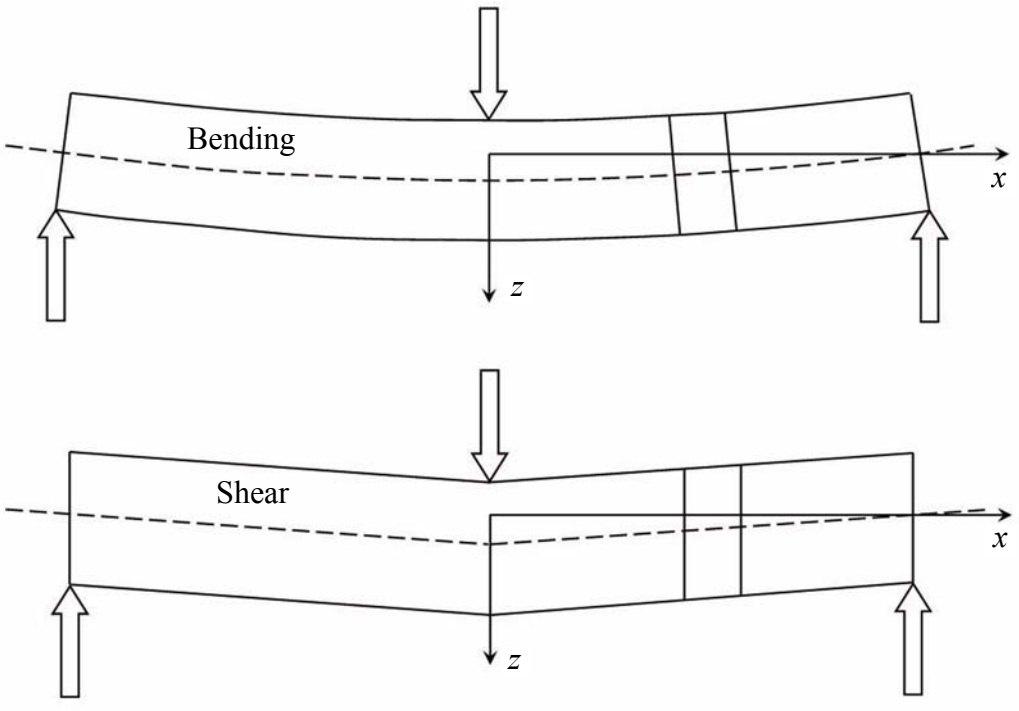

Figure 2.4: Shear plus bending theory

In the pure shear solution, vertical lines do not rotate with the beam as it deforms. Allen defines

$$A^* = \frac{b(t+c)^2}{c} \tag{2.124}$$

For a core with shear modulus G, the shear stiffness of the beam is GA^*. The shear displacement is a linear function of x given by

$$w_L^2(x) = \frac{P}{2GA^*}x + \frac{PL}{4GA^*} \tag{2.125}$$

$$w_R^2(x) = -\frac{P}{2GA^*}x + \frac{PL}{4GA^*} \tag{2.126}$$

where the superscript 2 represents the shear solution. Note that the displacements given by Eqs. (2.122) and (2.125) are zero at $x = -L/2$, and the displacements given by Eqs. (2.123) and (2.126) are zero at $x = L/2$. The total displacement (superscript 1+2) is the sum of the displacements due to bending and the displacement due to pure shear, i.e.,

$$w_L^{1+2}(x) = -\frac{P}{12EI}x^3 - \frac{PL}{8EI}x^2 + \frac{P}{2GA^*}x + \frac{PL^3}{48EI} + \frac{PL}{4GA^*} \tag{2.127}$$

$$w_R^{1+2}(x) = \frac{P}{12EI}x^3 - \frac{PL}{8EI}x^2 - \frac{P}{2GA^*}x + \frac{PL^3}{48EI} + \frac{PL}{4GA^*} \tag{2.128}$$

This solution compares very well to the previous exact solution for a wide range of material properties and beam dimensions. Figure 2.5 shows the nondimensional displacements of the exact solution and the shear plus bending theory solution with $\eta = 0.04$ and $g = 10$. The solutions are practically indistinguishable.

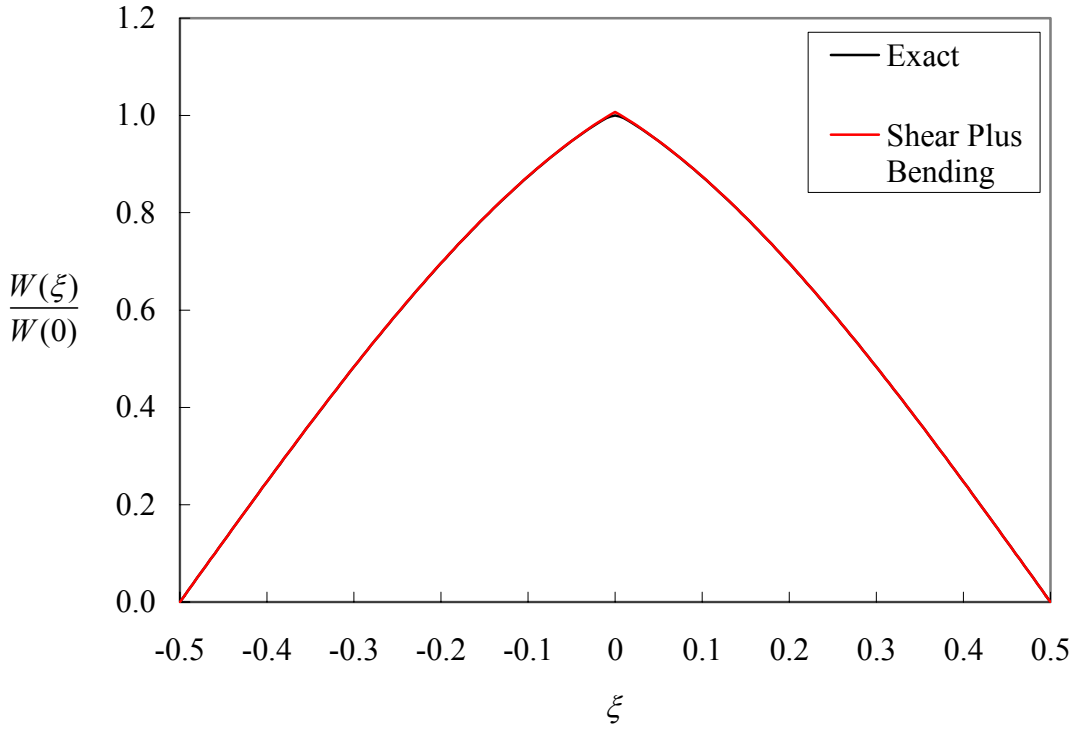

Figure 2.5: Exact and shear plus bending theory solutions for displacement of simply-supported sandwich beam

The shear plus bending theory does not include the rotation angle α of the original theory. While this angle is useful to describe the behavior of the beam, it is not possible to validate in an experiment. The only continuity condition that is satisfied in the center of the beam is the displacement. Unlike the previous theory, the slope of the midsurface is discontinuous due to the assumed linear nature of the pure shear displacement.

2.6 Comparison to Timoshenko Beam Theory

The shear plus bending theory is comparable to standard Timoshenko beam theory [14]. For Timoshenko beam theory, the two degrees of freedom are the vertical displacement, w, and the rotation angle, α, similar to those of the core of the sandwich beam. Unlike the standard Euler beam theory, the rotation of the cross-section does not have to be equivalent to the derivative of the vertical displacement.

The strain energy of a Timoshenko beam of total length L is given by

$$U_{Timo} = \frac{1}{2}\int_0^L \left[EI\left(\frac{d\alpha}{dx}\right)^2 + GA\left(\frac{dw}{dx}+\alpha\right)^2 \right] dx \tag{2.129}$$

where E is the elastic modulus, I is the cross-sectional moment of inertia, G is the shear modulus, and A is the cross-sectional area. If this discussion is extended to a Timoshenko beam that is simply supported on each end with a point load P in the center, it is necessary to divide the beam into left (w_L, α_L) and right (w_R, α_R) halves in exactly the same manner as the sandwich beam. For this case, the total potential energy is written

$$\begin{aligned}\Pi_{Timo} = &\frac{1}{2}\int_{-L/2}^0 \left[EI\left(\frac{d\alpha_L}{dx}\right)^2 + GA\left(\frac{dw_L}{dx}+\alpha_L\right)^2 \right] dx \\ &+\frac{1}{2}\int_0^{L/2} \left[EI\left(\frac{d\alpha_R}{dx}\right)^2 + GA\left(\frac{dw_R}{dx}+\alpha_R\right)^2 \right] dx - Pw(0)\end{aligned} \tag{2.130}$$

After much algebra, the first variation of the total potential energy is

$$\begin{aligned}\delta^{(1)}\Pi_{Timo} = &\int_{-L/2}^0 \left\{ \left[-GA(w_L'' + \alpha_L') \right]\delta w_L + \left[-EI\alpha_L'' + GA(w_L' + \alpha_L) \right]\delta\alpha_L \right\} dx \\ &+\int_0^{L/2} \left\{ \left[-GA(w_R'' + \alpha_R') \right]\delta w_R + \left[-EI\alpha_R'' + GA(w_R' + \alpha_R) \right]\delta\alpha_R \right\} dx \\ &+\left[GA(w_L' + \alpha_L) \right]\delta w_L \Big]_{-L/2}^0 + \left(EI\alpha_L' \right)\delta\alpha_L \Big]_{-L/2}^0 \\ &+\left[GA(w_R' + \alpha_R) \right]\delta w_R \Big]_0^{L/2} + \left(EI\alpha_R' \right)\delta\alpha_R \Big]_0^{L/2} - P\delta w(0) = 0\end{aligned} \tag{2.131}$$

For the integrals in this equation to be zero, the following four Euler-Lagrange equations must be satisfied:

$$GA(w_L'' + \alpha_L') = 0 \tag{2.132}$$

$$GA(w_R'' + \alpha_R') = 0 \tag{2.133}$$

$$-EI\alpha_L'' + GA(w_L' + \alpha_L) = 0 \tag{2.134}$$

$$-EI\alpha_R'' + GA(w_R' + \alpha_R) = 0 \tag{2.135}$$

The boundary term yields two boundary conditions on each end of the beam and two additional conditions in the middle of the beam. The boundary conditions are

$$w_L(-L/2) = 0 \tag{2.136}$$

$$EI\alpha_L'(-L/2) = 0 \tag{2.137}$$

$$w_R(L/2) = 0 \tag{2.138}$$

$$EI\alpha_R'(L/2) = 0 \tag{2.139}$$

For continuity purposes, $w_L(0) = w_R(0) = w(0)$ and $\alpha_L(0) = \alpha_R(0)$. Note that unlike the sandwich beam, the slope of the midsurface is not required to be continuous at the middle of the beam, $w_L'(0) \neq w_R'(0)$. Thus, the other two conditions at the center of the beam are

$$GA\left(w_L'(0) + \alpha_L(0)\right) - GA\left(w_R'(0) + \alpha_R(0)\right) - P = 0 \tag{2.140}$$

$$EI\alpha_L'(0) - EI\alpha_R'(0) = 0 \tag{2.141}$$

The differential equations are solved by integrating Eqs. (2.132) and (2.133) and substituting into Eqs. (2.134) and (2.135). After further integration and use of the boundary conditions, the displacements and rotations are found to be simple polynomials given by

$$w_L(x) = -\frac{P}{12EI}x^3 - \frac{PL}{8EI}x^2 + \frac{P}{2GA}x + \frac{PL^3}{48EI} + \frac{PL}{4GA} \tag{2.142}$$

$$w_R(x) = \frac{P}{12EI}x^3 - \frac{PL}{8EI}x^2 - \frac{P}{2GA}x + \frac{PL^3}{48EI} + \frac{PL}{4GA} \tag{2.143}$$

$$\alpha_L(x) = \frac{P}{4EI}x^2 + \frac{PL}{4EI}x \tag{2.144}$$

$$\alpha_R(x) = -\frac{P}{4EI}x^2 + \frac{PL}{4EI}x \tag{2.145}$$

The polynomials for the displacements are nearly identical to the those obtained from the bending plus shear theory of the previous section. The primary difference is that the Timoshenko beam uses the entire cross-sectional area A, but the sandwich uses the modified A^*. The flexural rigidity EI is defined differently for each case. The Timoshenko solution also gives a prediction of the rotation α.

2.7 Comparison to ASTM C 393

A general guideline for testing simply supported sandwich beams is given in ASTM C 393 entitled "Standard Test Method for Flexural Properties of Sandwich Constructions" [11]. The actual test procedure will be discussed in Chapter 5, but it is useful to compare the results from the sandwich beam theory developed previously with the deflection calculation given in the standard. The deflection in the center of the beam, Δ, is given in the standard to be

$$\Delta = \frac{PL^3}{48D} + \frac{PL}{4U} \tag{2.146}$$

where D is the bending stiffness and U is the shear rigidity defined in the standard by

$$D = \frac{E\left(d^3 - c^3\right)b}{12} \tag{2.147}$$

$$U = \frac{G\left(d + c\right)^2 b}{4c} \tag{2.148}$$

The variable d is introduced as the total beam thickness given by

$$d = c + 2t \tag{2.149}$$

The center deflection has a similar form to that of the displacement predicted by the shear plus bending theory given in Eqs. (2.127) or (2.128) at $x = 0$. After simple algebra, it is found that

$$D = EI \tag{2.150}$$

$$U = GA^* \tag{2.151}$$

Therefore, the ASTM result is a special case for the center deflection of the shear plus bending theory, which is valid for all values of x. As was shown in Figure 2.5, the shear plus bending theory gives very good agreement with the exact solution. Thus, the sandwich beam theory can be applied to predict the deflection of a sandwich beam tested according the procedures outlined in ASTM C 393.

2.8 Effect of Non-Uniform Facesheet Thickness

To this point, it has been assumed that the facesheets in the sandwich are identical and uniform in thickness. It will be shown in Chapter 4 that it is difficult to control the uniformity and thickness during the compression molding process used to fabricate random wetlay composite panels. This dilemma serves as motivation for developing a sandwich beam theory for facesheets with thickness that varies in the x-direction.

Consider the sandwich beam shown in Figure 2.1 with a top facesheet thickness of $t_T(x)$ and a bottom facesheet thickness of $t_B(x)$. The displacements, strains, and stresses given by Eqs. (2.1) through (2.9) remain the same. The limits of integration for the strain energy of the sandwich given by Eq. (2.11) must be modified to become

$$U = \frac{1}{2}\int_0^L \int_{-(c/2+t_B(x))}^{-c/2} (b\sigma_x\varepsilon_x)_B \, dz dx + \frac{1}{2}\int_0^L \int_{-c/2}^{c/2} (b\sigma_{xz}\gamma_{xz})_C \, dz dx + \frac{1}{2}\int_0^L \int_{c/2}^{c/2+t_T(x)} (b\sigma_x\varepsilon_x)_T \, dz dx \tag{2.152}$$

Integration through the thickness gives

$$U = \frac{1}{2}\int_0^L \left\{ B_3(x)\left[w''(x)\right]^2 - 2B_2(x)w''(x)\alpha'(x) + B_1(x)\left[\alpha'(x)\right]^2 + GA\left[w'(x)+\alpha(x)\right]^2 \right\} dx \tag{2.153}$$

where

$$B_1(x) = \frac{1}{4} Ebc^2 \left[t_B(x) + t_T(x) \right] \tag{2.154}$$

$$B_2(x) = \frac{1}{4} Ebc \left[t_B^2(x) + t_T^2(x) \right] \tag{2.155}$$

$$B_3(x) = \frac{1}{3} Eb \left[t_B^3(x) + t_T^3(x) \right] \tag{2.156}$$

This form is similar to that of Eq. (2.12) except that B_1, B_2, and B_3 are now functions of x.

Now consider the simply-supported sandwich beam shown in Figure 2.2 with facesheet thicknesses that vary as smooth, continuous, non-zero functions of x along the entire length of the beam. The total potential energy of the system is the same as that given by Eq. (2.61) with B_1, B_2, and B_3 defined by Eqs. (2.154) through (2.156). After much algebra and several integrations by parts, the first variation of the total potential energy is found to be very similar to Eq. (2.62). The four Euler-Lagrange equations revealed through the first variation are

$$\frac{d^2}{dx^2}\left[B_3(x) \frac{d^2 w_L}{dx^2} \right] - \frac{d^2}{dx^2}\left[B_2(x) \frac{d\alpha_L}{dx} \right] - GA\left[\frac{d^2 w_L}{dx^2} + \frac{d\alpha_L}{dx} \right] = 0 \tag{2.157}$$

$$\frac{d}{dx}\left[B_2(x) \frac{d^2 w_L}{dx^2} \right] - \frac{d}{dx}\left[B_1(x) \frac{d\alpha_L}{dx} \right] + GA\left[\frac{dw_L}{dx} + \alpha_L \right] = 0 \tag{2.158}$$

$$\frac{d^2}{dx^2}\left[B_3(x) \frac{d^2 w_R}{dx^2} \right] - \frac{d^2}{dx^2}\left[B_2(x) \frac{d\alpha_R}{dx} \right] - GA\left[\frac{d^2 w_R}{dx^2} + \frac{d\alpha_R}{dx} \right] = 0 \tag{2.159}$$

$$\frac{d}{dx}\left[B_2(x) \frac{d^2 w_R}{dx^2} \right] - \frac{d}{dx}\left[B_1(x) \frac{d\alpha_L}{dx} \right] + GA\left[\frac{dw_L}{dx} + \alpha_L \right] = 0 \tag{2.160}$$

The three boundary conditions at each end of the beam are the same as the sandwich beam with facesheets of uniform thickness given by Eqs. (2.67), (2.68), and (2.73) through (2.76). Five of the six conditions in the center of the beam given by Eqs. (2.77), (2.78), (2.79), (2.83), and (2.84) are also the same. The final center condition of Eq. (2.85) is

$$\frac{d}{dx}\left\{B_2(x)\left[\frac{d\alpha_L}{dx}-\frac{d\alpha_R}{dx}\right]-B_3(x)\left[\frac{d^2w_L}{dx^2}-\frac{d^2w_R}{dx^2}\right]\right\}_{x=0}=P \tag{2.161}$$

An exact solution to the above differential equations is difficult because B_1, B_2, and B_3 are no longer constant coefficients. Therefore, an approximate Rayleigh-Ritz solution will be developed similar to the procedure used in Section 2.4. Approximate functions of the form

$$w_{app}(x)=\sum_{i=1,3,5\ldots}^{\infty}W_i\cos\left(\frac{i\pi x}{L}\right)+\sum_{i=2,4,6\ldots}^{\infty}W_i\sin\left(\frac{i\pi x}{L}\right) \tag{2.162}$$

$$\alpha_{app}(x)=\sum_{i=1,3,5\ldots}^{\infty}\Omega_i\sin\left(\frac{i\pi x}{L}\right)+\sum_{i=2,4,6\ldots}^{\infty}\Omega_i\cos\left(\frac{i\pi x}{L}\right) \tag{2.163}$$

satisfy all of the boundary conditions at $x = \pm L/2$. The first set of terms in the approximate solutions are the same as those of Eqs. (2.104) and (2.105). An extra set of terms has been included because the beam is no long necessarily symmetric in x. These approximate functions are substituted into the total potential energy of the system with a finite number of terms in each series. The unknown constants are found by minimizing the total potential energy such that

$$\frac{\partial\Pi}{\partial W_i}=0 \text{ and } \frac{\partial\Pi}{\partial\Omega_i}=0 \qquad i = 1, 2, 3\ldots \tag{2.164}$$

and solving the resulting set of linear equations.

As an example, consider a sandwich beam with non-uniform facesheets that can be described by the polynomial

$$t_T(x)=t_B(x)=-\frac{9t}{4L^2}x^2+\frac{t}{4L}x+\frac{19t}{16} \tag{2.165}$$

where t is the average thickness that represents a uniform facesheet. In this case, the non-uniform facesheet is $0.5t$ at $x = -L/2$ and $0.75t$ at $x = L/2$. The shape of the top facesheet is shown in Figure 2.6. This shape is similar to those obtained when manufacturing random wetlay composite panels.

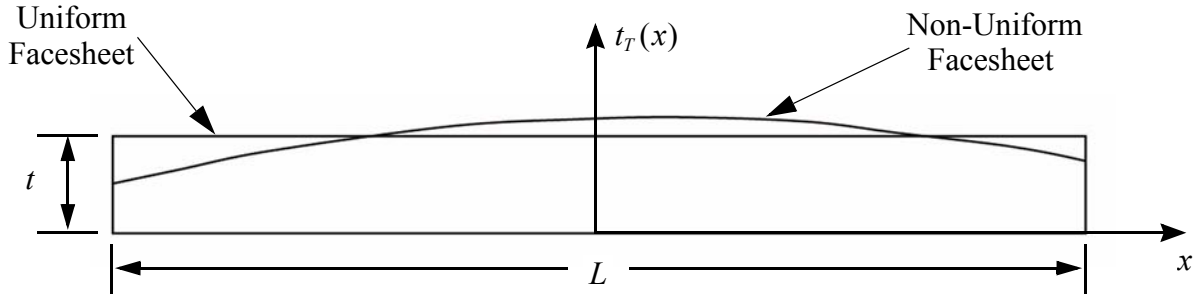

Figure 2.6: Example of non-uniform facesheet for sandwich beam

Functions of the form given by Eqs. (2.162) and (2.163) can be used to approximate the displacement and rotation of a simply-supported sandwich beam with the non-uniform facesheets described by Eq. (2.165). The displacements are shown in Figure 2.7. The displacement of the beam with non-uniform facesheets is less than the displacement of the beam with uniform facesheets because the bending stiffness is greater in the center of the beam with non-uniform facesheets. Careful examination will reveal that the displacement of the beam with non-uniform facesheets is not symmetric because of the linear term in Eq. (2.165).

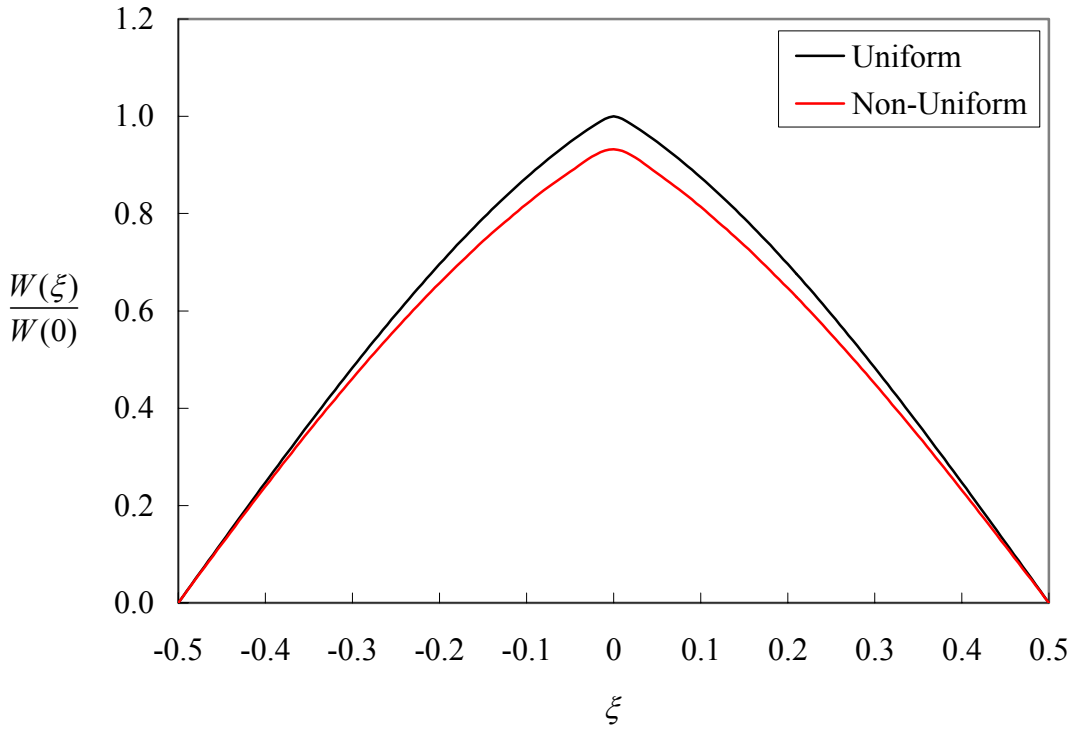

Figure 2.7: Uniform and non-uniform facesheet thickness solutions for displacement of simply-supported sandwich beam

This concludes the development and discussion of sandwich beam theories. In Chapter 5, the predictions of these theories will be compared with experimental results for random wetlay composite honeycomb sandwich beams. Attention now turns to the extension of the theory developed in Sections 2.2 and 2.3 to sandwich plates.

Chapter 3 Sandwich Plate Theory

3.1 Introduction

A plate is a structural member in which one dimension is significantly less than the other two. Figure 3.1 shows a rectangular sandwich plate of length a and width b. As with the beam in Figure 2.1, the thickness of each facesheet is t, and the thickness of the core is c. It is assumed that the midsurface of the plate remains neutral, or stress-free, during bending. This assumption restricts the analysis to plates with identical facesheets. The deflection of the plate in the z-direction can be described entirely by the displacement $w(x,y)$ of the midsurface. This displacement is considered small in comparison to the facesheet thickness. A state of plane-stress is assumed such that the transverse normal stresses are negligible. Therefore, plate theory is used to reduce the complicated three-dimensional elasticity problem to two dimensions. The facesheets are modeled as isotropic plates that are assumed to satisfy the Kirchhoff hypothesis, and the core is assumed to exhibit only shear deformations. In this chapter, Kirchhoff plate theory will be briefly reviewed, including the solution of several example problems, then the sandwich plate theory will be fully developed. Various boundary conditions and loading conditions will be explored.

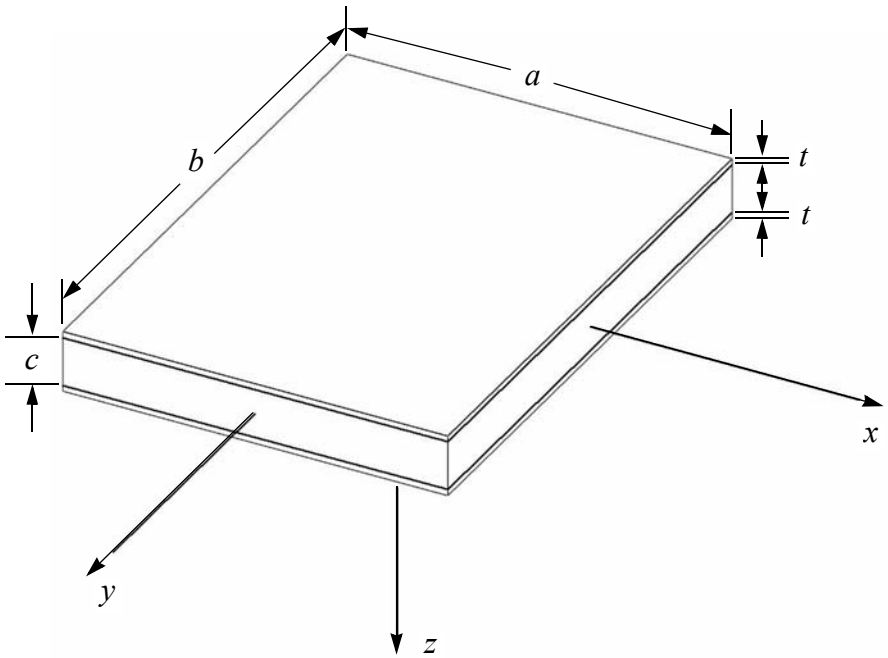

Figure 3.1: Rectangular sandwich plate

3.2 Brief Overview of Kirchhoff Plate Theory

Kirchhoff plate theory, which is an extension of Euler beam theory to two dimensions, is based upon the assumption that a straight line perpendicular to the midsurface of the plate before deformation remains straight and perpendicular to the midsurface after deformation. Timoshenko [15] discusses Kirchhoff plate theory and presents several unique solutions for plates with various loading and boundary conditions.

Within the context of Kirchhoff plate theory, the transverse deflections of an isotropic plate subjected to a transverse distributed load $q(x,y)$ are governed by the equation

$$\frac{\partial^2 M_x}{\partial x^2} + 2\frac{\partial^2 M_{xy}}{\partial x \partial y} + \frac{\partial^2 M_y}{\partial y^2} + q = 0 \tag{3.1}$$

where M_x, M_y, and M_{xy} are the bending and twisting moment resultants with sign conventions consistent with the theory of elasticity, as shown in Figure 3.2. The moment results are assumed to act on the midsurface of the plate. They can be expressed in terms of the deflection $w(x,y)$, plate geometry, and material properties as

$$M_x = -D\left(\frac{\partial^2 w}{\partial x^2} + \nu\frac{\partial^2 w}{\partial y^2}\right) \tag{3.2}$$

$$M_y = -D\left(\frac{\partial^2 w}{\partial y^2} + \nu\frac{\partial^2 w}{\partial x^2}\right) \tag{3.3}$$

$$M_{xy} = -D(1-\nu)\frac{\partial^2 w}{\partial x \partial y} \tag{3.4}$$

where the flexural rigidity D is given by

$$D = \frac{Eh^3}{12(1-\nu)^2} \tag{3.5}$$

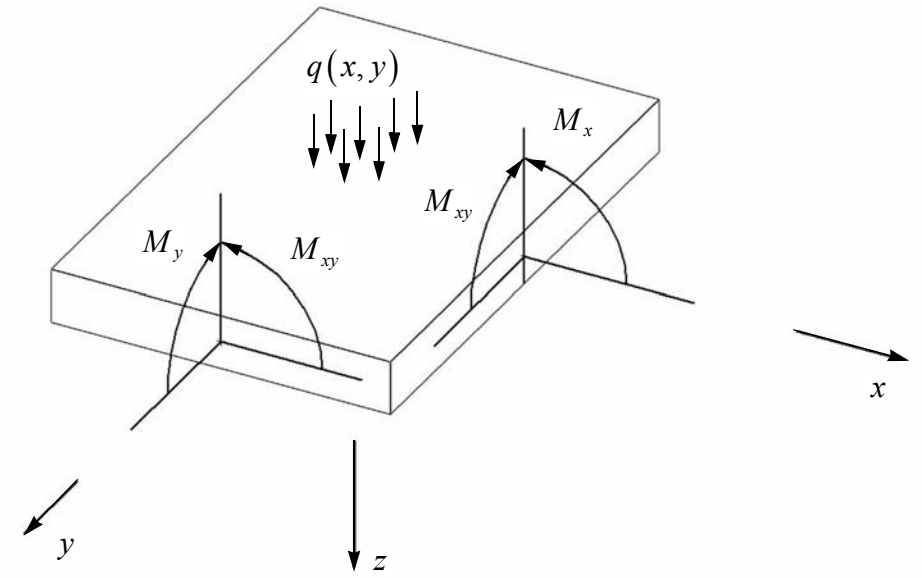

Figure 3.2: Moment resultants

and where E is the extensional modulus, ν is Poisson's ratio, and h is the thickness of the plate. Substituting the definitions of the moment resultants into the governing equation, the following 4th-order partial differential equation for $w(x,y)$ is obtained:

$$\frac{\partial^4 w}{\partial x^4} + 2\frac{\partial^4 w}{\partial x^2 \partial y^2} + \frac{\partial^4 w}{\partial y^4} = \frac{q}{D} \tag{3.6}$$

In addition to the moment resultants, there are transverse shear force resultants acting on the mid-surface of the plate. Because of equilibrium requirements, these force resultants are related to the moment resultants, and in turn, the displacements, by

$$Q_x = \frac{\partial M_x}{\partial x} + \frac{\partial M_{xy}}{\partial y} = -D\left(\frac{\partial^3 w}{\partial x^3} + \frac{\partial^3 w}{\partial x \partial y^2}\right) \tag{3.7}$$

$$Q_y = \frac{\partial M_y}{\partial y} + \frac{\partial M_{xy}}{\partial x} = -D\left(\frac{\partial^3 w}{\partial y^3} + \frac{\partial^3 w}{\partial x^2 \partial y}\right) \tag{3.8}$$

There are also effective transverse shear force resultants, Q_x^{eff} and Q_y^{eff}, that are developed through the variational process. They are not obvious resultants when using the force equilibrium approach. The effective transverse shear force resultants are given by

$$Q_x^{eff} = Q_x + \frac{\partial M_{xy}}{\partial y} = -D\left[\frac{\partial^3 w}{\partial x^3} + (2-\nu)\frac{\partial^3 w}{\partial x \partial y^2}\right] \tag{3.9}$$

$$Q_y^{eff} = Q_y + \frac{\partial M_{xy}}{\partial x} = -D\left[\frac{\partial^3 w}{\partial y^3} + (2-\nu)\frac{\partial^3 w}{\partial x^2 \partial y}\right] \tag{3.10}$$

Consider a rectangular plate of length a in the x-direction and width b in the y-direction as shown in Figure 3.3. The origin is in the center of the plate, and the z-axis is pointing into the page. There are two boundary conditions which must be satisfied along each edge. For a transversely loaded plate, the following boundary conditions must hold at $x = a/2$:

$$Q_x^{eff}(a/2, y) = 0 \quad \text{OR} \quad w(a/2, y) \text{ must be specified} \tag{3.11}$$

AND

$$M_x(a/2, y) = 0 \quad \text{OR} \quad \frac{\partial w}{\partial x}(a/2, y) \text{ must be specified} \tag{3.12}$$

Similarly, the boundary conditions at $y = b/2$ are

$$Q_y^{eff}(x, b/2) = 0 \quad \text{OR} \quad w(x, b/2) \text{ must be specified} \tag{3.13}$$

AND

$$M_y(x, b/2) = 0 \quad \text{OR} \quad \frac{\partial w}{\partial y}(x, b/2) \text{ must be specified} \tag{3.14}$$

The boundary conditions at $x = -a/2$ and $y = -b/2$ are the same as at their opposite edges.

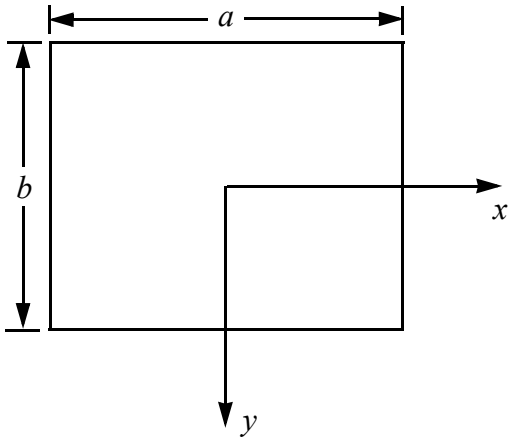

Figure 3.3: Rectangular plate dimensions

In addition to the boundary conditions given above, there are also corner conditions that are easily derived using the variational process. At each corner of the plate, the following condition must apply:

$$-2M_{xy}\left(\pm a/2, \pm b/2\right) = 0 \quad \text{OR} \quad w\left(\pm a/2, \pm b/2\right) \text{ must be specified} \tag{3.15}$$

If the displacement at a corner is specified to be zero, a concentrated reaction force is necessary to prevent this displacement. The magnitude of this reaction force is

$$R = -2M_{xy} \tag{3.16}$$

3.3 Uniformly-Loaded Isotropic Plate Simply Supported Along Four Edges

One of the easiest types of boundary conditions to analyze is that of a simply-supported edge. The displacement and bending moments are specified to be zero on all four edges, but nothing is said about the slopes. Consider a square plate ($a = b$) under a uniform distributed load q_o that is simply supported on all four edges. The specific boundary conditions are

$$\begin{aligned} w\left(\pm a/2, y\right) &= 0 \\ M_x\left(\pm a/2, y\right) &= 0 \\ w\left(x, \pm a/2\right) &= 0 \\ M_y\left(x, \pm a/2\right) &= 0 \end{aligned} \tag{3.17}$$

An assumed solution of the form

$$w(x,y) = \sum_{m=1,3,5\ldots}^{\infty} \sum_{n=1,3,5\ldots}^{\infty} W_{mn} \cos\left(\frac{m\pi x}{a}\right) \cos\left(\frac{n\pi y}{a}\right) \tag{3.18}$$

where W_{mn} are unknown constants, satisfies all of the boundary conditions. The uniform distributed load can be approximated by a double-infinite summation as

$$q(x,y) = \sum_{m=1,3,5\ldots}^{\infty} \sum_{n=1,3,5\ldots}^{\infty} \frac{16q_o}{\pi^2 mn} \sin\left(\frac{m\pi}{2}\right) \sin\left(\frac{n\pi}{2}\right) \cos\left(\frac{m\pi x}{a}\right) \cos\left(\frac{n\pi y}{a}\right) \tag{3.19}$$

The unknown constants W_{mn} are found by substituting Eqs. (3.18) and (3.19) into the governing differential equation given by Eq. (3.6). Equating like coefficients of $\cos\left(\frac{m\pi x}{a}\right)\cos\left(\frac{n\pi y}{a}\right)$ gives

$$W_{mn} = \frac{16q_o a^4}{D\pi^6 mn\left(m^2+n^2\right)^2} \sin\left(\frac{m\pi}{2}\right) \sin\left(\frac{n\pi}{2}\right) \qquad m, n = 1, 3, 5\ldots \tag{3.20}$$

This solution rapidly converges, and sufficient accuracy to three significant figures is obtained with just two terms in each series. To visualize the shape of the displacement, it is convenient to nondimensionalize the variables in the following manner:

$$\begin{aligned} W(x,y) &= \frac{w(x,y)}{\left(q_o a^4/D\right)} \\ \overline{x} &= \frac{x}{a} \\ \overline{y} &= \frac{y}{a} \end{aligned} \tag{3.21}$$

The nondimensional displacement is illustrated in Figure 3.4. The displacement is positive because the load is down in the positive z-direction in accordance with Figure 3.3. The maximum normalized deflection is 0.00406 at the center of the plate. A similar procedure will be used to find the deflection of a sandwich plate under uniform load with simply-supported boundary conditions.

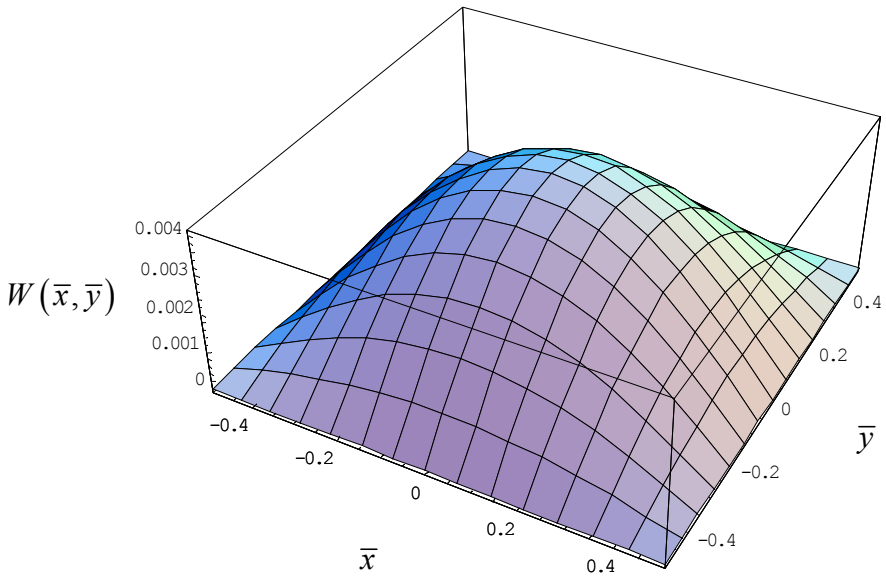

Figure 3.4: Displacement of uniformly-loaded isotropic plate simply supported along four edges

3.4 Uniformly-Loaded Isotropic Plate Simply Supported Along Two Edges

Timoshenko [16] presents a solution for the displacement of a rectangular isotropic plate under a uniform load q_o with simply-supported boundary conditions along the edges $x = \pm a/2$ and arbitrary boundary conditions at $y = \pm b/2$. The displacement is assumed to have the form

$$w(x,y) = w^1(x) + w^2(x,y) \tag{3.22}$$

where

$$w^1(x) = \frac{q_o}{384D}\left(16x^4 - 24a^2x^2 + 5a^4\right) \tag{3.23}$$

$$w^2(x,y) = \sum_{m=1,3,5\ldots}^{\infty} W_m(y)\cos\left(\frac{m\pi x}{a}\right) \tag{3.24}$$

The first part of the solution, $w^1(x)$, satisfies the particular solution of Eq. (3.6) when it is assumed that $\frac{\partial}{\partial y} = 0$. It represents the "deflection of a uniformly loaded strip parallel to the x-axis" [15] and satisfies the simply-supported boundary conditions at $x = \pm a/2$. The secondary part of the solution, $w^2(x,y)$, satisfies the simply-supported boundary conditions at $x = \pm a/2$, but it also con-

tains an unknown function $W_m(y)$ which must satisfy the homogeneous part of Eq. (3.6) as well as the boundary conditions at $y = \pm b/2$. One such function is

$$W_m(y) = \frac{q_o a^4}{D}\left[A_m \cosh\left(\frac{m\pi y}{a}\right) + B_m \frac{m\pi y}{a}\sinh\left(\frac{m\pi y}{a}\right)\right] \tag{3.25}$$

where A_m and B_m are constants used to satisfy the boundary conditions at $y = \pm b/2$.

As an application of this solution technique, consider such a square plate ($a = b$) free along the edges $y = \pm a/2$. The boundary conditions at the free edges are

$$\begin{aligned} Q_y^{eff}(x, \pm a/2) &= 0 \\ M_y(x, \pm a/2) &= 0 \end{aligned} \tag{3.26}$$

To satisfy these boundary conditions exactly, it is necessary to approximate the strip solution given in Eq. (3.23) with an infinite series as

$$w^1(x) = \frac{4q_o a^4}{\pi^5 D}\sum_{m=1,3,5\ldots}^{\infty}\frac{1}{m^5}\sin\left(\frac{m\pi}{2}\right)\cos\left(\frac{m\pi x}{a}\right) \tag{3.27}$$

Application of the boundary conditions, gives the unknown constants in the secondary part of the solution for any term m in the series as

$$\begin{aligned} A_m &= \frac{4\nu\left[2(1+\nu)\sinh\left(\frac{m\pi}{2}\right) - m\pi(1-\nu)\cosh\left(\frac{m\pi}{2}\right)\right]}{m^5\pi^5(1-\nu)\left[(3+\nu)\sinh(m\pi) - m\pi(1-\nu)\right]}\sin\left(\frac{m\pi}{2}\right) \\ B_m &= \frac{8\nu\sinh\left(\frac{m\pi}{2}\right)}{m^5\pi^5\left[(3+\nu)\sinh(m\pi) - m\pi(1-\nu)\right]}\sin\left(\frac{m\pi}{2}\right) \end{aligned} \tag{3.28}$$

The series converges very rapidly and two terms in the series are found to give sufficient accuracy to three significant figures. The nondimensional displacement, using Eq. (3.21), is illustrated in Figure 3.5 for $\nu = 0.3$. Notice the anticlastic curvature the develops because of the Poisson effect. The maximum normalized displacement of 0.01501 occurs at the free edges of the plate where $x = 0$ and $y = \pm a/2$. The normalized displacement in the center of the plate is 0.01309.

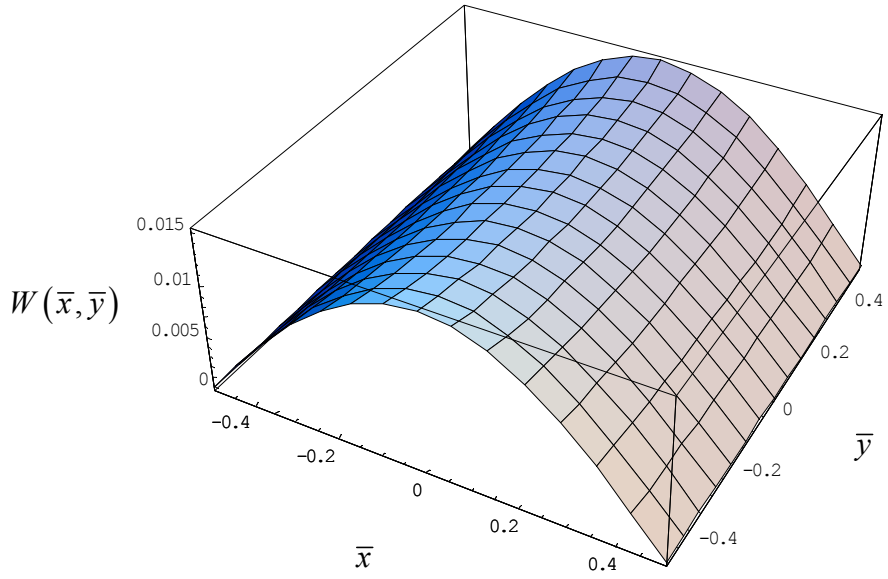

Figure 3.5: Displacement of uniformly-loaded isotropic plate simply supported along two opposite edges

Rayleigh-Ritz Solution

Another method to determine the unknown constants in Eq. (3.25) is to minimize the total potential energy with respect to each unknown. In calculating the total potential energy, the exact strip solution of Eq. (3.23) can be used. The strain energy of a square plate assumed to satisfy the assumption of Kirchhoff plate theory is given by

$$U = \frac{D}{2}\int_{-\frac{a}{2}}^{\frac{a}{2}}\int_{-\frac{a}{2}}^{\frac{a}{2}}\left\{\left(\frac{\partial^2 w}{\partial x^2}+\frac{\partial^2 w}{\partial y^2}\right)^2 - 2(1-\nu)\left[\frac{\partial^2 w}{\partial x^2}\frac{\partial^2 w}{\partial y^2}-\left(\frac{\partial^2 w}{\partial x \partial y}\right)^2\right]\right\}dxdy \tag{3.29}$$

The work done by the uniform external load is

$$W = q_o\int_{-\frac{a}{2}}^{\frac{a}{2}}\int_{-\frac{a}{2}}^{\frac{a}{2}}\left[w(x,y)\right]dxdy \tag{3.30}$$

The total potential energy is

$$\Pi = U - W \tag{3.31}$$

For static equilibrium, using the solution assumed by Eqs. (3.22) through (3.25), it is necessary that

$$\frac{\partial \Pi}{\partial A_m} = 0 \text{ and } \frac{\partial \Pi}{\partial B_m} = 0 \qquad m = 1, 3, 5\ldots \tag{3.32}$$

This method gives a normalized displacement of 0.01309 in the center of plate with only two terms in the series of Eq. (3.24). An energy approach will be used for sandwich plates with similar boundary conditions.

3.5 Sandwich Plate Equations and Boundary Conditions

As mentioned earlier, the sandwich plate model developed here is an extension of the sandwich beam theory presented in Chapter 2. The composite facesheets in the sandwich plate are assumed to behave as isotropic plates which satisfy the Kirchhoff hypothesis. The in-plane extensional moduli of the sandwich core are assumed to be negligible in both directions. The out-of-plane extensional modulus is considered infinite, so there is no out-of-plane strain. Thus, the core undergoes only transverse shear deformations. Because of the manner by which honeycomb core is often constructed, the shear modulus in the y-z plane can be different than the shear modulus in the x-z plane. As stated in Chapter 1, this is the case for the honeycomb considered here. Specifically, the core will be assumed to behave in an orthotropic manner. The governing equations and boundary conditions will be derived using energy and variational methods. Several example problems will be solved, including one with loading and boundary conditions which represent those used to test sandwich plates. The testing will be discussed in a later chapter.

Kinematics

It is assumed that the displacement of any point in the sandwich plate is dependent upon the midsurface deflection $w(x,y)$, and two rotations: $\alpha_x(x,y)$ and $\alpha_y(x,y)$. Figure 3.6 shows a cross-section of the plate with the y-axis coming out of the page. Initially, the lines A-B and B-C are both straight and normal to the geometric midsurface of the plate. After deformation, line A-B in the core has a rotation angle α_x as shown. Because the facesheets behave as plates, line B-C in the bottom facesheet undergoes a rotation $\partial w/\partial x$ and remains normal to the midsurface. In-plane displacements of the midsurface are not considered because the sandwich plate is assumed to be

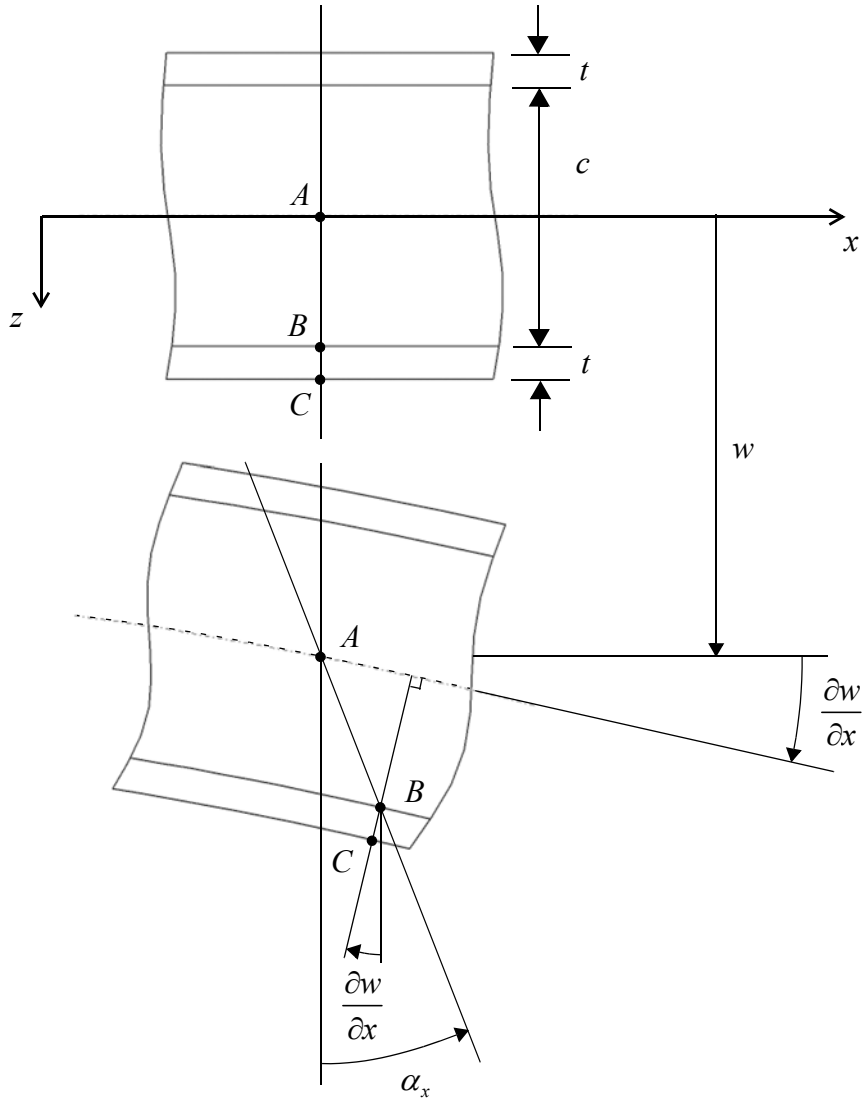

Figure 3.6: Sandwich plate deformations as viewed in the *x*-*z* plane

of symmetric construction. That is, the facesheets are identical in thickness and material properties and are located a distance $c/2$ on opposite sides of the midsurface. In composite literature, this is equivalent to saying that the **B** matrix is zero.

Because of the assumed kinematics of the cross-section, the displacements in the x-direction for the top facesheet (u_T), core (u_C), and bottom facesheet (u_B) consistent with Figure 3.6 are

$$u_T(x,y,z) = -\left(\frac{c}{2}\right)\alpha_x - \left(z+\frac{c}{2}\right)\frac{\partial w}{\partial x} \tag{3.33}$$

$$u_C(x,y,z) = z\alpha_x \tag{3.34}$$

$$u_B(x,y,z) = \left(\frac{c}{2}\right)\alpha_x - \left(z - \frac{c}{2}\right)\frac{\partial w}{\partial x} \tag{3.35}$$

Note that because the z-axis is directed downward, the displacements for the top and bottom facesheets are reversed from those of the sandwich beam in Chapter 2. In a similar manner, the displacements in the y-direction for the top facesheet (v_T), core (v_C), and bottom facesheet (v_B) are

$$v_T(x,y,z) = -\left(\frac{c}{2}\right)\alpha_y - \left(z + \frac{c}{2}\right)\frac{\partial w}{\partial y} \tag{3.36}$$

$$v_C(x,y,z) = z\alpha_y \tag{3.37}$$

$$v_B(x,y,z) = \left(\frac{c}{2}\right)\alpha_y - \left(z - \frac{c}{2}\right)\frac{\partial w}{\partial y} \tag{3.38}$$

The nine relevant strain components are found to be

$$(\varepsilon_x)_T = \frac{\partial u_T}{\partial x} = -\left(\frac{c}{2}\right)\frac{\partial \alpha_x}{\partial x} - \left(z + \frac{c}{2}\right)\frac{\partial^2 w}{\partial x^2} \tag{3.39}$$

$$(\varepsilon_y)_T = \frac{\partial v_T}{\partial y} = -\left(\frac{c}{2}\right)\frac{\partial \alpha_y}{\partial y} - \left(z + \frac{c}{2}\right)\frac{\partial^2 w}{\partial y^2} \tag{3.40}$$

$$(\gamma_{xy})_T = \frac{\partial u_T}{\partial y} + \frac{\partial v_T}{\partial x} = -\frac{c}{2}\left(\frac{\partial \alpha_x}{\partial y} + \frac{\partial \alpha_y}{\partial x}\right) - 2\left(z + \frac{c}{2}\right)\frac{\partial^2 w}{\partial x \partial y} \tag{3.41}$$

$$(\gamma_{xz})_C = \frac{\partial u_C}{\partial z} + \frac{\partial w}{\partial x} = \alpha_x + \frac{\partial w}{\partial x} \tag{3.42}$$

$$(\gamma_{yz})_C = \frac{\partial v_C}{\partial z} + \frac{\partial w}{\partial y} = \alpha_y + \frac{\partial w}{\partial y} \tag{3.43}$$

$$(\gamma_{xy})_C = \frac{\partial u_C}{\partial y} + \frac{\partial v_C}{\partial x} = z\left(\frac{\partial \alpha_x}{\partial y} + \frac{\partial \alpha_y}{\partial x}\right) \tag{3.44}$$

$$(\varepsilon_x)_B = \frac{\partial u_B}{\partial x} = \left(\frac{c}{2}\right)\frac{\partial \alpha_x}{\partial x} - \left(z - \frac{c}{2}\right)\frac{\partial^2 w}{\partial x^2} \tag{3.45}$$

$$(\varepsilon_y)_B = \frac{\partial v_B}{\partial y} = \left(\frac{c}{2}\right)\frac{\partial \alpha_y}{\partial y} - \left(z - \frac{c}{2}\right)\frac{\partial^2 w}{\partial y^2} \tag{3.46}$$

$$(\gamma_{xy})_B = \frac{\partial u_B}{\partial y} + \frac{\partial v_B}{\partial x} = \frac{c}{2}\left(\frac{\partial \alpha_x}{\partial y} + \frac{\partial \alpha_y}{\partial x}\right) - 2\left(z - \frac{c}{2}\right)\frac{\partial^2 w}{\partial x \partial y} \tag{3.47}$$

Stresses

The facesheets are assumed to behave as isotropic plates, but for convenience the stresses are expressed with the notation of computing the stresses in a composite laminate using classical lamination theory, as given by Hyer [17]. The stress-strain relationship for an isotropic material in a state of plane-stress is

$$\begin{Bmatrix} \sigma_x \\ \sigma_y \\ \tau_{xy} \end{Bmatrix} = \begin{bmatrix} Q_{11} & Q_{12} & 0 \\ Q_{12} & Q_{22} & 0 \\ 0 & 0 & Q_{66} \end{bmatrix} \begin{Bmatrix} \varepsilon_x \\ \varepsilon_y \\ \gamma_{xy} \end{Bmatrix} \tag{3.48}$$

where

$$Q_{11} = Q_{22} = \frac{E}{1-\nu^2} \tag{3.49}$$

$$Q_{12} = \frac{E\nu}{1-\nu^2} \tag{3.50}$$

$$Q_{66} = G_{xy}^F = \frac{E}{2(1+\nu)} \tag{3.51}$$

As the core is assumed to be orthotropic, there is no coupling of shear stresses. Thus, the three shear stresses are easily expressed by

$$(\tau_{yz})_C = G_{yz}(\gamma_{yz})_C \tag{3.52}$$

$$(\tau_{xz})_C = G_{xz}(\gamma_{xz})_C \tag{3.53}$$

$$(\tau_{xy})_C = G_{xy}(\gamma_{xy})_C \tag{3.54}$$

Note the use of the superscript F in Eq. (3.51) to indicate the in-plane facesheet shear modulus. The symbols Q_{11}, Q_{12}, and Q_{66} will be used throughout the rest of the text to distinguish the facesheet properties from the core shear properties. A soft core is one in which the in-plane shear modulus of the core, G_{xy}, is negligible compared to the transverse shear moduli and the extensional modulus of the facesheets. A soft core is capable of carrying only transverse shear stresses. A stiff core is capable of carrying both in-plane and transverse shear stresses [9]. For completeness, both soft and stiff cores will be considered in this analysis.

Total Potential Energy

To develop the total potential energy for use in the variational process, consider a rectangular sandwich plate with length a and width b like that of Figure 3.1. The strain energy given by Eq. (2.10) must be calculated separately for the top facesheet, bottom facesheet, and core. For the facesheets, the out-of-plane strains, γ_{yz} and γ_{xz}, are both zero because of the Kirchhoff hypothesis, and the out-of-plane stress, σ_z, is zero due to the plane-stress assumption. Therefore, the strain energy of the top facesheet reduces to

$$U_T = \frac{1}{2}\int_V (\sigma_x \varepsilon_x + \sigma_y \varepsilon_y + \tau_{xy}\gamma_{xy})_T \, dV \tag{3.55}$$

Substitution of the stresses and strains found previously, and integration through the thickness from $z = -(c/2 + t)$ to $z = -c/2$, gives the strain energy of the top facesheet to be

$$
\begin{aligned}
U_T = \frac{1}{2}\int_{-\frac{a}{2}}^{\frac{a}{2}}\int_{-\frac{b}{2}}^{\frac{b}{2}}\Bigg\{ & \frac{1}{3}t^3 Q_{11}\left[\left(\frac{\partial^2 w}{\partial x^2}\right)^2+\left(\frac{\partial^2 w}{\partial y^2}\right)^2\right]+\frac{1}{4}tc^2 Q_{11}\left[\left(\frac{\partial \alpha_x}{\partial x}\right)^2+\left(\frac{\partial \alpha_y}{\partial y}\right)^2\right] \\
& -\frac{1}{2}t^2 cQ_{11}\left(\frac{\partial \alpha_x}{\partial x}\frac{\partial^2 w}{\partial x^2}+\frac{\partial \alpha_y}{\partial y}\frac{\partial^2 w}{\partial y^2}\right)+\frac{2}{3}t^3 Q_{12}\frac{\partial^2 w}{\partial x^2}\frac{\partial^2 w}{\partial y^2}+\frac{1}{2}tc^2 Q_{12}\frac{\partial \alpha_x}{\partial x}\frac{\partial \alpha_y}{\partial y} \\
& -\frac{1}{2}t^2 cQ_{12}\left(\frac{\partial^2 w}{\partial x^2}\frac{\partial \alpha_y}{\partial y}+\frac{\partial^2 w}{\partial y^2}\frac{\partial \alpha_x}{\partial x}\right)+\frac{4}{3}t^3 Q_{66}\left(\frac{\partial^2 w}{\partial x \partial y}\right)^2+\frac{1}{2}tc^2 Q_{66}\frac{\partial \alpha_x}{\partial y}\frac{\partial \alpha_y}{\partial x} \\
& +\frac{1}{4}tc^2 Q_{66}\left[\left(\frac{\partial \alpha_x}{\partial y}\right)^2+\left(\frac{\partial \alpha_y}{\partial x}\right)^2\right]-t^2 cQ_{66}\frac{\partial^2 w}{\partial x \partial y}\left(\frac{\partial \alpha_x}{\partial y}+\frac{\partial \alpha_y}{\partial x}\right)\Bigg\}dxdy
\end{aligned}
\tag{3.56}
$$

A similar procedure for the bottom facesheet with different limits of integration in the z-direction reveals that the strain energy of both facesheets are identical. Thus,

$$U_B = U_T \tag{3.57}$$

The strain energy of the core contains only the three shear strains, so Eq. (2.10) reduces to

$$U_C = \frac{1}{2}\int_V (\tau_{xy}\gamma_{xy}+\tau_{xz}\gamma_{xz}+\tau_{yz}\gamma_{yz})_C\, dV \tag{3.58}$$

Integration of this equation through the thickness from $z = -c/2$ to $z = c/2$ gives the strain energy of the core as

$$U_C = \frac{1}{2}\int_{-\frac{a}{2}}^{\frac{a}{2}}\int_{-\frac{b}{2}}^{\frac{b}{2}}\left[cG_{xz}\left(\alpha_x+\frac{\partial w}{\partial x}\right)^2+cG_{yz}\left(\alpha_y+\frac{\partial w}{\partial y}\right)^2+\frac{1}{12}c^3 G_{xy}\left(\frac{\partial \alpha_x}{\partial y}+\frac{\partial \alpha_y}{\partial x}\right)^2\right]dxdy \tag{3.59}$$

If the rectangular plate is subjected to a transverse distributed load $q(x,y)$ in the positive z-direction, the work done by the external load is

$$W = \int_{-\frac{a}{2}}^{\frac{a}{2}}\int_{-\frac{b}{2}}^{\frac{b}{2}}\left[w(x,y)\; q(x,y)\right]dxdy \tag{3.60}$$

The total potential energy of the system, Π, is the sum of the strain energies minus the work done by the external load:

$$\Pi = U_T + U_B + U_C - W \tag{3.61}$$

For equilibrium, the first variation of the total potential energy must equal zero. To find the equilibrium equations and boundary conditions, thirty-three separate terms must be integrated by parts. In addition, three of these terms must integrated by parts a second time to reveal corner conditions similar to those found in an isotropic plate. The first variation is much too lengthy to be written here, but one advantage of using the variational approach is that it automatically provides the groupings for the governing differential equations, boundary conditions, and corner conditions.

Governing Equations

The presence of three independent variables $w(x,y)$, $\alpha_x(x,y)$, and $\alpha_y(x,y)$ indicates that there should be three governing differential equations, or three Euler-Lagrange equations. As expected, these three equations are revealed when the first variation of the total potential energy is set to zero. The first equilibrium equation is equivalent to summing forces in the transverse z-direction. It is the only non-homogeneous equation and is given by:

$$\begin{aligned}&\frac{2}{3}t^3Q_{11}\left(\frac{\partial^4 w}{\partial x^4}+\frac{\partial^4 w}{\partial y^4}\right)-\frac{1}{2}t^2cQ_{11}\left(\frac{\partial^3 \alpha_x}{\partial x^3}+\frac{\partial^3 \alpha_y}{\partial y^3}\right)+\frac{4}{3}t^3Q_{12}\frac{\partial^4 w}{\partial x^2\partial y^2}\\&-\frac{1}{2}t^2cQ_{12}\left(\frac{\partial^3 \alpha_x}{\partial x\partial y^2}+\frac{\partial^3 \alpha_y}{\partial x^2\partial y}\right)-cG_{xz}\left(\frac{\partial \alpha_x}{\partial x}+\frac{\partial^2 w}{\partial x^2}\right)-cG_{yz}\left(\frac{\partial \alpha_y}{\partial y}+\frac{\partial^2 w}{\partial y^2}\right)\\&+\frac{8}{3}t^3Q_{66}\frac{\partial^4 w}{\partial x^2\partial y^2}-t^2cQ_{66}\left(\frac{\partial^3 \alpha_x}{\partial x\partial y^2}+\frac{\partial^3 \alpha_y}{\partial x^2\partial y}\right)=q(x,y)\end{aligned} \tag{3.62}$$

The second and third equations are equivalent to summing the moments about the x- and y-axes:

$$\begin{aligned}&\frac{1}{2}t^2cQ_{11}\frac{\partial^3 w}{\partial x^3}-\frac{1}{2}tc^2Q_{11}\frac{\partial^2 \alpha_x}{\partial x^2}+\frac{1}{2}t^2cQ_{12}\frac{\partial^3 w}{\partial x\partial y^2}-\frac{1}{2}tc^2Q_{12}\frac{\partial^2 \alpha_y}{\partial x\partial y}+cG_{xz}\left(\alpha_x+\frac{\partial w}{\partial x}\right)\\&-\frac{1}{2}tc^2Q_{66}\left(\frac{\partial^2 \alpha_x}{\partial y^2}+\frac{\partial^2 \alpha_y}{\partial x\partial y}\right)+t^2cQ_{66}\frac{\partial^3 w}{\partial x\partial y^2}-\frac{1}{12}c^3G_{xy}\left(\frac{\partial^2 \alpha_x}{\partial y^2}+\frac{\partial^2 \alpha_y}{\partial x\partial y}\right)=0\end{aligned} \tag{3.63}$$

$$\begin{aligned}&\frac{1}{2}t^2cQ_{11}\frac{\partial^3 w}{\partial y^3}-\frac{1}{2}tc^2Q_{11}\frac{\partial^2 \alpha_y}{\partial y^2}+\frac{1}{2}t^2cQ_{12}\frac{\partial^3 w}{\partial x^2\partial y}-\frac{1}{2}tc^2Q_{12}\frac{\partial^2 \alpha_x}{\partial x\partial y}+cG_{yz}\left(\alpha_y+\frac{\partial w}{\partial y}\right)\\&-\frac{1}{2}tc^2Q_{66}\left(\frac{\partial^2 \alpha_y}{\partial x^2}+\frac{\partial^2 \alpha_x}{\partial x\partial y}\right)+t^2cQ_{66}\frac{\partial^3 w}{\partial x^2\partial y}-\frac{1}{12}c^3G_{xy}\left(\frac{\partial^2 \alpha_y}{\partial x^2}+\frac{\partial^2 \alpha_x}{\partial x\partial y}\right)=0\end{aligned} \tag{3.64}$$

The last two equations have a similar form to one another, the only difference being that the *x*- and *y*-coordinates are reversed.

The first variation of the total potential energy reveals boundary conditions and corner conditions for the sandwich plate which are not obvious through an equilibrium approach. These boundary conditions are expressed in terms of force and moment resultants that are defined as a result of the variational process. Effective transverse shear force resultants are given by

$$\begin{aligned} Q_x^{eff} &= cG_{xz}\left(\alpha_x + \frac{\partial w}{\partial x}\right) - \frac{2}{3}t^3 Q_{11}\frac{\partial^3 w}{\partial x^3} + \frac{1}{2}t^2 cQ_{11}\frac{\partial^2 \alpha_x}{\partial x^2} - \frac{2}{3}t^3 Q_{12}\frac{\partial^3 w}{\partial x \partial y^2} \\ &+ \frac{1}{2}t^2 cQ_{12}\frac{\partial^2 \alpha_y}{\partial x \partial y} - \frac{8}{3}t^3 Q_{66}\frac{\partial^3 w}{\partial x \partial y^2} + t^2 cQ_{66}\left(\frac{\partial^2 \alpha_x}{\partial y^2} + \frac{\partial^2 \alpha_y}{\partial x \partial y}\right) \end{aligned} \tag{3.65}$$

$$\begin{aligned} Q_y^{eff} &= cG_{yz}\left(\alpha_y + \frac{\partial w}{\partial y}\right) - \frac{2}{3}t^3 Q_{11}\frac{\partial^3 w}{\partial y^3} + \frac{1}{2}t^2 cQ_{11}\frac{\partial^2 \alpha_y}{\partial y^2} - \frac{2}{3}t^3 Q_{12}\frac{\partial^3 w}{\partial x^2 \partial y} \\ &+ \frac{1}{2}t^2 cQ_{12}\frac{\partial^2 \alpha_x}{\partial x \partial y} - \frac{8}{3}t^3 Q_{66}\frac{\partial^3 w}{\partial x^2 \partial y} + t^2 cQ_{66}\left(\frac{\partial^2 \alpha_y}{\partial x^2} + \frac{\partial^2 \alpha_x}{\partial x \partial y}\right) \end{aligned} \tag{3.66}$$

The sandwich plate is more complicated than an isotropic plate because there are four bending moment resultants and two twisting moment resultants. The four bending moment resultants are

$$M_x = -\frac{2}{3}t^3 Q_{11}\frac{\partial^2 w}{\partial x^2} + \frac{1}{2}t^2 cQ_{11}\frac{\partial \alpha_x}{\partial x} - \frac{2}{3}t^3 Q_{12}\frac{\partial^2 w}{\partial y^2} + \frac{1}{2}t^2 cQ_{12}\frac{\partial \alpha_y}{\partial y} \tag{3.67}$$

$$M_x^C = -\frac{1}{2}t^2 cQ_{11}\frac{\partial^2 w}{\partial x^2} + \frac{1}{2}tc^2 Q_{11}\frac{\partial \alpha_x}{\partial x} - \frac{1}{2}t^2 cQ_{12}\frac{\partial^2 w}{\partial y^2} + \frac{1}{2}tc^2 Q_{12}\frac{\partial \alpha_y}{\partial y} \tag{3.68}$$

$$M_y = -\frac{2}{3}t^3 Q_{11}\frac{\partial^2 w}{\partial y^2} + \frac{1}{2}t^2 cQ_{11}\frac{\partial \alpha_y}{\partial y} - \frac{2}{3}t^3 Q_{12}\frac{\partial^2 w}{\partial x^2} + \frac{1}{2}t^2 cQ_{12}\frac{\partial \alpha_x}{\partial x} \tag{3.69}$$

$$M_y^C = -\frac{1}{2}t^2 cQ_{11}\frac{\partial^2 w}{\partial y^2} + \frac{1}{2}tc^2 Q_{11}\frac{\partial \alpha_y}{\partial y} - \frac{1}{2}t^2 cQ_{12}\frac{\partial^2 w}{\partial x^2} + \frac{1}{2}tc^2 Q_{12}\frac{\partial \alpha_x}{\partial x} \tag{3.70}$$

The two twisting moment resultants are

$$M_{xy} = -\frac{4}{3}t^3 Q_{66}\frac{\partial^2 w}{\partial x \partial y} + \frac{1}{2}t^2 c Q_{66}\left(\frac{\partial \alpha_x}{\partial y} + \frac{\partial \alpha_y}{\partial x}\right) \tag{3.71}$$

$$M_{xy}^C = \frac{1}{2}tc^2 Q_{66}\left(\frac{\partial \alpha_x}{\partial y} + \frac{\partial \alpha_y}{\partial x}\right) - t^2 c Q_{66}\frac{\partial^2 w}{\partial x \partial y} + \frac{1}{12}c^3 G_{xy}\left(\frac{\partial \alpha_x}{\partial y} + \frac{\partial \alpha_y}{\partial x}\right) \tag{3.72}$$

The superscript C is used to indicate a moment resultant that is due only to the presence of the core. It is interesting to compare the complexity of Eqs. (3.67) through (3.72) with the simplicity of the equivalent equations for an isotropic plate given by Eqs. (3.2) through (3.4).

In the standard literature dealing with the mechanics of composite materials [17], the total bending moment resultant, M_x^T, in a composite laminate due to a stress σ_x is defined to be

$$M_x^T \equiv \int_{-H/2}^{H/2} \sigma_x z dz \tag{3.73}$$

where H is the total thickness of the laminate. When applying this definition to a sandwich plate, it is only necessary to integrate through the thickness of the top and bottom facesheets because the extensional modulus of the core, and thus the stress σ_x, is considered negligible. After much algebra, it is found that applying Eq. (3.73) to the problem here results in

$$M_x^T = M_x + M_x^C \tag{3.74}$$

Thus, the total bending moment resultant in a sandwich plate is the algebraic sum of the bending moment resultants defined by Eqs. (3.67) and (3.68). Similar results are obtained for the additional total bending moment resultant, M_y^T, and the total twisting moment resultant, M_{xy}^T, defined by

$$M_y^T \equiv \int_{-H/2}^{H/2} \sigma_y z dz \tag{3.75}$$

$$M_{xy}^T \equiv \int_{-H/2}^{H/2} \tau_{xy} z dz \tag{3.76}$$

It is necessary to integrate through the thickness of the entire sandwich panel for the total twisting moment resultant, M_{xy}^T, because the shear stress τ_{xy} is not considered to be negligible in the core.

The governing differential equations can written in a much more compact form using the force and moment resultants. The transverse shear force resultants in the facesheets, Q_x and Q_y, are defined to be the same as those of an isotropic plate given by the first equality of Eqs. (3.7) and (3.8). It is also necessary to define the transverse shear force resultants in the core as

$$Q_x^C = \int_{-\frac{c}{2}}^{\frac{c}{2}} \tau_{xz} dz = cG_{xz}\left(\alpha_x + \frac{\partial w}{\partial x}\right) \tag{3.77}$$

$$Q_y^C = \int_{-\frac{c}{2}}^{\frac{c}{2}} \tau_{yz} dz = cG_{yz}\left(\alpha_y + \frac{\partial w}{\partial y}\right) \tag{3.78}$$

Use of the moment resultants defined previously for a sandwich plate reveals that the effective transverse shear force resultants for the sandwich plate, Q_x^{eff} and Q_y^{eff}, can be written in terms of the shear force and moment resultants as

$$Q_x^{eff} = Q_x^C + Q_x + \frac{\partial M_{xy}}{\partial y} \tag{3.79}$$

$$Q_y^{eff} = Q_y^C + Q_y + \frac{\partial M_{xy}}{\partial x} \tag{3.80}$$

After careful algebraic manipulation, the first governing differential equation can be written strictly in terms of the transverse shear force resultants and the applied load. The first differential equation, Eq. (3.62), becomes

$$\frac{\partial}{\partial x}\left(Q_x + Q_x^C\right) + \frac{\partial}{\partial y}\left(Q_y + Q_y^C\right) + q = 0 \tag{3.81}$$

The second and third differential equations, Eqs. (3.63) and (3.64), can also be simplified to the following forms:

$$Q_x^C - \frac{\partial M_x^C}{\partial x} - \frac{\partial M_{xy}^C}{\partial y} = 0 \tag{3.82}$$

$$Q_y^C - \frac{\partial M_y^C}{\partial y} - \frac{\partial M_{xy}^C}{\partial x} = 0 \tag{3.83}$$

These three simplified equations closely resemble those of a first-order shear deformation composite plate theory given by Reddy [18]. If the core thickness is zero, all force and moment resultants reduce to those of an isotropic plate of thickness $2t$. The first differential equation is then equivalent to that of an isotropic plate given in Eq. (3.1), and the second and third differential equations are identically satisfied.

Boundary Conditions

Four separate boundary conditions are found on each of the four edges of the plate. The first boundary condition along the edges $x = \pm a/2$ states that the effective shear force resultant, Q_x^{eff}, at any point along the edge must be zero, or the midsurface vertical displacement at that point must be specified. Symbolically this boundary condition is written as

$$Q_x^{eff}\left(\pm a/2, y\right) = 0 \quad \text{OR} \quad w\left(\pm a/2, y\right) \text{ must be specified} \tag{3.84}$$

The second and third boundary conditions along the edges $x = \pm a/2$ state that the bending moment resultants M_x and M_x^C must be zero, or the corresponding slope $\partial w/\partial x$ and rotation α_x must be specified, respectively. These conditions are given by

$$M_x\left(\pm a/2, y\right) = 0 \quad \text{OR} \quad \frac{\partial w}{\partial x}\left(\pm a/2, y\right) \text{ must be specified} \tag{3.85}$$

AND

$$M_x^C\left(\pm a/2, y\right) = 0 \quad \text{OR} \quad \alpha_x\left(\pm a/2, y\right) \text{ must be specified} \tag{3.86}$$

The fourth and final boundary condition along the edges $x = \pm a/2$ states that the twisting moment resultant M_{xy}^C is zero, or the rotation α_y must be specified. Thus,

$$M_{xy}^C\left(\pm a/2, y\right) = 0 \quad \text{OR} \quad \alpha_y\left(\pm a/2, y\right) \text{ must be specified} \tag{3.87}$$

A similar set of four boundary conditions are obtained for the edges of the plate corresponding to $y = \pm b/2$. They are given by:

$$Q_y^{eff}\left(x, \pm b/2\right) = 0 \quad \text{OR} \quad w\left(x, \pm b/2\right) \text{ must be specified} \tag{3.88}$$

AND

$$M_y\left(x,\pm b/2\right)=0 \quad \text{OR} \quad \frac{\partial w}{\partial y}\left(x,\pm b/2\right) \text{ must be specified} \tag{3.89}$$

AND

$$M_y^C\left(x,\pm b/2\right)=0 \quad \text{OR} \quad \alpha_{\text{y}}\left(x,\pm b/2\right) \text{ must be specified} \tag{3.90}$$

AND

$$M_{xy}^C\left(x,\pm b/2\right)=0 \quad \text{OR} \quad \alpha_{\text{x}}\left(x,\pm b/2\right) \text{ must be specified} \tag{3.91}$$

Because the facesheets are considered to be isotropic plates satisfying the Kirchhoff hypothesis, the sandwich plate also has corner conditions. These corner conditions come directly from the first variation of the total potential energy. At each corner, the following condition must apply:

$$-2M_{xy}\left(\pm a/2,\pm b/2\right)=0 \quad \text{OR} \quad w\left(\pm a/2,\pm b/2\right) \text{ must be specified} \tag{3.92}$$

Like the isotropic plate, if the vertical displacement is specified to be zero at a corner, the reaction force R necessary to keep the corner of the plate from moving is $-2M_{xy}$.

3.6 Uniformly-Loaded Sandwich Plate Simply Supported Along Four Edges

As with an isotropic plate, one of the simplest types of boundary conditions to analyze for a sandwich plate is that of a simply-supported edge. As an example, consider a square sandwich plate ($a = b$) that is simply supported on all four edges and subjected to a uniform distributed load q_{o}. The boundary conditions along the edges $x = \pm a/2$ must be those given by Eqs. (3.84) through (3.87). The displacement is specified to be zero, so the first boundary condition is satisfied. For a simply-supported boundary condition, nothing is said about the slope $\partial w/\partial x$ or the rotation α_x, so therefore the bending moment resultants M_x and M_x^C must be zero. Here, the rotation α_y is specified to be zero for ease of computation. Mathematically, the simply-supported boundary conditions considered here are:

$$\begin{aligned} w(\pm a/2, y) &= 0 \\ M_x(\pm a/2, y) &= 0 \\ M_x^C(\pm a/2, y) &= 0 \\ \alpha_y(\pm a/2, y) &= 0 \end{aligned} \tag{3.93}$$

Similarly, boundary conditions along the edges $y = \pm a/2$ are:

$$\begin{aligned} w(x, \pm a/2) &= 0 \\ M_y(x, \pm a/2) &= 0 \\ M_y^C(x, \pm a/2) &= 0 \\ \alpha_x(x, \pm a/2) &= 0 \end{aligned} \tag{3.94}$$

One method of finding the displacement and rotations for a uniformly loaded sandwich plate is to approximate the load with an double-infinite trigonometric series, and then assume a similar form for the displacement and rotations. This type of solution was shown previously for an isotropic plate. As in Eq. (3.19), the uniform distributed load can be approximated by

$$q(x,y) = \sum_{m=1,3,5\ldots}^{\infty} \sum_{n=1,3,5\ldots}^{\infty} \frac{16 q_o}{\pi^2 mn} \sin\left(\frac{m\pi}{2}\right) \sin\left(\frac{n\pi}{2}\right) \cos\left(\frac{m\pi x}{a}\right) \cos\left(\frac{n\pi y}{a}\right) \tag{3.95}$$

The displacement and rotations are then assumed to have the following forms:

$$w(x,y) = \sum_{m=1,3,5\ldots}^{\infty} \sum_{n=1,3,5\ldots}^{\infty} W_{mn} \cos\left(\frac{m\pi x}{a}\right) \cos\left(\frac{n\pi y}{a}\right) \tag{3.96}$$

$$\alpha_x(x,y) = \sum_{m=1,3,5\ldots}^{\infty} \sum_{n=1,3,5\ldots}^{\infty} A_{mn} \sin\left(\frac{m\pi x}{a}\right) \cos\left(\frac{n\pi y}{a}\right) \tag{3.97}$$

$$\alpha_y(x,y) = \sum_{m=1,3,5\ldots}^{\infty} \sum_{n=1,3,5\ldots}^{\infty} B_{mn} \cos\left(\frac{m\pi x}{a}\right) \sin\left(\frac{n\pi y}{a}\right) \tag{3.98}$$

where W_{mn}, A_{mn}, and B_{mn} are unknown constants. These solutions satisfy all of boundary conditions given in Eqs. (3.93) and (3.94).

To find the unknown constants, one must consider only a finite number of terms in each series. It has been found that three terms in each series (m = 1, 3, 5 and n = 1, 3, 5) gives solutions that are within 0.5% of the converged series results. Thus, there are 9 unknown W_{mn}, A_{mn}, and B_{mn} for a total of 27 constants. The series are substituted into the governing differential equations given by Eqs. (3.62) through (3.64). Every term in the first differential equation contains the terms from the trigonometric series $\cos\left(\frac{m\pi x}{a}\right)\cos\left(\frac{n\pi y}{a}\right)$. The entire equation must hold true for all x and y, so the coefficients of each term in the trigonometric series must equal zero. Similarly, the second equation contains $\sin\left(\frac{m\pi x}{a}\right)\cos\left(\frac{n\pi y}{a}\right)$ and the third equation contains $\cos\left(\frac{m\pi x}{a}\right)\sin\left(\frac{n\pi y}{a}\right)$. This results in a set of 27 linear equations to solve for the unknown constants. A closed-form solution for the constants is not presented here because it far too lengthy.

As with the isotropic plate, to visualize the shape of the displacement, it is convenient to nondimensionalize the displacement and rotations by

$$W\left(x,y\right)=\frac{w\left(x,y\right)}{\left(q_o a^4/D\right)} \tag{3.99}$$

$$\bar{\alpha}_x\left(x,y\right)=\frac{\alpha_x\left(x,y\right)}{\left(q_o a^3/D\right)} \tag{3.100}$$

$$\bar{\alpha}_y\left(x,y\right)=\frac{\alpha_y\left(x,y\right)}{\left(q_o a^3/D\right)} \tag{3.101}$$

where

$$D=Q_{11}\left(\frac{1}{2}c^2t+ct^2+\frac{2}{3}t^3\right) \tag{3.102}$$

is the flexural rigidity for a sandwich plate. The flexural rigidity is an extension of the flexural rigidity of a sandwich beam given by Eq. (2.17), where the factor Eb has been replaced with Q_{11}. This extension is analogous to the relationship between the flexural rigidity of an Euler beam and an isotropic plate.

The nondimensional displacement is shown in Figure 3.7 using material properties and geometry that are representative of the plate to be tested. The coordinate axes have been nondimensionalized by the length of the side of the sandwich plate. The ribbon direction (L) of the core is the $\bar{y}$-coordinate. The in-plane shear modulus is assumed to be zero because the core is considered to be soft. The maximum normalized displacement in the center of the plate is 0.01059. The overall shape of the displacement is similar to that of the isotropic plate shown in Figure 3.4. However, because of the differences in the transverse shear moduli of the core, the variation of the displacement is not the same with the $\bar{x}$- and $\bar{y}$-coordinates, as in the case of the isotropic plate. Figure 3.8 gives a contour plot of the displacement to show that the shape is slightly elongated in the $\bar{x}$-direction due to the lower transverse shear modulus. This elongation would be much more exaggerated if the two transverse shear moduli were greatly different.

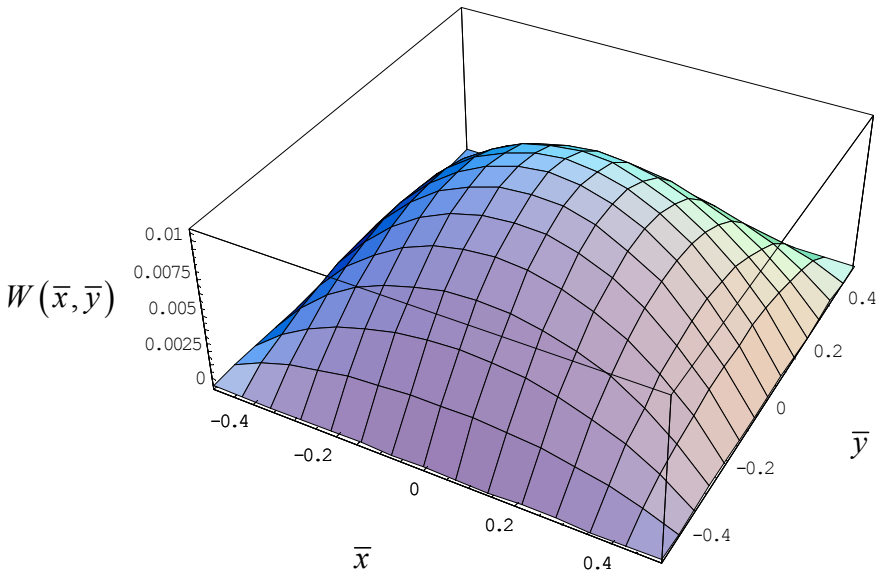

Figure 3.7: Displacement of uniformly-loaded sandwich plate simply supported along four edges

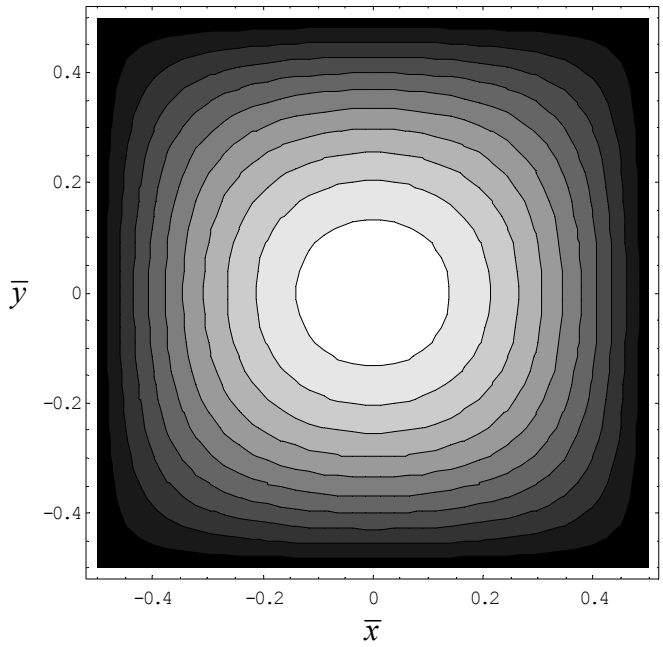

Figure 3.8: Displacement contours of uniformly-loaded sandwich plate simply supported along four edges

The difference in transverse shear moduli has a greater affect on the rotations $\bar{\alpha}_x$ and $\bar{\alpha}_y$, as shown in Figures 3.9 and 3.10. The rotation $\bar{\alpha}_x$ has a maximum value of 0.00842 and a minimum value of –0.00842 due to symmetry. It is zero along the boundaries $\bar{y} = \pm 0.5$, as specified by the boundary conditions given in Eq. (3.94). The rotation $\bar{\alpha}_y$ has a maximum value of 0.01553 and a minimum value of –0.01553. It is zero along the boundaries $\bar{x} = \pm 0.5$, as specified by the boundary conditions given in Eq. (3.93). The rotation $\bar{\alpha}_y$ is larger than the rotation $\bar{\alpha}_x$. One would expect larger shear strains in the *x*-*z* plane than in the *y*-*z* plane because the shear modulus G_{xz} is less than the shear modulus G_{yz}. This fact is found to be true using the definition of the shear strains $(\gamma_{xz})_C$ and $(\gamma_{yz})_C$ given in Eqs. (3.42) and (3.43) because the slopes and rotations are defined to be in opposite directions according to Figure 3.6.

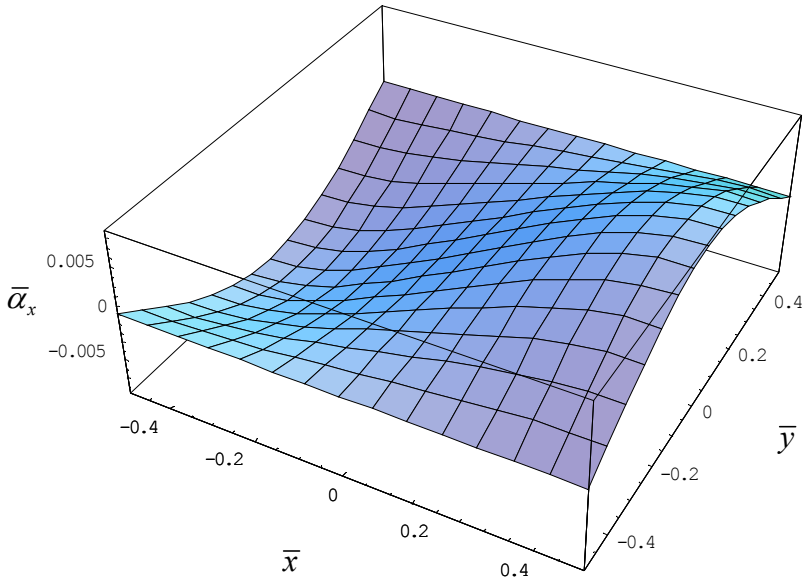

Figure 3.9: Rotation $\bar{\alpha}_x$ of uniformly-loaded sandwich plate simply supported along four edges

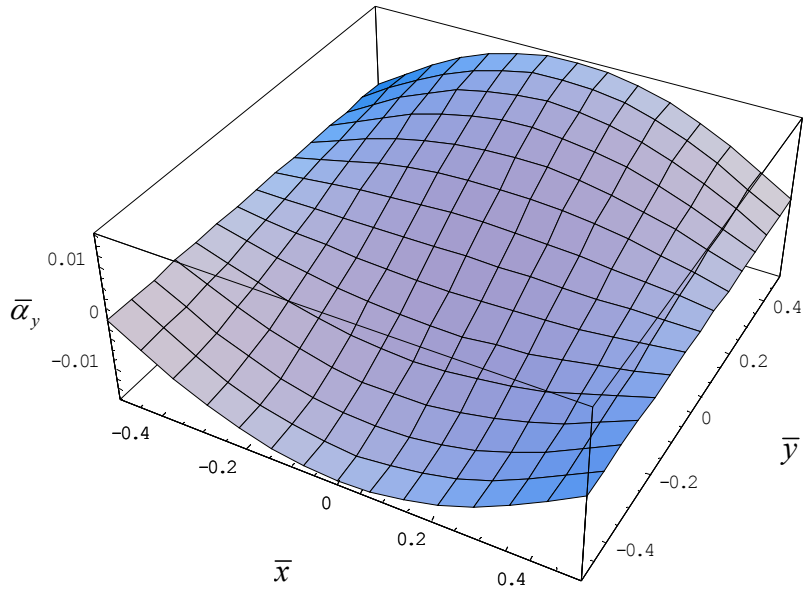

Figure 3.10: Rotation $\bar{\alpha}_y$ of uniformly-loaded sandwich plate simply supported along four edges

To satisfy the satisfy the first governing differential equation, the plate must be in vertical equilibrium. The forces acting on the plate are the distributed load, the effective shear forces along the edges, and the reactions at the corners. For vertical equilibrium, the following forces must sum to zero:

$$\sum F_z = \int_{-\frac{a}{2}}^{\frac{a}{2}}\int_{-\frac{a}{2}}^{\frac{a}{2}} q(x,y)\,dxdy + \int_{-\frac{a}{2}}^{\frac{a}{2}} Q_x^{eff}(a/2,y)\,dy + \int_{-\frac{a}{2}}^{\frac{a}{2}} Q_x^{eff}(-a/2,y)\,dy$$
$$+ \int_{-\frac{a}{2}}^{\frac{a}{2}} Q_y^{eff}(x,a/2)\,dx + \int_{-\frac{a}{2}}^{\frac{a}{2}} Q_y^{eff}(x,-a/2)\,dx - 2M_{xy}(a/2,a/2) \qquad (3.103)$$
$$- 2M_{xy}(-a/2,a/2) + 2M_{xy}(a/2,-a/2) + 2M_{xy}(-a/2,-a/2) = 0$$

The effective shear forces on opposite edges of the plate are the same due to symmetry. They act in the negative z-direction because they are reactions to the positively distributed load. The reaction force at each corner acts in the positive *z*-direction. In practice, full simply-supported boundary conditions are difficult to achieve because this reaction force must be applied at the corners of the plate to keep the corners at zero displacement. Therefore, other boundary conditions, which are easier to simulate in the laboratory, will be explored later.

Rayleigh-Ritz Solution

An approximate solution for this problem can be found using the Rayleigh-Ritz method discussed in Section 3.4 for an isotropic plate. In this method, the displacement and rotations are assumed to have the same form as those in Eqs. (3.96) through (3.98) because they satisfy all of the simply-supported boundary conditions. Instead of substituting directly into the differential equations, these solutions are used to minimize the total potential energy of the system. The elastic potential energy of the facesheets and core are very complicated integral expressions given by Eqs. (3.56) and (3.59) which require a great deal of computation time as the number of terms is increased. The load does not need to be written in terms of a trigonometric series because the work done by the external load can be calculated directly from Eq. (3.60). The total potential energy of the system must be minimized with respect to the unknown constants W_{mn}, A_{mn}, B_{mn}. Thus,

$$\frac{\partial \Pi}{\partial W_{mn}} = 0 \text{ and } \frac{\partial \Pi}{\partial A_{mn}} = 0 \text{ and } \frac{\partial \Pi}{\partial B_{mn}} = 0 \quad m, n = 1, 3, 5\ldots \qquad (3.104)$$

The resulting equations are solved simultaneously for the unknown constants. Table 3.1 gives a comparison of the normalized displacement in the center of the plate between the solution

obtained by substituting the various series directly into the governing differential equations and the Rayleigh-Ritz approximation. The running time of *Mathematica* for these computations is also given. The results are very similar, but the Rayleigh-Ritz solution takes much more time to compute because of the complex elastic potential energy functions given by Eqs. (3.56) and (3.59). Despite the increased computation time, the advantage of such a solution is that it can be used for loads that are not easily written as an infinite trigonometric series, such as complex distributed loads or concentrated point loads. Note that to use this approach directly, the applied load must still be symmetric with respect to the x-axis and y-axis because of the symmetry of the assumed solution.

Table 3.1: Normalized displacements for uniformly-loaded sandwich plate simply supported along four edges

Terms in Series	Differential Equation		Rayleigh-Ritz	
	W(0,0)	Time (s)	W(0,0)	Time (s)
1	0.01143	0.172	0.02821	1.47
2	0.01044	0.250	0.01044	11.2
3	0.01063	0.342	0.01063	53.8
4	0.01056	0.544	0.01056	194
5	0.01059	0.951	0.01059	657
6	0.01058	1.782	0.01058	2090

3.7 Uniformly-Loaded Sandwich Plate Simply Supported Along Two Edges

As discussed previously, a fully simply-supported sandwich plate under uniform load is difficult to achieve in practice because the corners tend to deflect unless a reaction force at each corner is applied. Therefore, consider a square sandwich plate ($a = b$) subjected to a uniform load, q_o, that is simply supported at $x = \pm a/2$ and free at $y = \pm a/2$, as shown in Figure 3.11. A similar set of boundary conditions was discussed previously in Section 3.4 for an isotropic plate. The displacement and x-rotation are assumed to have the form

$$w(x,y) = w^1(x) + w^2(x,y) \tag{3.105}$$

$$\alpha_x(x,y) = \alpha_x^1(x) + \alpha_x^2(x,y) \tag{3.106}$$

where $w^1(x)$ and $\alpha_x^1(x)$ are the solutions for a sandwich strip parallel to the x-axis, and $w^2(x,y)$ and $\alpha_x^2(x)$ are secondary solutions used to satisfy the boundary conditions at $y = \pm a/2$. The y-rotation is given by

$$\alpha_y(x,y) = \alpha_y^2(x,y) \tag{3.107}$$

because $a_y^1(x) = 0$ for a strip solution.

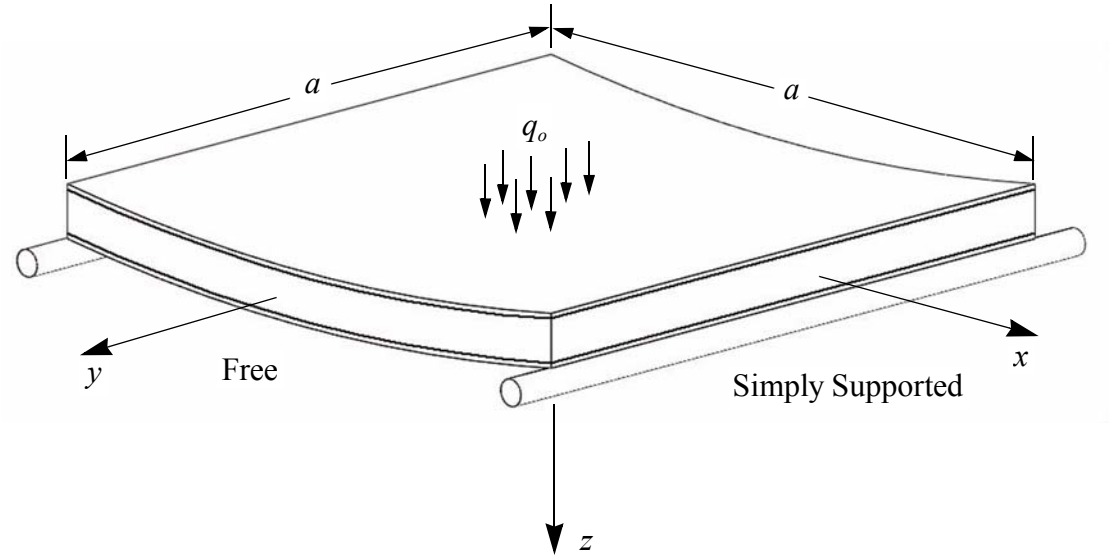

Figure 3.11: Uniformly-loaded sandwich plate simply supported along two edges

Exact Strip Solution

To find the solution for the sandwich strip, the strip solutions are substituted into the governing differential equations given by Eqs. (3.62) through (3.64). The first two partial differential equations become ordinary differential equations given by

$$\frac{2}{3}t^3Q_{11}\frac{d^4w^1}{dx^4} - \frac{1}{2}t^2cQ_{11}\frac{d^3\alpha_x^1}{dx^3} - cG_{xz}\left(\frac{d\alpha_x^1}{dx} + \frac{d^2w^1}{dx^2}\right) = q_o \tag{3.108}$$

$$\frac{1}{2}t^2cQ_{11}\frac{d^3w^1}{dx^3} - \frac{1}{2}tc^2Q_{11}\frac{d^2\alpha_x^1}{dx^2} + cG_{xz}\left(\alpha_x^1 + \frac{dw^1}{dx}\right) = 0 \tag{3.109}$$

The third governing differential equation is identically zero. The solution contains both homogeneous and particular parts, and it must satisfy the boundary conditions at $x = \pm a/2$ given in Eq. (3.93). The total solution for $w^1(x)$ and $\alpha_x^1(x)$ is

$$w^1(x) = \frac{q_o}{3c^2+6ct+4t^2}\left[\frac{1}{4Q_{11}t}x^4 + \left(\frac{24-3a^2\lambda^2}{8Q_{11}t\lambda^2} - \frac{3c}{2G_{xz}}\right)x^2 + \frac{5a^4\lambda^4 - 48a^2\lambda^2 + 384}{64Q_{11}t\lambda^4} + \frac{3ca^2\lambda^2 - 24c}{8G_{xz}\lambda^2} - \frac{12e^{a\lambda/2}\cosh(\lambda x)}{\left(1+e^{a\lambda}\right)Q_{11}t\lambda^4} + \frac{6ce^{a\lambda/2}\cosh(\lambda x)}{\left(1+e^{a\lambda}\right)G_{xz}\lambda^2}\right] \tag{3.110}$$

$$\alpha_x^1(x) = \frac{q_o}{3c^2+6ct+4t^2}\left[-\frac{1}{Q_{11}t}x^3 + \left(\frac{3a^2\lambda^2-24}{4Q_{11}t\lambda^2} - \frac{3t}{G_{xz}}\right)x + \frac{6Q_{11}ct^2\lambda e^{a\lambda/2}\sinh(\lambda x)}{\left(1+e^{a\lambda}\right)\left(Q_{11}ct\lambda^2 - 2G_{xz}\right)G_{xz}} - \frac{24G_{xz}e^{a\lambda/2}\sinh(\lambda x)}{\left(1+e^{a\lambda}\right)\left(Q_{11}ct\lambda^2 - 2G_{xz}\right)Q_{11}t\lambda^3} + \frac{12(c-t)e^{a\lambda/2}\sinh(\lambda x)}{\left(1+e^{a\lambda}\right)\left(Q_{11}ct\lambda^2 - 2G_{xz}\right)\lambda}\right] \tag{3.111}$$

where

$$\lambda = \sqrt{\frac{2G_{xz}\left(3c^2+6ct+4t^2\right)}{Q_{11}ct^3}} \tag{3.112}$$

Notice that the displacement is an even function of x and the rotation is an odd function of x.

Approximate Strip Solution

Instead of using the exact solution of Eqs. (3.108) and (3.109) for the sandwich strip, an approximate strip solution can be found by assuming

$$w^1(x) = \sum_{m=1,3,5\ldots}^{\infty} W_m \cos\left(\frac{m\pi x}{a}\right)$$
$$\alpha_x^1(x) = \sum_{m=1,3,5\ldots}^{\infty} A_m \sin\left(\frac{m\pi x}{a}\right) \tag{3.113}$$

where W_m and A_m are unknown constants. This assumed form of the solution satisfies the simply-supported boundary conditions at $x = \pm a/2$. Because a strip is essentially a wide beam, the constants are found by minimizing the total potential energy in a similar manner to that discussed in Section 2.4. After much algebra, the constants for any term m in the series are found to be

$$W_m = \frac{24a^4 q_o \left(2G_{xz}a^2 + m^2\pi^2 Q_{11} ct\right)}{m^5\pi^5 Q_{11} t\left[m^2\pi^2 Q_{11} ct^3 + 2G_{xz}a^2\left(3c^2 + 6ct + 4t^2\right)\right]} \sin\left(\frac{m\pi}{2}\right)$$

$$A_m = \frac{24a^3 q_o \left(2G_{xz}a^2 - m^2\pi^2 Q_{11} t^2\right)}{m^4\pi^4 Q_{11} t\left[m^2\pi^2 Q_{11} ct^3 + 2G_{xz}a^2\left(3c^2 + 6ct + 4t^2\right)\right]} \sin\left(\frac{m\pi}{2}\right) \tag{3.114}$$

Table 3.2 gives a comparison of the exact strip solution and the approximate solutions with various numbers of terms in the series. The displacement in the center of the plate has been nondimensionalized in accordance with Eq. (3.99). Agreement to four significant figures is achieved with five terms in the series. This approximate solution will prove to be a convenient form when applying the free edge boundary conditions at $y = \pm a/2$.

Table 3.2: Normalized displacements for uniformly-loaded sandwich strip

Terms in Series	W(0,0)
1	0.02765
2	0.02706
3	0.02718
4	0.02713
5	0.02715
Exact	0.02715

Secondary Solution

The remaining secondary part of the solution, $w^2(x,y)$, $\alpha_x^2(x,y)$, and $\alpha_y^2(x,y)$ from Eqs. (3.105) through (3.107), should satisfy the homogeneous form of the governing differential equations given by Eqs. (3.62) through (3.64), and make the total solution for the displacement and rotations satisfy all of the boundary conditions of the plate. The solution developed is from a similar procedure done by Timoshenko [16] for an isotropic plate. The assumed forms of the displacement and rotations are

$$
\begin{aligned}
w^2(x,y) &= \sum_{m=1,3,5\ldots}^{\infty} \Omega_m(y)\cos\left(\frac{m\pi x}{a}\right) \\
\alpha_x^2(x,y) &= \sum_{m=1,3,5\ldots}^{\infty} X_m(y)\sin\left(\frac{m\pi x}{a}\right) \\
\alpha_y^2(x,y) &= \sum_{m=1,3,5\ldots}^{\infty} Y_m(y)\cos\left(\frac{m\pi x}{a}\right)
\end{aligned}
\tag{3.115}
$$

The simply-supported boundary conditions at $x = \pm a/2$ are thus all identically satisfied. The remaining free boundary conditions at $y = \pm a/2$ will be discussed at a later point.

To determine the functions $\Omega_m(y)$, $X_m(y)$, and $Y_m(y)$, the displacement and rotations are substituted into the homogeneous form of the governing differential equations for a sandwich plate given by Eqs. (3.62) through (3.64). The coefficients of every trigonometric term must be zero for the equations to hold true for all x and y. The result is a set of three homogeneous linear differential equations for each value of m in the series. Each function is then assumed to have an exponential form given by

$$
\begin{aligned}
\Omega_m(y) &= W_m e^{\beta_m y} \\
X_m(y) &= A_m e^{\beta_m y} \\
Y_m(y) &= B_m e^{\beta_m y}
\end{aligned}
\tag{3.116}
$$

where W_m, A_m, B_m, and β_m are constants. Substitution into the three homogeneous linear differential equations, and cancellation of the common exponential term, results in the following three equations for any term m in the series:

$$
\begin{aligned}
&\left[\frac{2}{3}Q_{11}t^3\beta_m^4 - \left(\frac{4m^2\pi^2(Q_{12}+2Q_{66})t^3}{3a^2} + G_{yz}c\right)\beta_m^2 + \frac{2m^4\pi^4Q_{11}t^3}{3a^4} + \frac{m^2\pi^2G_{xz}c}{a^2}\right]W_m \\
&\quad + \left[-\frac{m\pi(Q_{12}+2Q_{66})ct^2}{2a}\beta_m^2 + \frac{m^3\pi^3Q_{11}ct^2}{2a^3} - \frac{m\pi G_{xz}c}{a}\right]A_m \\
&\quad + \left[-\frac{1}{2}Q_{11}ct^2\beta_m^3 + \left(\frac{m^2\pi^2(Q_{12}+2Q_{66})ct^2}{2a^2} - G_{yz}c\right)\beta_m\right]B_m = 0
\end{aligned}
\tag{3.117}
$$

$$\left[-\frac{m\pi\left(Q_{12}+2Q_{66}\right)ct^2}{2a}\beta_m^2+\frac{m^3\pi^3Q_{11}ct^2}{2a^3}-\frac{m\pi G_{xz}c}{a}\right]W_m$$
$$+\left[\left(-\frac{1}{2}Q_{66}c^2t-\frac{1}{12}G_{xy}c^3\right)\beta_m^2+\frac{m^2\pi^2Q_{11}c^2t}{2a^2}+G_{xz}c\right]A_m \tag{3.118}$$
$$+\left[\left(\frac{m\pi\left(Q_{12}+Q_{66}\right)c^2t}{2a}+\frac{m\pi G_{xy}c^3}{12a}\right)\beta_m\right]B_m=0$$

$$\left[-\frac{1}{2}Q_{11}ct^2\beta_m^3+\left(\frac{m^2\pi^2\left(Q_{12}+2Q_{66}\right)ct^2}{2a^2}-G_{yz}c\right)\beta_m\right]W_m$$
$$+\left[\left(\frac{m\pi\left(Q_{12}+Q_{66}\right)c^2t}{2a}+\frac{m\pi G_{xy}c^3}{12a}\right)\beta_m\right]A_m \tag{3.119}$$
$$+\left[\frac{1}{2}Q_{11}c^2t\beta_m^2-\frac{m^2\pi^2Q_{66}c^2t}{2a^2}-\frac{m^2\pi^2G_{xy}c^3}{12a^2}-G_{yz}c\right]B_m=0$$

In order for this set of equations to have a solution other than $W_m = 0$, $A_m = 0$, $B_m = 0$, the determinant of the coefficient matrix must be zero. The determinant of this matrix is an eighth-order polynomial in β_m. A closed-form solution for the roots of this polynomial is much too lengthy to be written here. It is enough to say that the functions given by Eq. (3.116) can be written as a series of eight exponential functions

$$\Omega_m\left(y\right)=\sum_{i=1}^{8}W_m^ie^{\beta_m^iy}$$
$$X_m\left(y\right)=\sum_{i=1}^{8}A_m^ie^{\beta_m^iy} \tag{3.120}$$
$$Y_m\left(y\right)=\sum_{i=1}^{8}B_m^ie^{\beta_m^iy}$$

where W_m^i, A_m^i, B_m^i and β_m^i correspond to the i^{th} root of the m^{th} term the series given by Eq. (3.115). There are several different possibilities for the roots of the polynomial.

For a soft core in which $G_{xy} = 0$, the roots of the polynomial consist of two unique sets of opposite real numbers, $\pm\lambda_m^1$ and $\pm\lambda_m^2$, as well as one repeated set of opposite real numbers, $\pm\lambda_m^3$. The exponential functions of Eq. (3.120) can then be written in terms of hyperbolic trigonometric functions as

$$
\begin{aligned}
\Omega_m(y) &= \sum_{j=1}^{3}\left[W_m^{2j-1}\cosh\left(\lambda_m^j y\right)+W_m^{2j}\sinh\left(\lambda_m^j y\right)\right] \\
&\quad + y\left[W_m^7\cosh\left(\lambda_m^3 y\right)+W_m^8\sinh\left(\lambda_m^3 y\right)\right] \\
X_m(y) &= \sum_{j=1}^{3}\left[A_m^{2j-1}\cosh\left(\lambda_m^j y\right)+A_m^{2j}\sinh\left(\lambda_m^j y\right)\right] \\
&\quad + y\left[A_m^7\cosh\left(\lambda_m^3 y\right)+A_m^8\sinh\left(\lambda_m^3 y\right)\right] \\
Y_m(y) &= \sum_{j=1}^{3}\left[B_m^{2j-1}\cosh\left(\lambda_m^j y\right)+B_m^{2j}\sinh\left(\lambda_m^j y\right)\right] \\
&\quad + y\left[B_m^7\cosh\left(\lambda_m^3 y\right)+B_m^8\sinh\left(\lambda_m^3 y\right)\right]
\end{aligned}
\tag{3.121}
$$

The constants in Eqs. (3.120) and (3.121) are the not the same, but the symbols remain unchanged because the values for constants are unknown at this point.

For a stiff core in which $G_{xy} > 0$, the eight roots to the polynomial can be real or complex. The first possibility is four unique sets of opposite real numbers, $\pm\lambda_m^1$, $\pm\lambda_m^2$, $\pm\lambda_m^3$, and $\pm\lambda_m^4$, for which the functions can be written as

$$
\begin{aligned}
\Omega_m(y) &= \sum_{j=1}^{4}\left[W_m^{2j-1}\cosh\left(\lambda_m^j y\right)+W_m^{2j}\sinh\left(\lambda_m^j y\right)\right] \\
X_m(y) &= \sum_{j=1}^{4}\left[A_m^{2j-1}\cosh\left(\lambda_m^j y\right)+A_m^{2j}\sinh\left(\lambda_m^j y\right)\right] \\
Y_m(y) &= \sum_{j=1}^{4}\left[B_m^{2j-1}\cosh\left(\lambda_m^j y\right)+B_m^{2j}\sinh\left(\lambda_m^j y\right)\right]
\end{aligned}
\tag{3.122}
$$

The second possibility for the roots of the polynomial with a stiff core is two unique sets of opposite real numbers, $\pm\lambda_m^1$ and $\pm\lambda_m^2$, plus one set of opposite complex conjugates, $\pm\lambda_m^3 \pm i\mu_m^3$. To ensure that the constants are real, the complex exponentials are expressed in terms of trigonometric functions. In this case, the functions of Eq. (3.120) are given by

$$
\begin{aligned}
\Omega_m(y) &= \sum_{j=1}^{2}\left[W_m^{2j-1}\cosh\left(\lambda_m^j y\right)+W_m^{2j}\sinh\left(\lambda_m^j y\right)\right] \\
&\quad +\cos\left(\mu_m^3 y\right)\left[W_m^5\cosh\left(\lambda_m^3 y\right)+W_m^6\sinh\left(\lambda_m^3 y\right)\right] \\
&\quad +\sin\left(\mu_m^3 y\right)\left[W_m^7\cosh\left(\lambda_m^3 y\right)+W_m^8\sinh\left(\lambda_m^3 y\right)\right] \\
X_m(y) &= \sum_{j=1}^{2}\left[A_m^{2j-1}\cosh\left(\lambda_m^j y\right)+A_m^{2j}\sinh\left(\lambda_m^j y\right)\right] \\
&\quad +\cos\left(\mu_m^3 y\right)\left[A_m^5\cosh\left(\lambda_m^3 y\right)+A_m^6\sinh\left(\lambda_m^3 y\right)\right] \\
&\quad +\sin\left(\mu_m^3 y\right)\left[A_m^7\cosh\left(\lambda_m^3 y\right)+A_m^8\sinh\left(\lambda_m^3 y\right)\right] \\
Y_m(y) &= \sum_{j=1}^{2}\left[B_m^{2j-1}\cosh\left(\lambda_m^j y\right)+B_m^{2j}\sinh\left(\lambda_m^j y\right)\right] \\
&\quad +\cos\left(\mu_m^3 y\right)\left[B_m^5\cosh\left(\lambda_m^3 y\right)+B_m^6\sinh\left(\lambda_m^3 y\right)\right] \\
&\quad +\sin\left(\mu_m^3 y\right)\left[B_m^7\cosh\left(\lambda_m^3 y\right)+B_m^8\sinh\left(\lambda_m^3 y\right)\right]
\end{aligned}
\tag{3.123}
$$

Solution Satisfying Free Edge Boundary Conditions

The constants W_m^i, A_m^i, and B_m^i are not independent of one another as Eqs. (3.117) through (3.119) indicate. There are only eight independent constants for each value of *m* in the series. There are also four boundary conditions that must be satisfied at each of the two edges of the plate:

$$
\begin{aligned}
Q_y^{eff}\left(x,\pm a/2\right) &= 0 \\
M_y\left(x,\pm a/2\right) &= 0 \\
M_y^C\left(x,\pm a/2\right) &= 0 \\
M_{xy}^C\left(x,\pm a/2\right) &= 0
\end{aligned}
\tag{3.124}
$$

The displacement $w(x,y)$ is symmetric with respect to the x-axis, so the coefficients of any odd function of y must be zero. This leaves only four constants which must satisfy the four boundary conditions at $y = a/2$. If the approximate strip solutions for $w^1(x)$ and $\alpha_x^1(x)$ given by Eq. (3.113) are used with the same number of terms as the secondary solutions for $w^2(x,y)$, $\alpha_x^2(x,y)$, and $\alpha_y^2(x,y)$ given by Eq. (3.115), each of the four boundary condition reduces to a series of trigono-

metric functions. The coefficients of the trigonometric functions must be zero for the boundary conditions to be zero for all values of x. Each of the four boundary conditions contains a linear equation to solve for the four unknown constants for each term in the series.

As before, the normalized displacement is shown in Figure 3.12 for material properties and geometry representative of the plate to be tested. The anticlastic curvature is not as apparent as that of the isotropic plate in Figure 3.5. The rotation $\bar{\alpha}_x$ is given in Figure 3.13. Unlike the sandwich plate simply supported on all four edges, $\bar{\alpha}_x$ does not go to zero at $\bar{y} = \pm 0.5$. However, there is very little deviation in the $\bar{y}$-direction. The shape of the rotation $\bar{\alpha}_y$ shown in Figure 3.14 is also much different than the sandwich plate simply supported on all four edges previously shown in Figure 3.10. The rotation $\bar{\alpha}_y$ goes to zero on at the edges $\bar{x} = \pm 0.5$, but it is negative for positive values of $\bar{y}$ because of the anticlastic curvature of the plate.

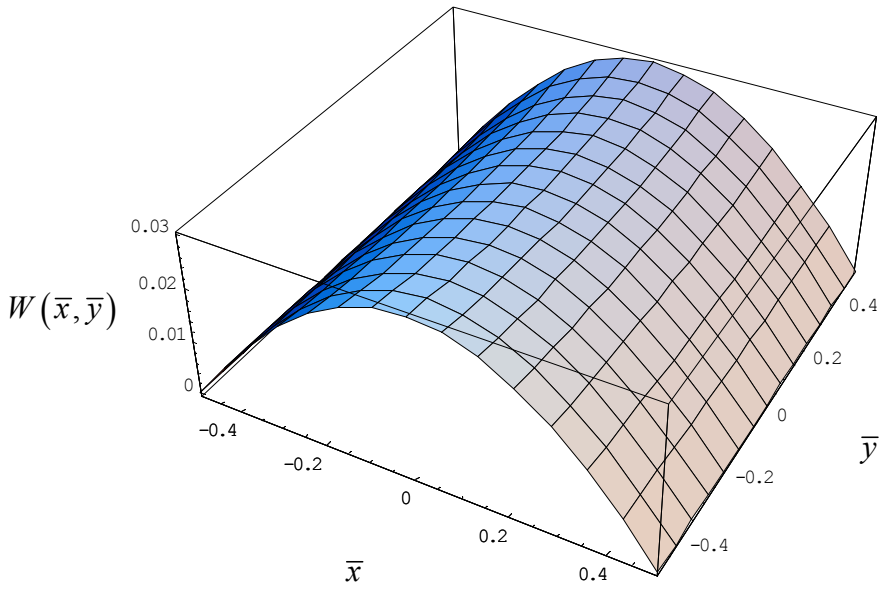

Figure 3.12: Displacement of uniformly-loaded sandwich plate simply supported along two opposite edges

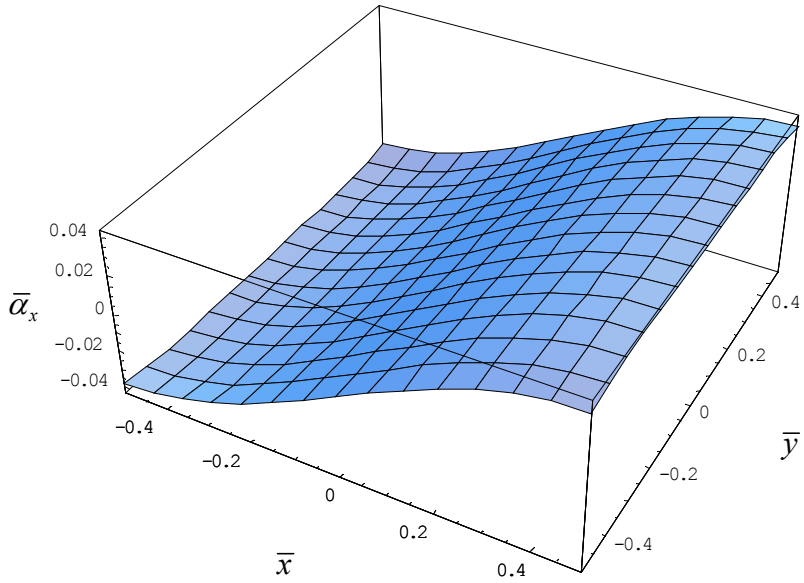

Figure 3.13: Rotation $\bar{\alpha}_x$ of uniformly-loaded sandwich plate simply supported along two opposite edges

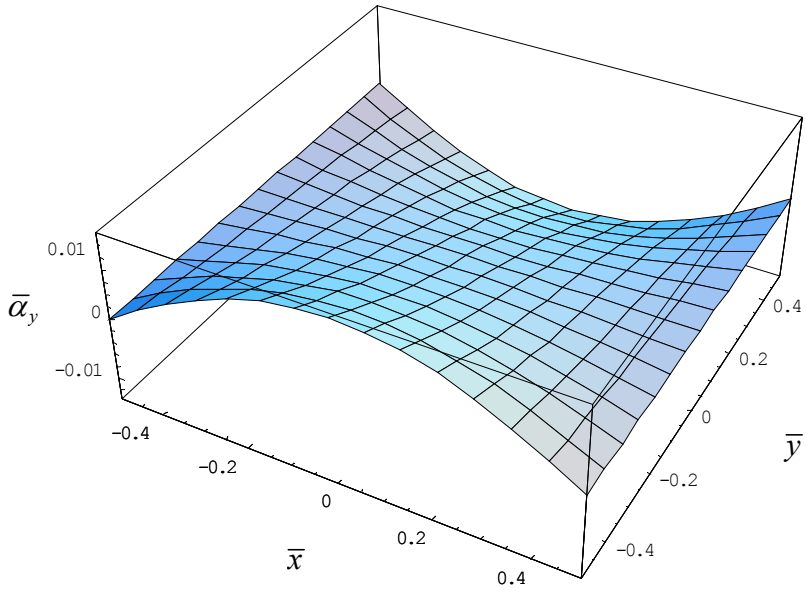

Figure 3.14: Rotation $\bar{\alpha}_y$ of uniformly-loaded sandwich plate simply supported along two opposite edges

It is important to note that the first governing differential equation, Eq. (3.62), is not identically satisfied because the approximate strip solution has been used. The forces in the vertical direction given by Eq. (3.103) do not equal zero, but the sum approaches zero as the number of

terms in the series is increased. The reaction force at the corners always acts in the negative z-direction. Therefore, unlike the fully simply-supported plate, the corners do not tend to deform away from the supports.

Rayleigh-Ritz Solution

An alternative method for studying the displacement and rotation response of the plate is to minimize the total potential using the Rayleigh-Ritz approach. The exact strip solution of Eqs. (3.110) and (3.111) can be used, and the secondary solution has the same form as that of Eq. (3.115). The total potential energy is then minimized with respect to the unknown constants found in Eqs. (3.121), (3.122), or (3.123), depending upon the types of roots of the polynomial. The displacement and rotations obtained in this way are in very good agreement with the results obtained from the previous solution by applying the boundary conditions directly. Table 3.3 gives the nondimensional displacement in the center of the plate for both solutions. The computational time for the Rayleigh-Ritz solution is larger because of the elastic strain energy integrals. However, only one term is needed to match the solution satisfying the free edge boundary conditions in the limit as the number of terms goes to infinity in that solution. The Rayleigh-Ritz solution gives boundary conditions at the free edges $y = \pm a/2$ that are not identically equal to zero for all values of x. They are actually functions of x that approach zero as the number of terms in the series is increased.

Table 3.3: Normalized displacements for uniformly-loaded sandwich plate simply supported along two edges

Terms in Series	B.C. Solution		Rayleigh-Ritz	
	W(0,0)	Time (s)	W(0,0)	Time (s)
1	0.02753	0.938	0.02703	4.92
2	0.02694	2.24	0.02703	33.6
3	0.02706	5.41	0.02703	94.1
4	0.02702	14.08	0.02703	203
10	0.02703	52.7	0.02703	3220

3.8 Line-Loaded Sandwich Plate Simply Supported Along Two Edges

It is difficult to apply a uniform distributed load in a mechanical test. Therefore, consider the sandwich plate shown in Figure 3.15 subjected to a uniform line load P along the y-axis. Similar to the simply-supported sandwich beam in Section 2.3, the exact solutions for the left ($x < 0$) and right ($x > 0$) halves of the plate must be written separately because of the discontinuity of shear due to the applied line load. As in Eqs. (3.105) through (3.107), assume the total solution for each half of the plate can be written as the sum of a strip solution and a secondary solution by

$$\begin{aligned} w_L(x,y) &= w_L^1(x) + w_L^2(x,y) \\ \alpha_{xL}(x,y) &= \alpha_{xL}^1(x) + \alpha_{xL}^2(x,y) \\ \alpha_{yL}(x,y) &= \alpha_{yL}^2(x,y) \end{aligned} \tag{3.125}$$

$$\begin{aligned} w_R(x,y) &= w_R^1(x) + w_R^2(x,y) \\ \alpha_{xR}(x,y) &= \alpha_{xR}^1(x) + \alpha_{xR}^2(x,y) \\ \alpha_{yR}(x,y) &= \alpha_{yR}^2(x,y) \end{aligned} \tag{3.126}$$

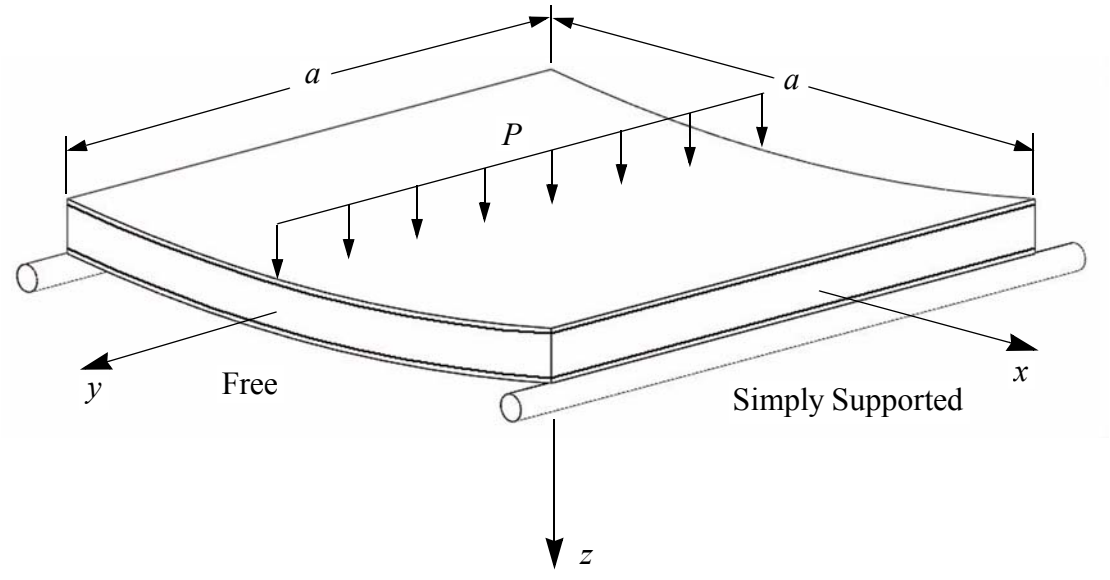

Figure 3.15: Line-loaded sandwich plate simply supported along two edges

Exact Strip Solution

Substitution of the left and right strip solutions into the governing partial differential equations given by Eqs. (3.62) through (3.64) gives the following four homogeneous ordinary differential equations:

$$\frac{2}{3}t^3Q_{11}\frac{d^4w_L^1}{dx^4}-\frac{1}{2}t^2cQ_{11}\frac{d^3\alpha_{xL}^1}{dx^3}-cG_{xz}\left(\frac{d\alpha_{xL}^1}{dx}+\frac{d^2w_L^1}{dx^2}\right)=0 \tag{3.127}$$

$$\frac{1}{2}t^2cQ_{11}\frac{d^3w_L^1}{dx^3}-\frac{1}{2}tc^2Q_{11}\frac{d^2\alpha_{xL}^1}{dx^2}+cG_{xz}\left(\alpha_{xL}^1+\frac{dw_L^1}{dx}\right)=0 \tag{3.128}$$

$$\frac{2}{3}t^3Q_{11}\frac{d^4w_R^1}{dx^4}-\frac{1}{2}t^2cQ_{11}\frac{d^3\alpha_{xR}^1}{dx^3}-cG_{xz}\left(\frac{d\alpha_{xR}^1}{dx}+\frac{d^2w_R^1}{dx^2}\right)=0 \tag{3.129}$$

$$\frac{1}{2}t^2cQ_{11}\frac{d^3w_R^1}{dx^3}-\frac{1}{2}tc^2Q_{11}\frac{d^2\alpha_{xR}^1}{dx^2}+cG_{xz}\left(\alpha_{xR}^1+\frac{dw_R^1}{dx}\right)=0 \tag{3.130}$$

These equations are identical in form to Eqs. (2.63) through (2.66) for a simply-supported sandwich beam, but with different constants. Thus, the displacements and rotations for the exact strip solution are the same as Eqs. (2.88) through (2.91) for a sandwich beam given by

$$w_L^1(x)=C_1e^{\lambda x}+C_2e^{-\lambda x}+C_3+C_4x+C_5x^2+C_6x^3 \tag{3.131}$$

$$\alpha_{xL}^1(x)=D_1e^{\lambda x}+D_2e^{-\lambda x}+D_3+D_4x+D_5x^2+D_6x^3 \tag{3.132}$$

$$w_R^1(x)=C_1e^{-\lambda x}+C_2e^{\lambda x}+C_3-C_4x+C_5x^2-C_6x^3 \tag{3.133}$$

$$\alpha_{xR}^1(x)=-D_1e^{-\lambda x}-D_2e^{\lambda x}-D_3+D_4x-D_5x^2+D_6x^3 \tag{3.134}$$

where λ is defined by Eq. (3.112).

The first variation of the total potential energy yields the following six conditions at $x = 0$ that relate the displacements and rotations for the left and right halves of the sandwich strip:

$$w_L^1(0) = w_R^1(0) \tag{3.135}$$

$$w_L^{1\prime}(0) = w_R^{1\prime}(0) \tag{3.136}$$

$$w_L^{1\prime\prime}(0) = w_R^{1\prime\prime}(0) \tag{3.137}$$

$$\alpha_{xL}^1(0) = \alpha_{xR}^1(0) \tag{3.138}$$

$$\alpha_{xL}^{1\prime}(0) = \alpha_{xR}^{1\prime}(0) \tag{3.139}$$

$$Q_{xL}^{eff}(0) - Q_{xR}^{eff}(0) = P \tag{3.140}$$

where Q_{xL}^{eff} and Q_{xR}^{eff} are defined by Eq. (3.65) and applied for only the strip solutions. As with the sandwich beam, three of the conditions are identically satisfied due to the symmetry of the assumed solution. Application of the three remaining conditions and the simply-supported boundary conditions at $x = -a/2$ gives the constants C_1 through C_6 in Eqs. (3.131) and (3.133) as

$$C_1 = \frac{3P(2G_{xz} - Q_{11}ct\lambda^2)e^{a\lambda}}{(1+e^{a\lambda})Q_{11}^2 ct^4\lambda^5} \tag{3.141}$$

$$C_2 = -\frac{3P(2G_{xz} - Q_{11}ct\lambda^2)}{(1+e^{a\lambda})Q_{11}^2 ct^4\lambda^5} \tag{3.142}$$

$$C_3 = \frac{Pa\left[6Q_{11}ct\lambda^2 + G_{xz}(a^2\lambda^2 - 12)\right]}{4Q_{11}^2 ct^4\lambda^4} \tag{3.143}$$

$$C_4 = -\frac{3P(2G_{xz} - Q_{11}ct\lambda^2)}{Q_{11}^2 ct^4\lambda^4} \tag{3.144}$$

$$C_5 = -\frac{3PaG_{xz}}{2Q_{11}^2 ct^4\lambda^2} \tag{3.145}$$

$$C_6 = -\frac{PG_{xz}}{Q_{11}^2 ct^4\lambda^2} \tag{3.146}$$

The remaining constants D_1 through D_6 are found by substituting the known displacements back into one of the differential equations given in Eqs. (3.127) through (3.130) and setting the coefficients of $e^{\lambda x}$, $e^{-\lambda x}$, x^3, x^2, x and the constant equal to zero. After much algebra, the remaining constants are given by

$$D_1 = -\frac{3P(2G_{xz} + Q_{11}t^2\lambda^2)e^{a\lambda}}{(1+e^{a\lambda})Q_{11}^2 ct^4\lambda^4} \tag{3.147}$$

$$D_2 = -\frac{3P(2G_{xz} + Q_{11}t^2\lambda^2)}{(1+e^{a\lambda})Q_{11}^2 ct^4\lambda^4} \tag{3.148}$$

$$D_3 = \frac{3P(2G_{xz} + Q_{11}t^2\lambda^2)}{Q_{11}^2 ct^4\lambda^4} \tag{3.149}$$

$$D_4 = \frac{3PaG_{xz}}{Q_{11}^2 ct^4\lambda^2} \tag{3.150}$$

$$D_5 = \frac{3PG_{xz}}{Q_{11}^2 ct^4\lambda^2} \tag{3.151}$$

$$D_6 = 0 \tag{3.152}$$

Approximate Strip Solution

It is convenient to find an approximate strip solution that is continuous over the entire plate. The strip solution is approximated in the same manner as Eq. (3.113) by

$$\begin{aligned} w^1(x) &= \sum_{m=1,3,5...}^{\infty} W_m \cos\left(\frac{m\pi x}{a}\right) \\ \alpha_x^1(x) &= \sum_{m=1,3,5...}^{\infty} A_m \sin\left(\frac{m\pi x}{a}\right) \end{aligned} \tag{3.153}$$

where

$$W_m = \frac{12a^3P\left(2G_{xz}a^2 + m^2\pi^2Q_{11}ct\right)}{m^4\pi^4Q_{11}t\left[m^2\pi^2Q_{11}ct^3 + 2G_{xz}a^2\left(3c^2 + 6ct + 4t^2\right)\right]}$$
$$A_m = \frac{12a^2P\left(2G_{xz}a^2 - m^2\pi^2Q_{11}t^2\right)}{m^3\pi^3Q_{11}t\left[m^2\pi^2Q_{11}ct^3 + 2G_{xz}a^2\left(3c^2 + 6ct + 4t^2\right)\right]} \tag{3.154}$$

are found by minimizing the total potential energy. To compare the exact and approximate strip solutions, the displacement is nondimensionalized by

$$W\left(x,y\right) = \frac{w\left(x,y\right)}{\left(Pa^3/D\right)} \tag{3.155}$$

where D is the flexural rigidity defined by Eq. (3.102). Table 3.4 gives the nondimensional displacement in the center of the strip for various numbers of terms in the approximate solution. The line-loaded sandwich strip takes many more terms than the uniformly-loaded sandwich strip to agree with the exact solution.

Table 3.4: Normalized displacements for line-loaded sandwich strip

Terms in Series	W(0,0)
1	0.04343
5	0.04787
10	0.04836
25	0.04856
50	0.04858
Exact	0.04859

Secondary Solution

The form of the secondary part of the solution for the line-loaded sandwich plate is the same as for the uniformly-loaded plate given by Eq. (3.115) because the secondary solution involves only the homogeneous governing differential equations and therefore does not depend on the type of applied load. This secondary solution is continuous over the entire plate. The simply-supported boundary conditions at $x = \pm a/2$ are identically satisfied. The unknown functions $\Omega_m(y)$, $X_m(y)$, and $Y_m(y)$ are given by Eqs. (3.121), (3.122), or (3.123), depending upon the types of roots of the polynomial.

Solution Satisfying Free Edge Boundary Conditions

As with the uniformly-loaded plate, using the approximate strip solution and applying the free edge boundary conditions given by Eq. (3.124) results in four equations with four unknown constants for each term in the series. The normalized displacement obtained in this manner is given in Figure 3.16 for the sandwich plate to be tested. The shape of the surface is not as smooth as the displacement for a uniformly loaded plate shown in Figure 3.12. The normalized displacement in the center of the plate is $W(0,0) = 0.0484$. Because of the anticlastic curvature, the maximum normalized displacement of 0.0523 occurs at the free edges of the plate. This effect is illustrated by the contour plot in Figure 3.17. A visualization of the contours found experimentally using shadow moiré will be discussed in Chapter 5.

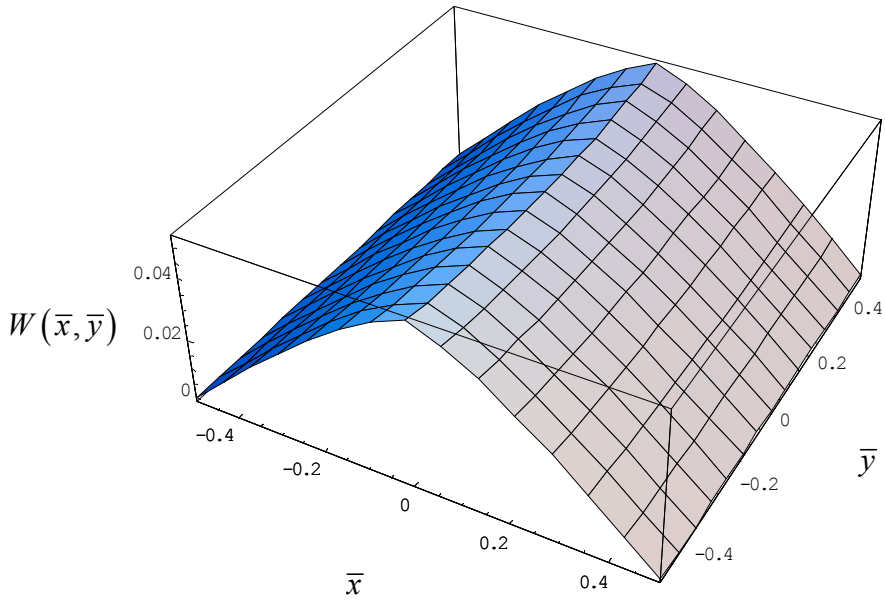

Figure 3.16: Displacement of line-loaded sandwich plate simply supported along two opposite edges

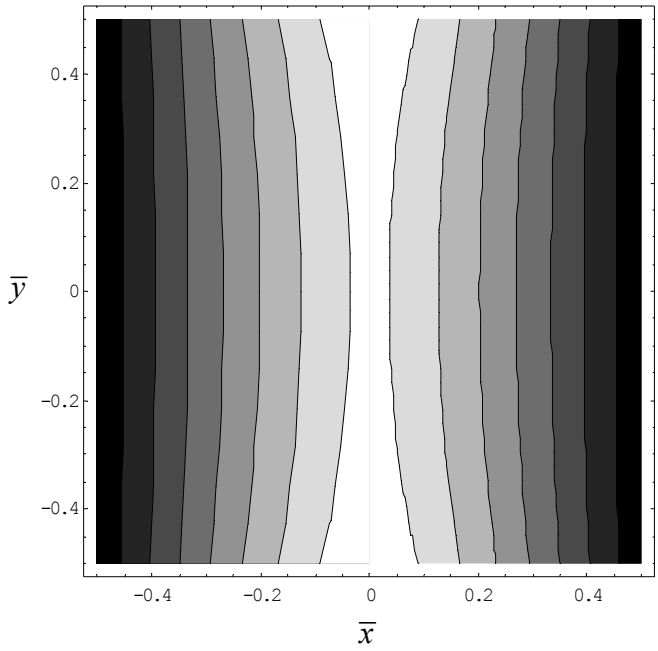

Figure 3.17: Displacement contours of line-loaded sandwich plate simply supported along two opposite edges

To visualize the rotations α_x and α_y, they are nondimensionalized by

$$\bar{\alpha}_x\left(x,y\right)=\frac{\alpha_x\left(x,y\right)}{\left(Pa^2/D\right)} \tag{3.156}$$

$$\bar{\alpha}_y\left(x,y\right)=\frac{\alpha_y\left(x,y\right)}{\left(Pa^2/D\right)} \tag{3.157}$$

The normalized rotations are given in Figures 3.18 and 3.19. As with the uniformly loaded sandwich plate shown in Figure 3.13, $\bar{\alpha}_x$ has little variation in the $\bar{y}$-direction. The maximum value is 0.0636. The rotation $\bar{\alpha}_y$ is similar in shape to that of the uniformly loaded plate shown in Figure 3.14, except with less variation. Once again, $\bar{\alpha}_y$ is negative for positive values of $\bar{y}$ because of the anticlastic curvature of the plate, and the maximum value is 0.0222.

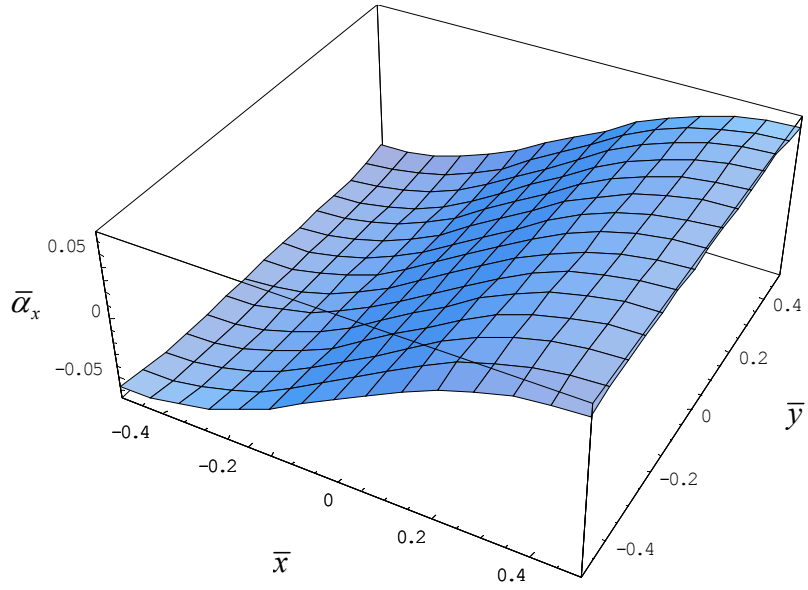

Figure 3.18: Rotation $\bar{\alpha}_x$ of line-loaded sandwich plate simply supported along two opposite edges

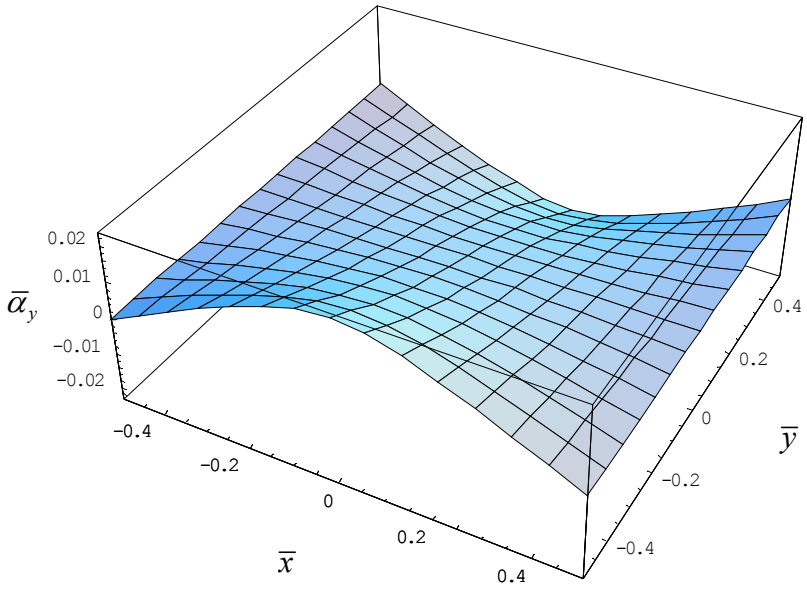

Figure 3.19: Rotation $\bar{\alpha}_y$ of line-loaded sandwich plate simply supported along two opposite edges

Because the approximate strip solution was used over the entire plate, the forces in the vertical direction given by Eq. (3.103) are not identically zero. As the number of terms Eq. (3.153) is increased, the sum of the forces approaches zero. Like the uniformly-loaded sandwich plate simply supported along two edges, the reaction forces at the corners act in the negative *z*-

direction. Thus, no external force is required to hold the corners in place. This condition, along with the use of a line load, makes this case ideal for testing purposes.

Rayleigh-Ritz Solution

The Rayleigh-Ritz method can also be used to determine the unknown constants in the secondary solution by minimizing the total potential energy. The exact strip solutions in Eqs. (3.131) through (3.134) should be used. The strain energy only needs to be calculated for either the left or right half of the plate, and then doubled, because both halves have the same strain energy due to symmetry. Table 3.5 gives the normalized displacement in the center of the plate for the Rayleigh-Ritz solution and the solution satisfying the free edge boundary conditions. The boundary condition solution requires over 50 terms to converge to the Rayleigh-Ritz solution obtained with just one term. The Rayleigh-Ritz solution was not calculated with 50 terms because the time required would be too great.

Table 3.5: Normalized displacements for line-loaded sandwich plate simply supported along two edges

Terms in Series	B.C. Solution		Rayleigh-Ritz	
	W(0,0)	Time (s)	W(0,0)	Time (s)
1	0.04324	0.342	0.04840	3.08
5	0.04768	7.83	0.04840	206
10	0.04817	33.1	0.04840	1091
25	0.04837	259	0.04840	13290
50	0.04839	1071	-	-

The sandwich plate models presented in this chapter will be used in Chapter 5 to predict the deflections of random wetlay composite sandwich plates. Before testing, sandwich specimens had to be manufactured in the laboratory. Chapter 4 discusses the compression molding of the composite facesheets, and the various adhesives used to used construct the sandwich specimens.

Chapter 4 Manufacturing

4.1 Materials

The random wetlay process is begun by intimately mixing the reinforcing fibers and thermoplastic polymer fibers together in an aqueous slurry using a pulper. The reinforcing fibers can be anywhere from 0.5 to 3 in. in length, and the polymer fibers can be up to 0.25 in. in length. The aqueous slurry consists of water, a viscosity modifier, a surfactant, and an antifoam agent to ensure good fiber dispersion. The slurry is drawn onto a forming wire and is de-watered through suction slots. This process creates a nonwoven mat of commingled reinforcing and matrix fibers. The composite mat is then passed through a convective oven which removes any remaining water and melts the polymer fibers into beads that hold the reinforcing fibers together. The mat is made in a continuous process so that it can be stored in roll form until ready for compression molding. Unlike many composite prepregs, these rolls do not require freezer storage and have an infinite shelf life [19].

The random wetlay composite facesheets used in this research consist of 25% E-glass fibers and 75% PET by weight. A substantial quantity of this wetlay mat was donated by DuPont [20] for research purposes. The glass fibers are 0.5 in. in length with a diameter of 0.531 mils. The polymer was initially chopped to a length of 0.250 in. Composite materials are typically described in terms of fiber volume fraction, not weight percent. The fiber volume fraction *VF* can be found by

$$VF = \frac{WF\,\rho_m}{WF\,\rho_m + (1 - WF)\,\rho_f} \tag{4.1}$$

where *WF* is the fiber weight percent, ρ_m is the matrix density, and ρ_f is the fiber density. For this particular composite, the density of the glass fibers is 5.03 slug/ft^3 and the density of the PET is 2.62 slug/ft^3. Thus, the fiber volume fraction is 14.8%. The density of the overall composite is 3.22 slug/ft^3. The material properties of the compression molded wetlay composite are considered to be in-plane isotropic because the glass fibers are randomly distributed in the isotropic PET matrix. The average tensile elastic modulus as measured by Lu [21] is 1.105 msi, and the average ultimate tensile strength is 11.08 ksi.

This random wetlay composite has a relatively low tensile modulus for structural purposes. For instance, the elastic modulus of a typical steel is 30.7 msi and the elastic modulus of aluminum is 10.2 msi. However, the densities of steel and aluminum are 15.27 slug/ft^3 and 5.24 slug/ft^3 respectively [22]. Thus, it was postulated that by using this composite as the facesheets of a sandwich plate, significant weight gains can be achieved while still maintaining adequate flexural rigidity.

The core material used in this research is HexWeb™ EM that has been donated by Hexcel [23]. It is a relatively inexpensive honeycomb composed of collinear nylon and PET fibers. The density of this material is 0.1289 slug/ft^3. Figure 4.1 shows a 6-in. x 6-in. square sample of the material with a thickness of 0.78 in. The honeycomb core exhibits orthotropic behavior due to the manufacturing process. The in-plane directions are denoted by the ribbon direction (L) and the transverse direction (W). Compared to the facesheet material, the honeycomb is assumed to have no in-plane extensional stiffness. However, it is assumed to be infinitely stiff in extension and compression in the thickness direction and linearly elastic in transverse, or through-the-thickness, shear. Thus, the only required core material properties are the three shear moduli. The transverse shear moduli are G_L = 2300 psi and G_W = 1400 psi [24]. For the core material here, the in-plane shear modulus is assumed to be zero [25], though for generality it has been included in the development of the sandwich plate model.

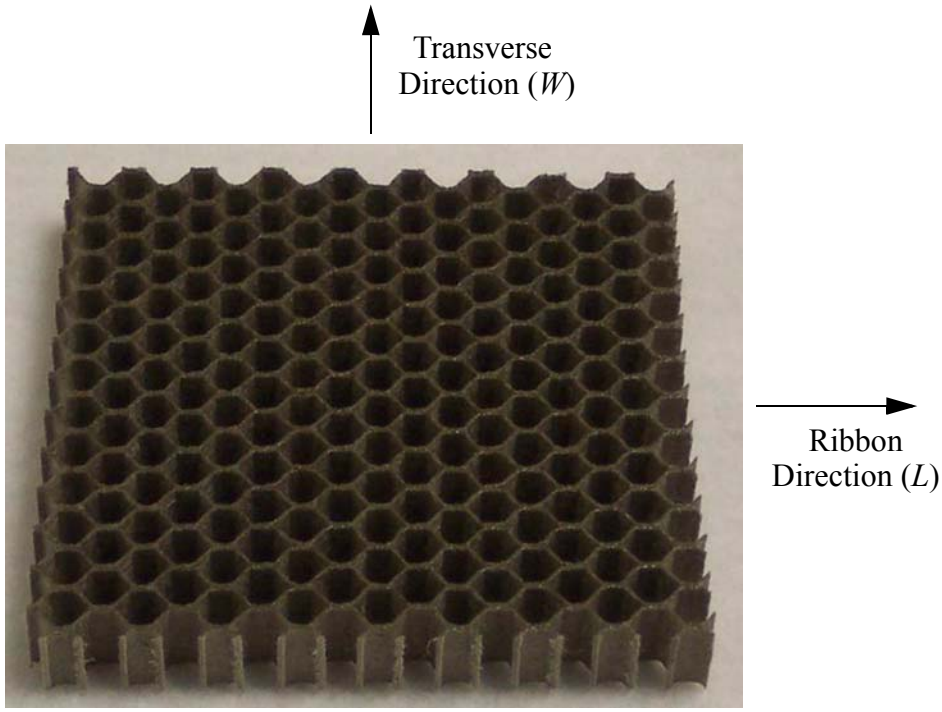

Figure 4.1: HexWeb™ EM honeycomb core

4.2 Compression Molding

The random wetlay mat discussed in Chapter 1 must be consolidated in a heated compression mold before it can be used in any structural application. This process fully melts the PET beads to flow and form into one continuous matrix to support the glass fibers. Lu [21] performed a variety of tests which determined the effects of temperature, molding pressure, and cooling rate on the mechanical properties of the composite. Lu's guidelines and recommendations were followed when manufacturing the composite facesheets.

A single layer of the random wetlay mat has a consolidated thickness of approximately 0.012 in. To make thicker specimens, several layers were stacked on top of one another and consolidated together. Three layers for each facesheet gives a total thickness of approximately 10% of the 0.78 in. thick core. Each layer was cut to the required dimensions using a paper cutter. Both 6-in. and 12-in. square specimens were made in a steel mold held together by bolts along the sides. Figure 4.2 shows an exploded view of three layers of wetlay mat in a 12-in. x 12-in. mold.

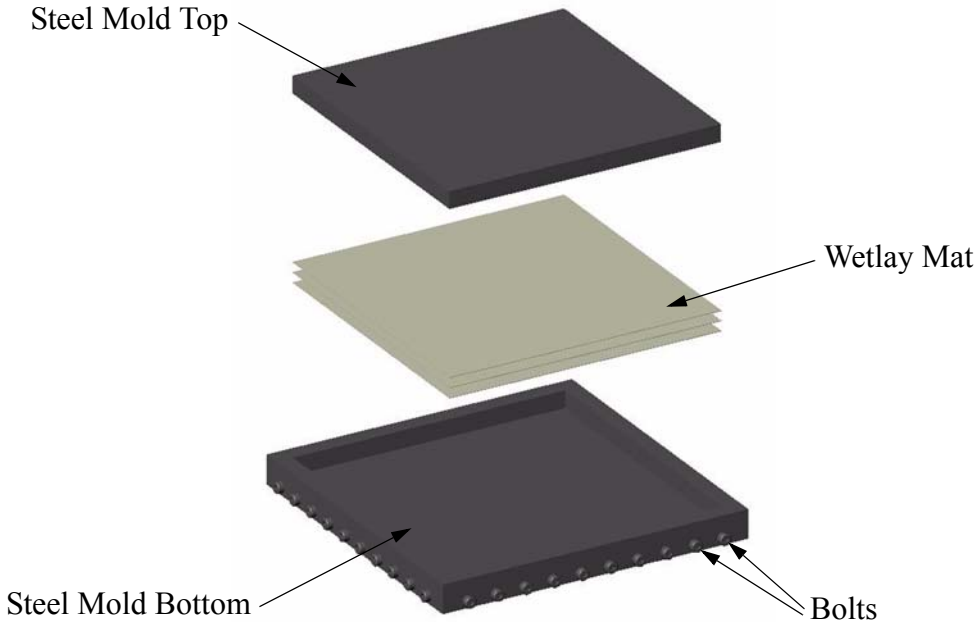

Figure 4.2: Exploded view of compression mold

Before processing, the mold was thoroughly cleaned and coated with mold release agent. The wetlay mat and mold were then placed into the hot press initially at room temperature, as shown in Figure 4.3. The bolts from Figure 4.2 can be seen on the mold. A thermocouple was attached in one corner of the mold to monitor the specimen temperature during cure. The temperature of both the top and bottom platen were raised at 5.4°F per minute while maintaining a constant contact pressure of approximately 15 psi. Once the part temperature reached 490°F, the consolidation pressure was increased to 700 psi. Lu [21] found that the best mechanical properties were achieved with a fast cooling rate. Air cooling was applied to the platens until the temperature reached 300°F, at which point water cooling was applied. The water cooling could not be applied above this temperature because it would produce too much steam in the pipes of the press. The mold was removed from press when it was cool to the touch. Figure 4.4 shows a typical temperature profile. The platen temperatures were not available after the heat was turned off. It is possible to see the distinct points at which the air and water cooling were applied.

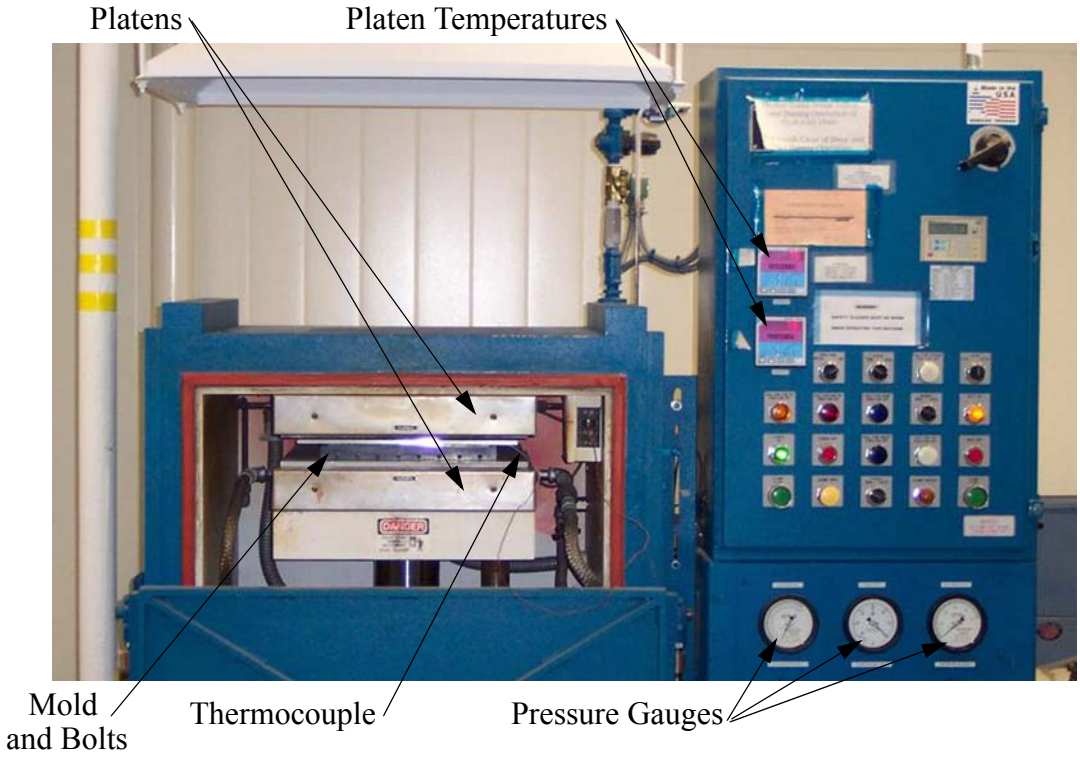

Figure 4.3: Hot press for compression molding of 12-in. x 12-in. facesheets

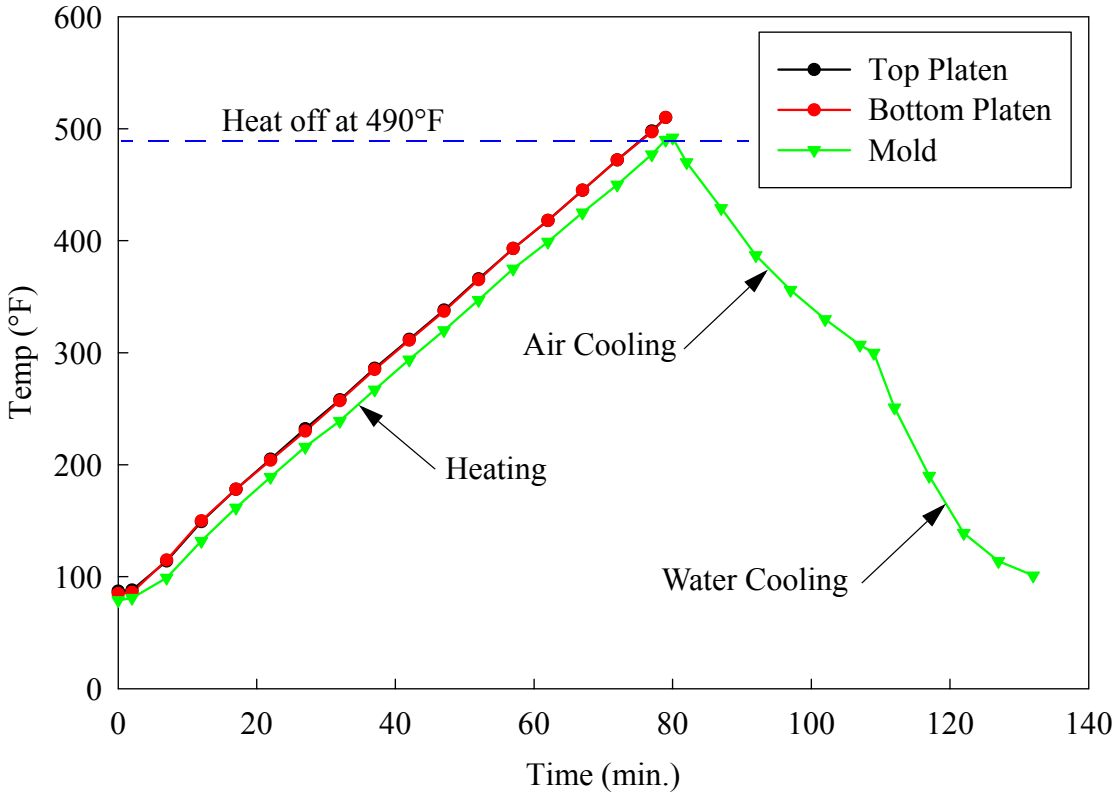

Figure 4.4: Temperature profile for compression molding

During consolidation, melted PET would squeeze out between the top of the mold and the sides. This excess material, or flash, was scraped off the edges of the finished composite panel. The ideal panel had very little flash with uniform melting of the PET. Too much flash would significantly change the fiber content and panel thickness. The primary factor controlling the amount of flash was the maximum temperature reached during processing. The temperature of the mold would continue to rise after the platen heaters were turned off, as shown by the top two green triangles in Figure 4.4. The amount of overshoot ranged from 2°F to 8°F and was not consistent from one panel to the next. Thus, the maximum temperature was difficult to control consistently. Table 4.1 gives the maximum mold temperature, cooling process, average thickness, standard deviation of thickness, and percent mass loss for panels identified with the nomenclature CG25.4 through CG25.15. A long-arm sheet metal micrometer was used to measure the thickness every 1 in. for the 6-in. x 6-in. panels and every 2 in. for the 12-in. x 12-in. panels.

Table 4.1: Composite facesheet data

Panel #	Size (in.)	Max Temp. (°F)	Cooling Process	Average (mils)	Std. Dev. (mils)	Percent Loss	Comments
CG25.4	12	507	None	25.4	3.00	25.1	
CG25.5	12	507	None	25.5	3.94	24.5	
CG25.6	12	502	None	35.0	3.07	6.20	
CG25.7	6	486	Air/Water	-	-	-	A
CG25.8	6	490	Air/Water	30.8	3.44	12.2	
CG25.9	6	492	Air/Water	33.7	1.75	5.83	
CG25.10	6	485	Air/Water	36.2	1.14	2.21	
CG25.11	12	490	Air/Water	35.5	1.50	0.00	B
CG25.12	12	495	Air/Water	36.2	1.12	1.30	
CG25.13	12	496	Air/Water	34.2	3.65	9.70	
CG25.14	12	492	Air/Water	38.5	1.10	0.92	
CG25.15	12	492	Air/Water	38.4	1.18	0.44	
A	High pressure (700 psi) on during entire process. Large amount of flash.						
B	PET not fully melted. No visible flash.						

The first three panels contained a large amount of flash because the maximum mold temperature was much too high. Without cooling the platens, the temperature remained above the melting point of PET for a long time, which allowed for more PET to be squeezed out of the mold under the high pressure. The next four panels were made in a smaller press with computerized control of the temperature and pressure. Lower temperatures and air/water cooling were sug-

gested [26] because Lu's research was not available at that time. Panel CG25.7 contained an error in the computer controls, which left the high pressure on during the entire process and pushed the majority of the PET out of the mold. The remaining smaller panels were successful in reducing the amount of flash. It was found that the larger mold required a higher maximum temperature than the smaller mold. Panel CG25.11 reached a maximum temperature of 490°F, but did not fully melt the PET. The last two panels contained the least flash with the best thickness uniformity. As an example, Figure 4.5 shows the measured thicknesses of panels CG25.4 and CG25.15. The thickness of all the panels are given in Appendix A. It is important to note that the thickness scale of both panels is the same, so the thickness of panel CG25.15 appears relatively uniform. As can be seen, there was a balance between reaching a temperature high enough to melt all the PET, but not having a temperature so high that the PET was squeezed out of the mold.

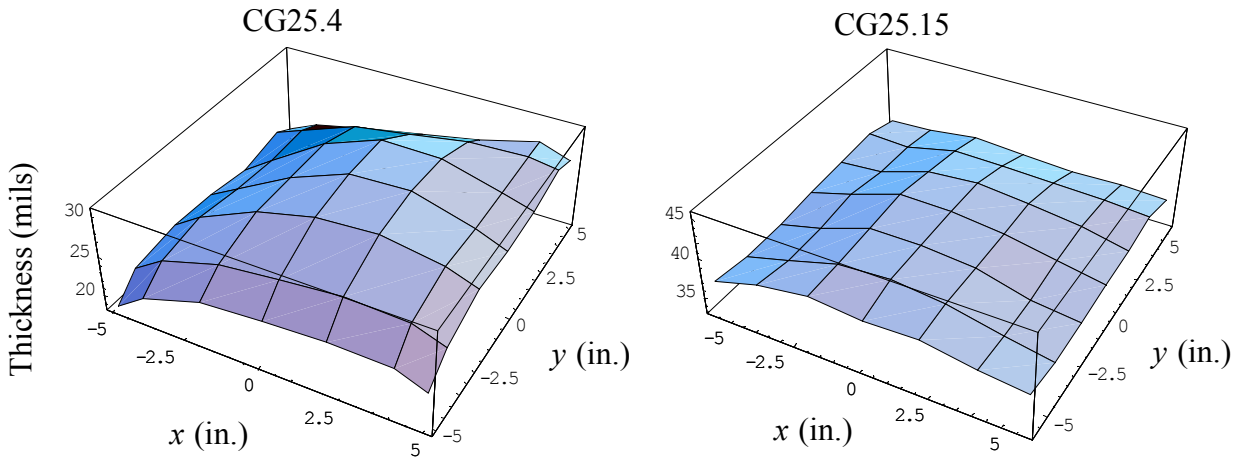

Figure 4.5: Panel thickness comparison

4.3 Sandwich Specimens

One common method of bonding the facesheets and core of a honeycomb sandwich panel is by using a film adhesive. A layer of film adhesive is cut to size and placed over the pre-molded facesheet. The honeycomb is then secondarily bonded to the facesheet by curing the adhesive at an elevated temperature. The contact pressure between the honeycomb and facesheets could be maintained by vacuum bagging the entire part. The film adhesive is typically easy to apply at room temperature and assures uniform thickness over the entire facesheet. Despite these advan-

tages, film adhesives were not examined in this research because they are generally more expensive than liquid/paste adhesives, need an additional step of heating to cure, require refrigeration storage, and have a limited shelf life.

Another method initially considered was thermally bonding the facesheets to the core. Because both the facesheets and core contain PET as the matrix material, it might be possible to melt the PET and fuse the facesheets and core together. Once again, this would require and additional step of applied heat. Also, the facesheets could not be fabricated and bonded to the core in the same step because the 700 psi pressure required for compression molding would crush the core. Melting the thermoplastic under less pressure would also reduce the mechanical properties of the facesheets.

Cagle [27] suggests some adhesives useful for bonding the polyethylene facesheets to the core include epoxies, polyesters, polyurethanes, and hot melts. The nylon polyamide core can be bonded with epoxies, nitril phenolics, and urethanes. It is important that the adhesive create a good fillet between the facesheets and the walls of the honeycomb core. In fact, this fillet is believed to be of such importance that a side study was done to determine the strengths of a variety of adhesives. Three different adhesives were examined in this phase of the research: polyurethane glue; epoxy paste; and 3M Scotch-Grip™ plastic adhesive [28].

Polyurethane Glue

The initial adhesive chosen was Elmer's Probond [29] polyurethane glue. It is a viscous yellow liquid that requires moisture to cure at room temperature. It was thought that this adhesive would form a good fillet because it expands as it cures. Several bottles were purchased from the local hardware store for about $9 per bottle. The first sandwich panel constructed using the polyurethane glue was cured at room temperature in a vacuum bag to hold the pre-molded facesheets in contact with the core. An exploded profile view of the bagging sequence is given in Figure 4.6. Both 6-in. x 6-in. facesheets of random wetlay composite were bonded in the same step. Before bonding, each facesheet was cleaned with isopropyl alcohol (IPA) and wiped with a damp cloth to provide moisture for the polyurethane glue to cure. A thin layer of polyurethane glue was applied using card stock. A layer of teflon was wrapped around the sandwich to prevent the adhesive

from getting on the breather, which was also wrapped around the sandwich. The breather allowed air to be drawn out of the bag without pinching. A wooden block with holes drilled through it was placed underneath the vacuum puck where the vacuum port was attached. The plastic bag was wrapped around the entire part and closed with sealant tape. The part was allowed to sit under full vacuum (14.7 psi) for 24 hours. This process proved unsuccessful because the core was crushed by the vacuum bag in the transverse direction (*W*) of Figure 4.1. Figure 4.7 shows the shape of the crushed core visible through the facesheet because the facesheet is only one layer thick. There was no fillet along the walls of the core because the adhesive was absorbed into the honeycomb.

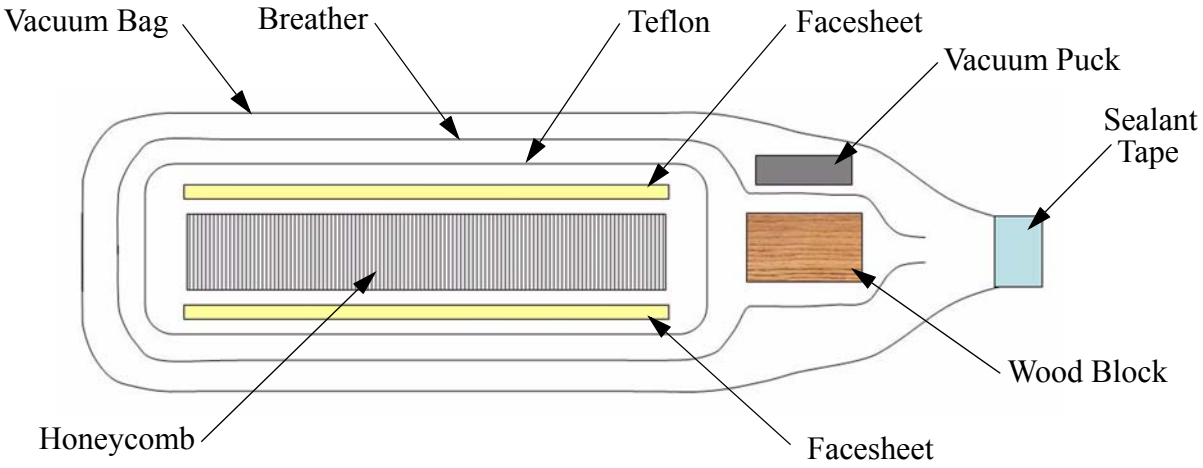

Figure 4.6: Initial vacuum bagging sequence

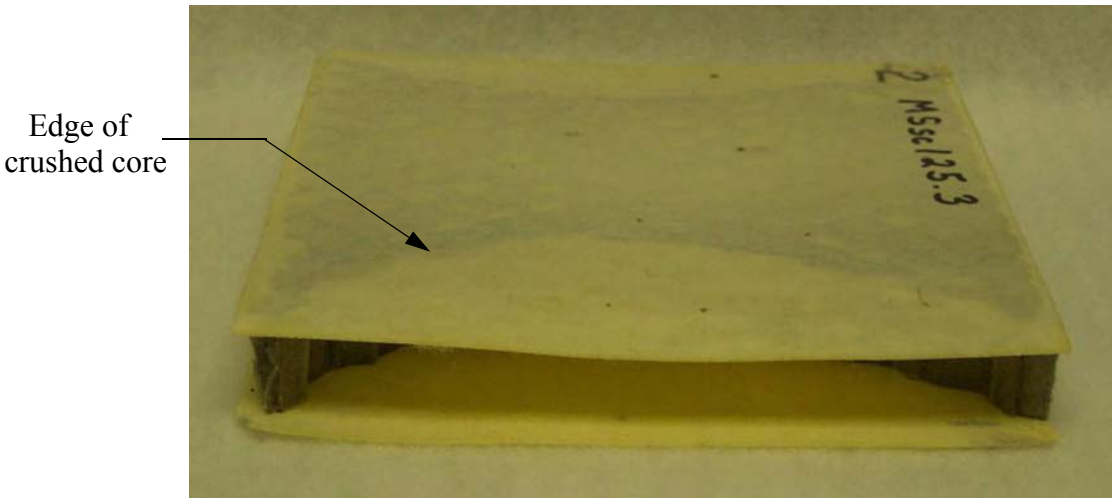

Figure 4.7: Initial sandwich panel with core crushing

Several process enhancements were made when fabricating the next sandwich panel. The thickness of the facesheets was increased to three layers of random wetlay mat. To prevent the crushing in the core, a wood frame was constructed to support all four sides of a 12-in. x 12-in. panel. Figure 4.8 shows the honeycomb, wood frame, and bagging materials before the bag was sealed and the vacuum was applied. The bagging sequence is the same as that given by Figure 4.6 with the addition of the wood frame. Initially, the facesheets were very smooth and shiny. Cagle [27] suggests that molded plastic parts should be sanded before bonding to remove any excess mold release and promote mechanical lock. Therefore, one side of each facesheet was sanded with 600 grit sandpaper until the surface appeared dull. As before, the surface was cleaned with IPA and wiped with a damp cloth to apply moisture for the cure. The polyurethane glue was spread onto both facesheets and placed in the vacuum bag. Full vacuum pressure was applied for 24 hours. After removal from the vacuum bag, the facesheets appeared to be bonded to the core, but there was very little fillet at the base of the honeycomb wall. The strength of the bond was tested in flatwise tension, and a beam specimen was cut from the center of the plate and tested in three-point bending. These results of these tests will be discussed in Chapter 5.

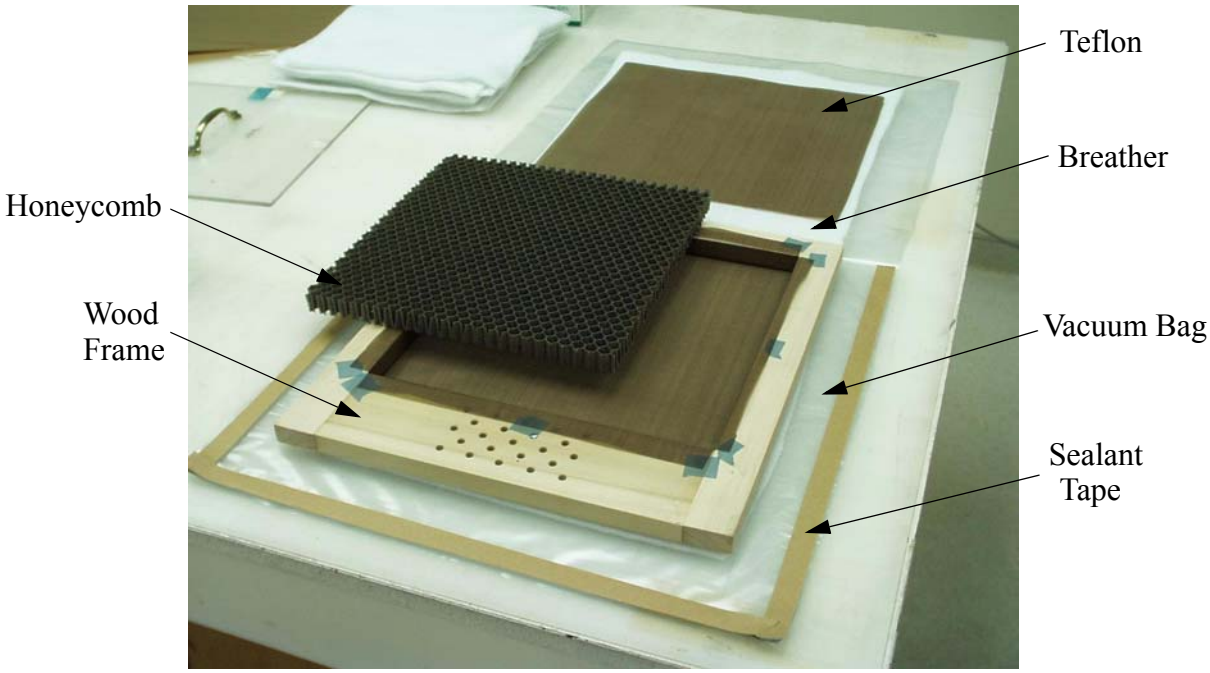

Figure 4.8: Honeycomb, bagging materials, and wood frame for sandwich construction

To further improve the bond strength, another 6-in. x 6-in. panel was fabricated using a thicker layer of adhesive. Instead of sanding, a grit blast machine was used to roughen the surface and remove the mold release. The surface was sprayed with many small grit particles until it had a dull finish. This process was thought to roughen the surface better than sandpaper. The amount of adhesive used on each facesheet was measured to be between 0.705 oz. and 0.741 oz. The thickness of the adhesive layer was considerably more than the amount used on the two previous sandwiches. Because of the horizontal orientation of the panel during the bonding operation as shown in Figure 4.6, the sandwich was constructed in two stages to prevent the adhesive on the top facesheet from running down the honeycomb walls during cure. After the bottom facesheet was bonded under full vacuum for 24 hours, the sandwich was turned over and the second facesheet was bonded using the same procedure. The final structure appeared to be well bonded, but much of the adhesive had been absorbed into the honeycomb walls, which left no fillet along the honeycomb wall. Figure 4.9 shows an end view of a piece of the sandwich. The adhesive was absorbed about 1/3 of the way up from each facesheet.

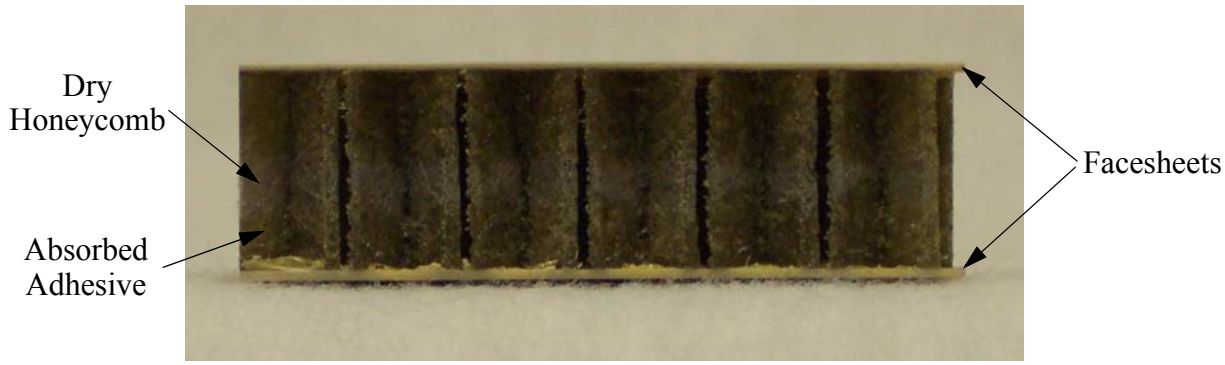

Figure 4.9: Sandwich specimen with polyurethane glue absorbed into honeycomb

The sandwich was cut using a diamond saw into four 2.75-in. x 2.75-in. square specimens labeled A, B, C, and D to measure the bond strength using a flatwise tension test. After the sandwich had been cut, it was noticed that the second facesheet was not bonded in one corner of each specimen. Arranging the specimens as they were situated on the original 6-in. x 6-in. panel revealed that there was a debond in the center of the panel, as shown in Figure 4.10. Thus, there was no need to test these specimens in flatwise tension. The cause of the debond was unknown, but it was thought to be associated with the adhesive being absorbed into the honeycomb.

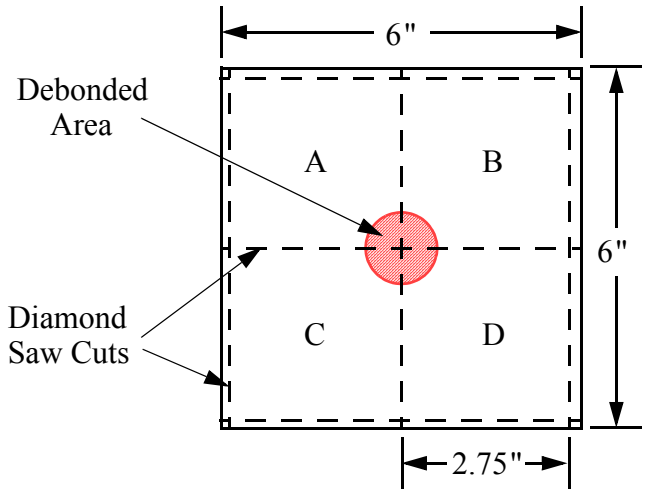

Figure 4.10: Debonded area of sandwich specimen

To prevent the polyurethane glue from absorbing into the honeycomb, it was suggested [24] to mix the polyurethane glue with Cab-O-Sil, which is a fumed silicon dioxide powder used as a thickening agent. It can be purchased at a variety of commercial internet sites for less than $20 per pound [30]. The weight density is approximately 2.30 lb/ft^3. Cab-O-Sil can be stored in a sealed bag at room temperature for an indefinite amount of time. The particles disperse easily in air, so a fume hood was used when working with this material. Typical amounts of Cab-O-Sil added to the adhesive range from 1% to 7% by weight [31]. Several different ratios were mixed together and spread onto a test surface to compare the thickness and ease of use. It was found that 3% Cab-O-Sil provided sufficient thickening without being difficult to spread. A mixture of 7% Cab-O-Sil had a consistency similar to vaseline.

In addition to adding Cab-O-Sil, it was thought that curing the adhesive at atmospheric conditions would strengthen the bond because the adhesive expands as it cures when left in the open air. No such expansion had occurred when constructing the previous sandwich panels in a vacuum bag. This expansion mechanism was thought to be able to create a fillet at the base of the honeycomb walls. To accomplish this without the use of a vacuum bag, a contact pressure of approximately 0.5 psi was maintained between the honeycomb and bottom facesheet with a steel plate as shown in Figure 4.11. As before, the bonding was performed in two steps to prevent the adhesive on the top facesheet from running down the honeycomb walls during the curing cycle.

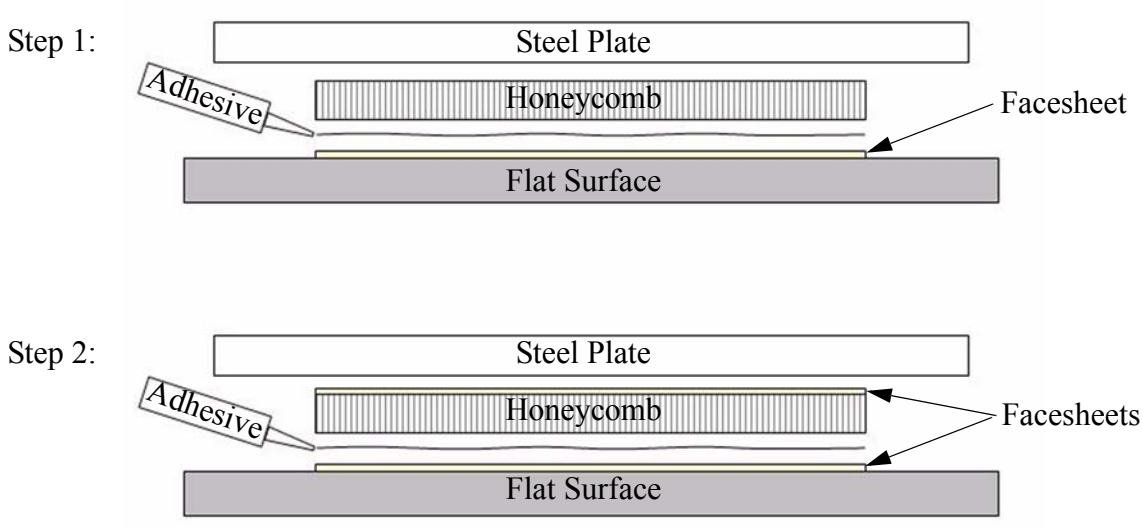

Figure 4.11: Atmospheric bonding of facesheets and honeycomb

The resulting bond appeared to be much more adequate than that of the polyurethane glue without Cab-O-Sil cured in a vacuum bag. Figure 4.12 shows the interior of a bonded specimen cut with a diamond saw. Unlike Figure 4.9, the adhesive expanded fully and was not absorbed into the honeycomb. This thick layer of adhesive had more surface area to bond along the honeycomb walls. The thickness of the adhesive was approximately uniform inside every honeycomb cell.

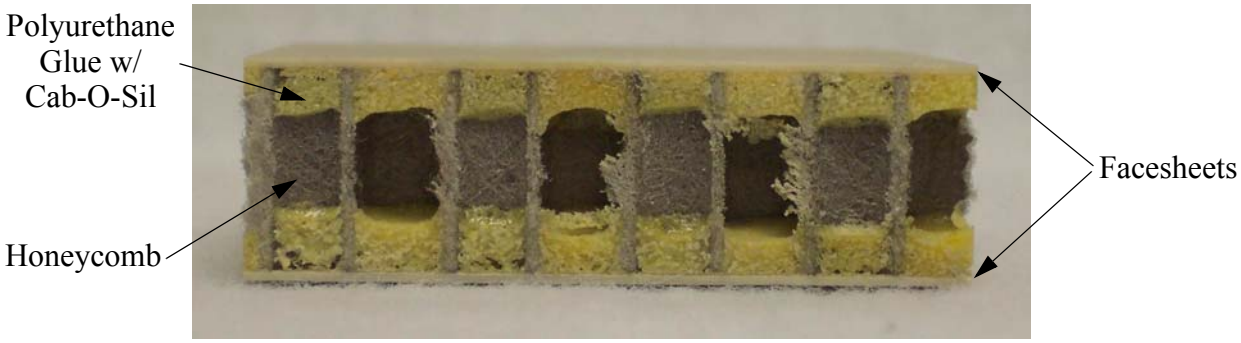

Figure 4.12: Polyurethane glue with Cab-O-Sil sandwich specimen

Epoxy Paste

For comparison, two other adhesives were used to construct sandwich panels. The first was PC-7 [32] two-part heavy duty epoxy paste. The cost of one 2-oz. tube was about $5 at the

local hardware store. The facesheets were grit blasted and cleaned as described previously. Two equal parts of epoxy were then mixed together on a sheet of teflon. The resulting mixture was spread onto the bottom facesheet and cured in a vacuum bag over night. The second facesheet was bonded in a similar fashion the following day. Applying the epoxy was much more difficult than applying the polyurethane glue because the epoxy was very viscous and stuck to the tools used for mixing and spreading. A thick layer was initially applied because the epoxy paste was not expected to form a fillet due to its high viscosity. The uniformity of the thickness was difficult to control, as seen in Figure 4.13. Therefore, almost one entire tube of epoxy paste was used for each facesheet of a 6-in. x 6-in. sandwich panel in order to create a thick enough layer of adhesive. The completed sandwich panel appeared to be well bonded. Flatwise tension test results will be given in Chapter 5.

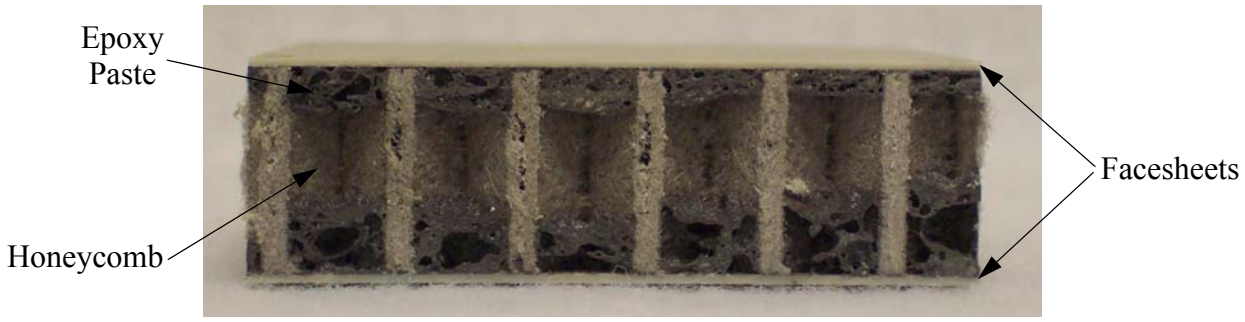

Figure 4.13: Epoxy paste sandwich specimen

Scotch-Grip™ Plastic Adhesive

The other adhesive considered for this research was a 3M Scotch-Grip™ plastic adhesive. A free 5-oz. sample was sent by 3M after discussing the problem with them in detail. It can be purchased from distributors for about $30 per quart. Approximately 0.952 oz. was applied directly to the 6-in. x 6-in. bottom facesheet and spread evenly over the entire surface. This adhesive does not require moisture to cure, so a vacuum bag was used to maintain contact pressure between the bottom facesheet and core for 24 hours. The second facesheet was then bonded using the same procedure. Initially, the viscosity of the plastic adhesive was greater than that of the polyurethane glue, but much less than the epoxy paste. However, it began to cure very rapidly when exposed to the atmosphere. After 10 minutes, the adhesive was nearly impossible to spread

further. While this was enough time to construct a 6-in. x 6-in. panel, the plastic adhesive would be very difficult to use for much larger panels. The adhesive was able to form a small fillet along the walls of the honeycomb to create an adequate bond as shown in Figure 4.14. The strength of the bond was tested under flatwise tension, and the results will be discussed in Chapter 5.

Figure 4.14: Scotch-Grip™ plastic adhesive sandwich specimen

Chapter 5 Experimental Procedures

5.1 Flatwise Tension Tests

To determine the strength of the various adhesives used to bond the facesheets to the core, a series of flatwise tension tests were performed in accordance with ASTM C 297 [33]. The flatwise tensile strength measurements are not used in any analysis developed herein, such as the beam or plate models discussed previously, but the bond between the facesheets and the core can be a weak point in sandwich construction. It is thus useful to know the strength of the bond for a particular adhesive, and to determine the range of strengths for several different adhesives. A *SolidWorks* [34] model of the flatwise tension test fixture is shown in Figure 5.1. The top and bottom surfaces of each 2.75-in. x 2.75-in. flatwise tension sandwich specimen were bonded to the center of 3 in. cube aluminum loading blocks. A 0.5-in. diameter hole was bored through the center of each aluminum block before bonding. The facesheets and aluminum were grit-blasted and cleaned thoroughly for proper bonding. Both sides of the flatwise tension sandwich specimen were bonded to the aluminum blocks with approximately 0.25 oz. of epoxy paste such that the holes in the two aluminum blocks were perpendicular to one another. This epoxy paste was the same as one of the adhesives used to bond the facesheets to the core, as discussed in Chapter 4. Care was taken to ensure that the faces of the aluminum blocks remained parallel. A 2-lb weight was used to maintain contact pressure while the epoxy paste cured for 24 hours at room temperature. A steel loading fixture consisting of two U-shaped brackets was made by the ESM machine shop. The specimen was free to rotate about two 0.5-in. diameter steel pins that passed through the holes in the aluminum blocks. The fixture was threaded at the top and bottom to attach directly to a load frame. A tensile load was applied at the rate of 0.01 in/min. with a sampling period of 6 sec. Both the load and the displacements between the platens of the load frame were recorded. The load was applied until the specimen failed, at which point the load dropped off significantly.

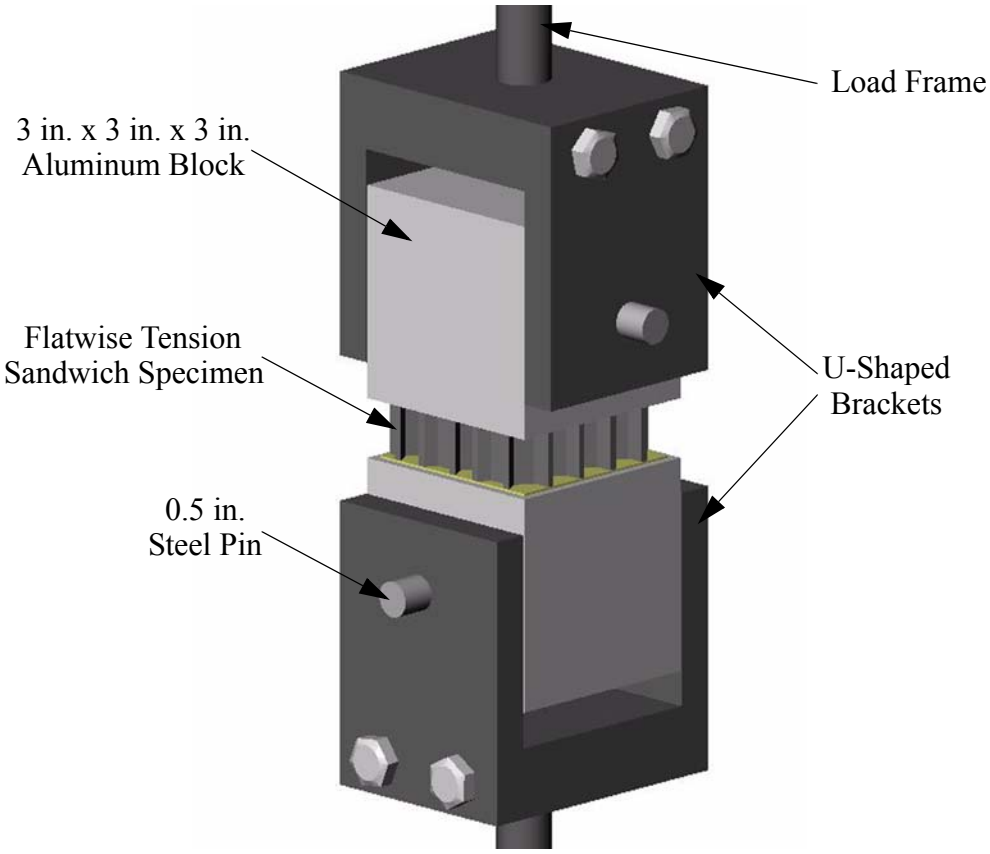

Figure 5.1: Flatwise tension text fixture model

The flatwise tensile strength is calculated by

$$\sigma = \frac{P}{A} \tag{5.1}$$

where P is the ultimate tensile load and A is the cross-sectional area of the sandwich specimen. For these tests, the cross-sectional area was 7.56 in.^{2}. The possible failure modes for a flatwise tension test are core failure, cohesive failure, adhesive failure, facesheet failure, or disbond between one of the facesheets and aluminum block. Core failure occurs when there are pieces of the core still bonded to both facesheets. In cohesive failure, there are remnants of the adhesive left on both the facesheet and core. Adhesive failure is characterized by disbonding of the adhesive from either the core or facesheets such that no adhesive remains on one surface. Facesheet failure is tensile failure of one of the facesheets, with delamination between the individual layers. Disbonding of the epoxy paste adhesive between the facesheets and aluminum block is not considered a valid failure mode.

Two 12-in. x 12-in. facesheets (CG25.4 and CG25.5) were fabricated from the random wetlay mat and then bonded to a 12-in. x-12 in. piece of honeycomb core using the polyurethane glue. A 2.75-in. x 2.75-in. flatwise tension sandwich specimen was cut from the center of the panel. A 2-in. wide beam specimen, which was to be tested in three-point bending, was also cut from the panel. All cutting was done using a diamond saw and liquid coolant. Extreme care was taken not to damage the bond between the facesheets and honeycomb. The stress vs. displacement relations for this specimen are given in Figure 5.2. The flatwise tensile strength was 39.8 psi at a displacement of 0.01150 in. There was no adhesive remaining on the core after failure, so the failure mode was adhesive in nature. As discussed in Section 4.3, the bond did not appear to be adequate because there was no fillet at the base of the honeycomb walls.

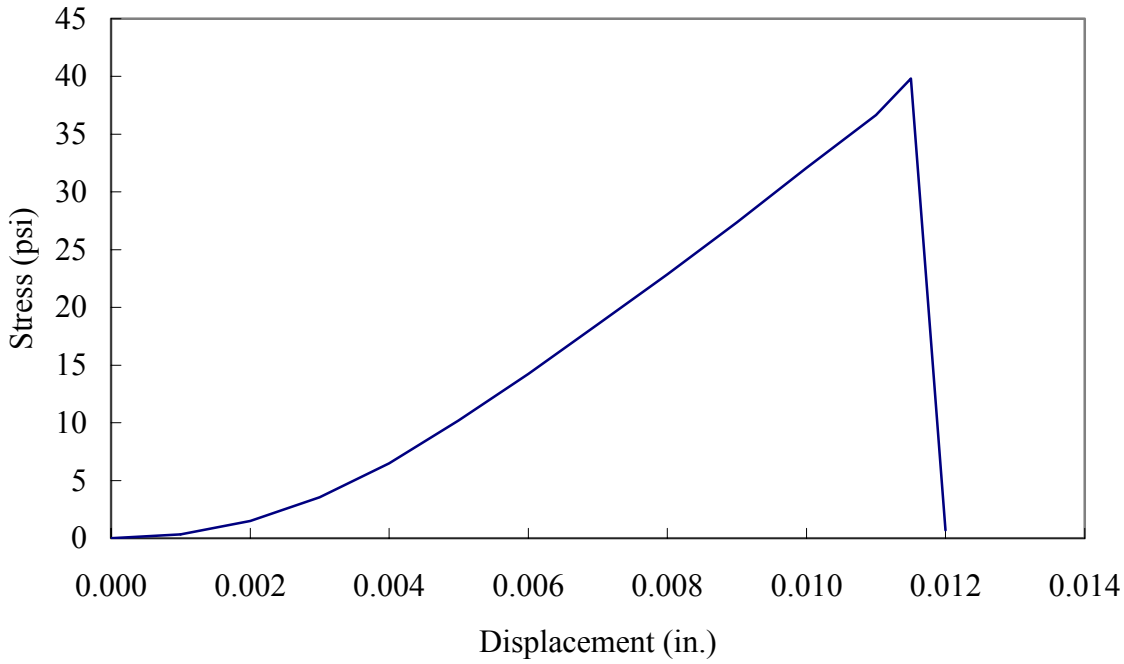

Figure 5.2: Flatwise tension test result for polyurethane glue

In an attempt to improve the flatwise tensile strength, additional flatwise tension tests were performed on sandwich panels bonded using three different adhesives: polyurethane glue with Cab-O-Sil filler; an epoxy paste; and a 3M Scotch-Grip™ plastic adhesive. Three 6-in. x 6-in. square sandwich panels were fabricated using each of the three different types of adhesives. Each 6-in. x 6-in. sandwich panel was cut into four 2.75-in. x 2.75-in. flatwise tension specimens. Three of the four specimens for each type of adhesive were then tested in flatwise tension. Table

5.1 lists the flatwise tensile strength and failure mode for each specimen. The measured stress vs. displacement relations are given in Figure 5.3. The previous results for polyurethane glue are shown on the same plot.

Table 5.1: Flatwise tension test results

	Polyurethane w/ Cab-O-Sil		Epoxy Paste		3M Plastic Adhesive	
Specimen #	Strength (psi)	Failure Mode	Strength (psi)	Failure Mode	Strength (psi)	Failure Mode
1	-	Cohesive	118.3	Adhesive	57.9	Adhesive
2	182.7	Disbond	114.4	Adhesive	101.8	Cohesive
3	177.4	Disbond	107.3	Adhesive	81.4	Adhesive
Average	180.0		113.3		80.3	

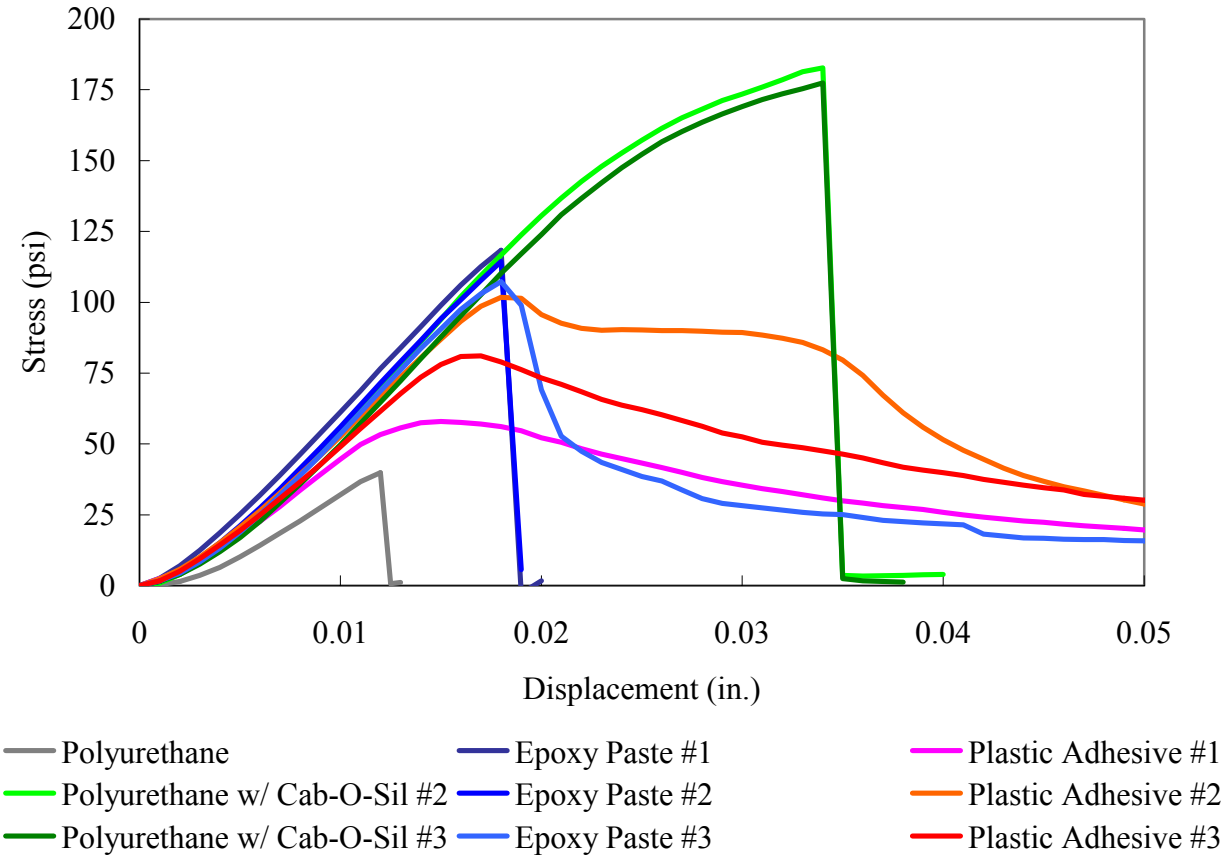

Figure 5.3: Flatwise tension test results for polyurethane glue with Cab-O-Sil, epoxy paste, and 3M Scotch-Grip™ plastic adhesive

The three tests of sandwich specimens bonded with polyurethane glue with Cab-O-Sil did not give an accurate description of the flatwise tensile strength. The first specimen failed cohe-

sively because there was polyurethane present on both the facesheet and core. Unfortunately, the data for this specimen were lost due to a floppy disk error. The other two tests were not valid because the epoxy paste bonding the facesheets to the aluminum blocks failed adhesively with the facesheets. These disbonds were characterized by a brittle fracture, with a dramatic decrease in the load. Although the second specimen initially failed due to disbond between the facesheet and one aluminum block, an interesting result was obtained when the sandwich specimen was completely separated from that block. As shown in Figure 5.4, a small portion in the bottom right corner of the specimen failed adhesively with the facesheet, and another small portion exhibited facesheet failure.

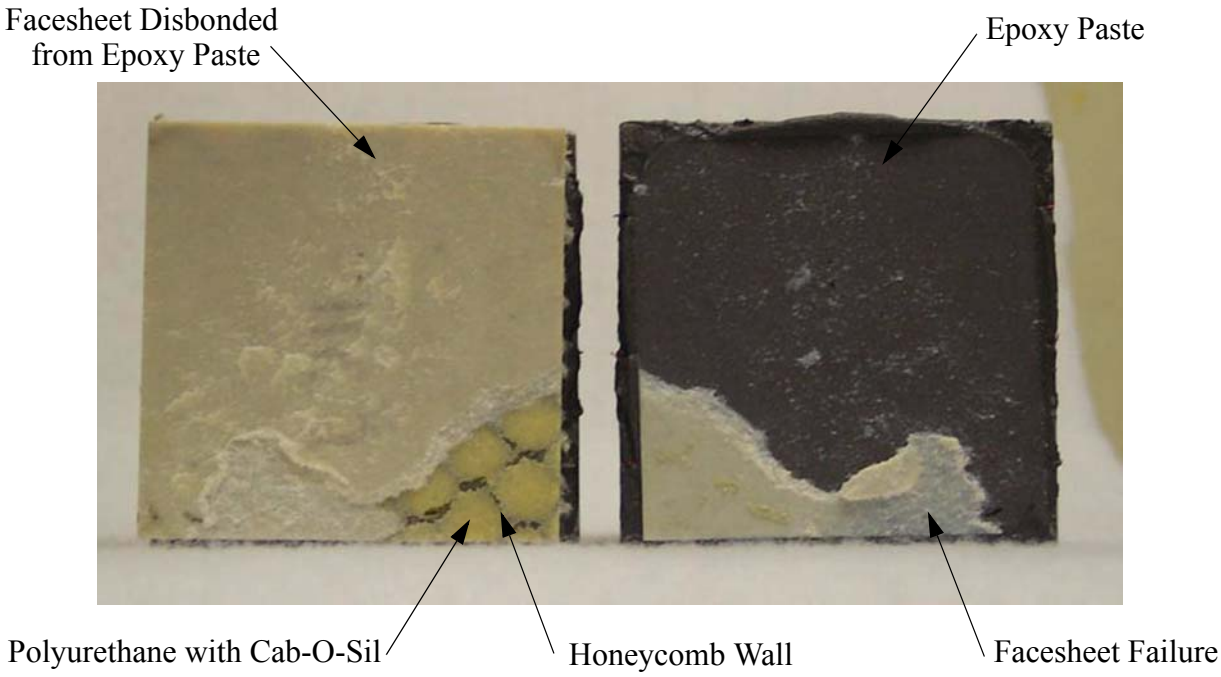

Figure 5.4: Mixed failure mode of polyurethane glue with Cab-O-Sil specimen #2

The flatwise tensile strength of the sandwich specimens bonded with the epoxy paste was considerably less than the strength of the bond between the facesheets and aluminum blocks. The first two specimens experienced abrupt failures, while the third showed a gradual decrease in load. In all three specimens, the epoxy failed adhesively with the facesheet. Figure 5.5 shows the honeycomb pattern still visible on the facesheet where the adhesive failed. It was concluded that the epoxy paste does not bond well to the surface of the glass/PET composite facesheets.

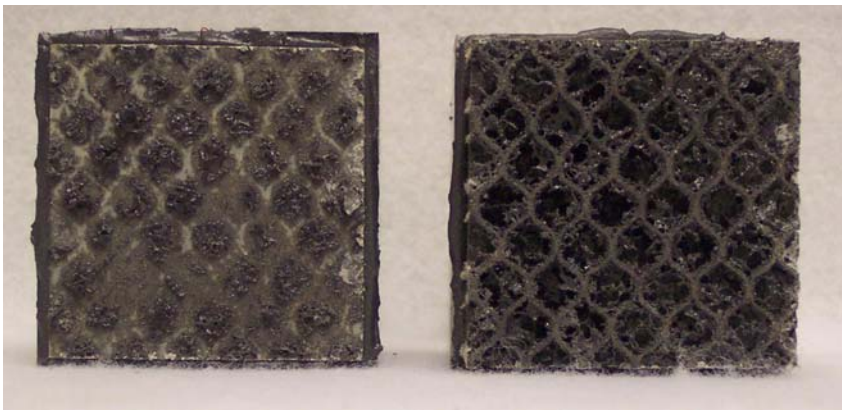

Figure 5.5: Adhesive failure of epoxy paste specimen #1

The Scotch-Grip™ plastic adhesive showed a wide variability results, despite the fact that all three specimens were cut from the same original 6-in. x 6-in. panel. The only similarity was the fact that the load decreased in a smooth gradual manner, unlike the more sudden failure of the epoxy paste. The second specimen had the highest strength and failed cohesively with adhesive remaining on both the facesheet and core, as shown in Figure 5.6. The other two specimens had less strength and failed adhesively with the honeycomb core. One possible explanation for this result is that the adhesive layer was not uniform when spread onto the facesheet. The plastic adhesive cured so rapidly in the atmosphere that the uniformity was very difficult to control.

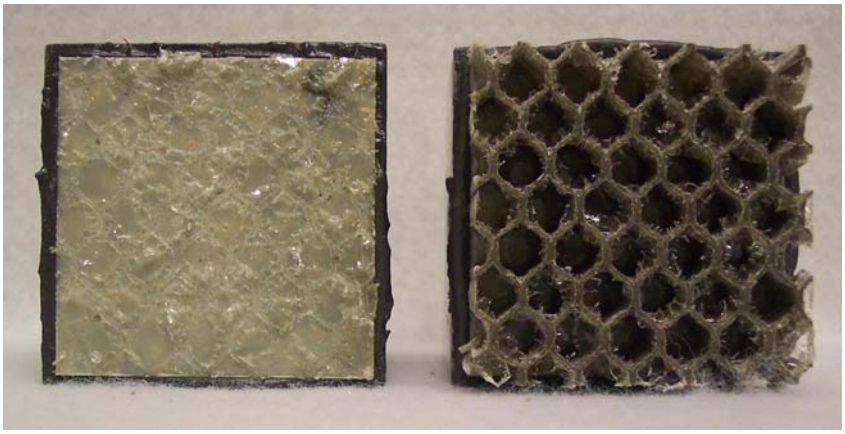

Figure 5.6: Cohesive failure of Scotch-Grip™ plastic adhesive specimen #2

The initial flatwise tension tests of the sandwich panels bonded using the polyurethane glue with Cab-O-Sil proved inconclusive, so additional flatwise tension tests were performed. In this set of tests, the polyurethane glue was used instead of the epoxy paste to bond the facesheets

to the aluminum blocks because it was thought that the polyurethane glue would be less likely to disbond from the facesheets. The results from the first specimen tested in this manner are shown by the brown curve (Polyurethane w/ Cab-O-Sil #4) in Figure 5.7. This curve closely matches the two previous green curves from Figure 5.3 until the point of failure. Once again, one of the facesheets disbonded from an aluminum block because the majority of the liquid polyurethane glue had been squeezed out from between the facesheets and aluminum blocks before it had a chance to cure. A second specimen was bonded to the aluminum blocks by adding three strips of thin wire between the facesheets and aluminum blocks to prevent the polyurethane glue from being squeezed out. The results from this specimen are shown by the pink curve (Polyurethane w/ Cab-O-Sil #5) in Figure 5.7. The flatwise tensile strength was much less because the polyurethane glue between the facesheets and aluminum blocks failed cohesively. A more suitable adhesive was necessary for bonding the facesheets and aluminum blocks. However, from the results in Table 5.1, it can be seen that the strength of the polyurethane glue with Cab-O-Sil bond between the facesheets and core was greater than 182.7 psi.

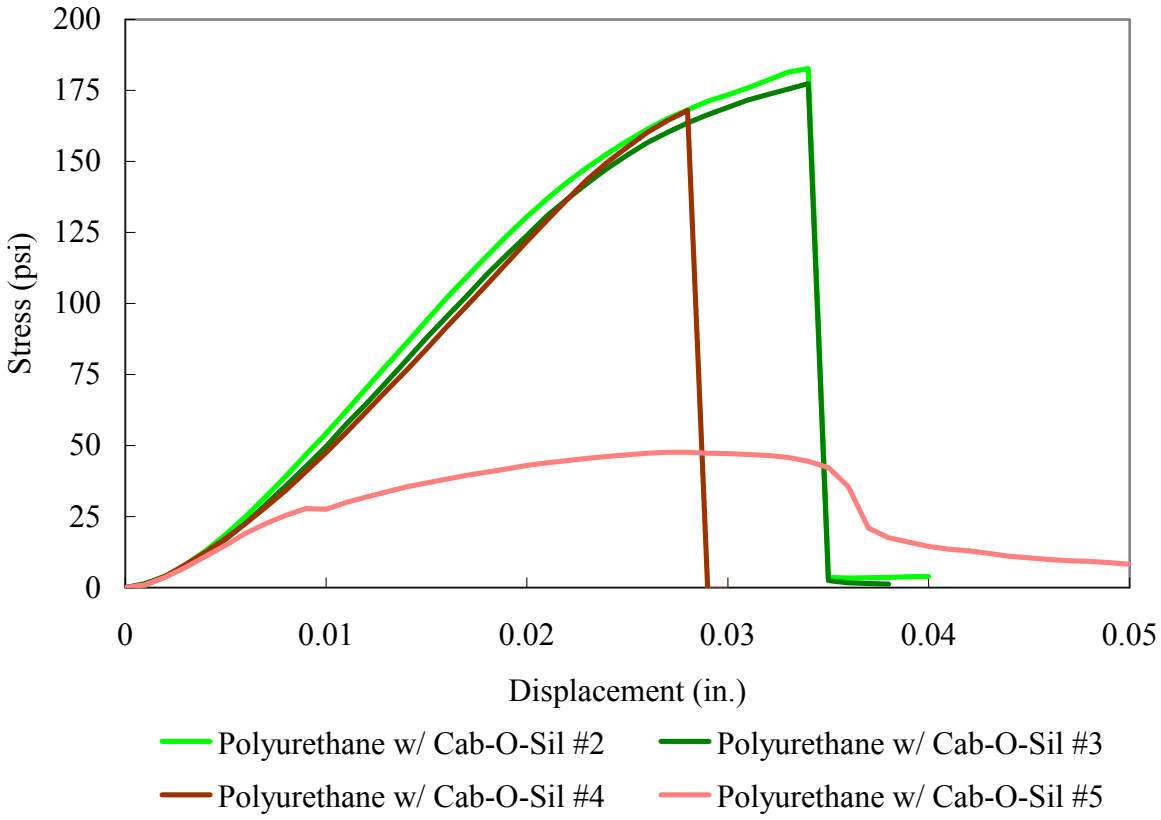

Figure 5.7: Additional flatwise tension test results for polyurethane glue with Cab-O-Sil

5.2 Displacement Tests of Sandwich Beam

To determine the accuracy of the simply-supported beam model from Section 2.3, a three-point bend test was performed according to ASTM C 393 [11]. The 2-in. wide beam specimen cut from the sandwich panel bonded with the polyurethane glue, and mentioned in the previous section, was used. The ribbon direction of the core was along the length of the beam.

The experimental setup for the three-point bend test is shown in Figure 5.8. The span of the beam was 10 in. from one simple support to the other. The beam was loaded with a series of weights hanging underneath the simple support fixture on a weight pan. The load was transferred to the beam through a steel rod which supported the weight pan with a tension wire. The three dial gauges used for displacement measurements were attached to the steel plates using magnetic bases. The entire fixture was supported by steel bars which spanned two sawhorses. A *Solid-Works* model of the test fixture is shown in Figure 5.9.

Figure 5.8: Displacement test of sandwich beam

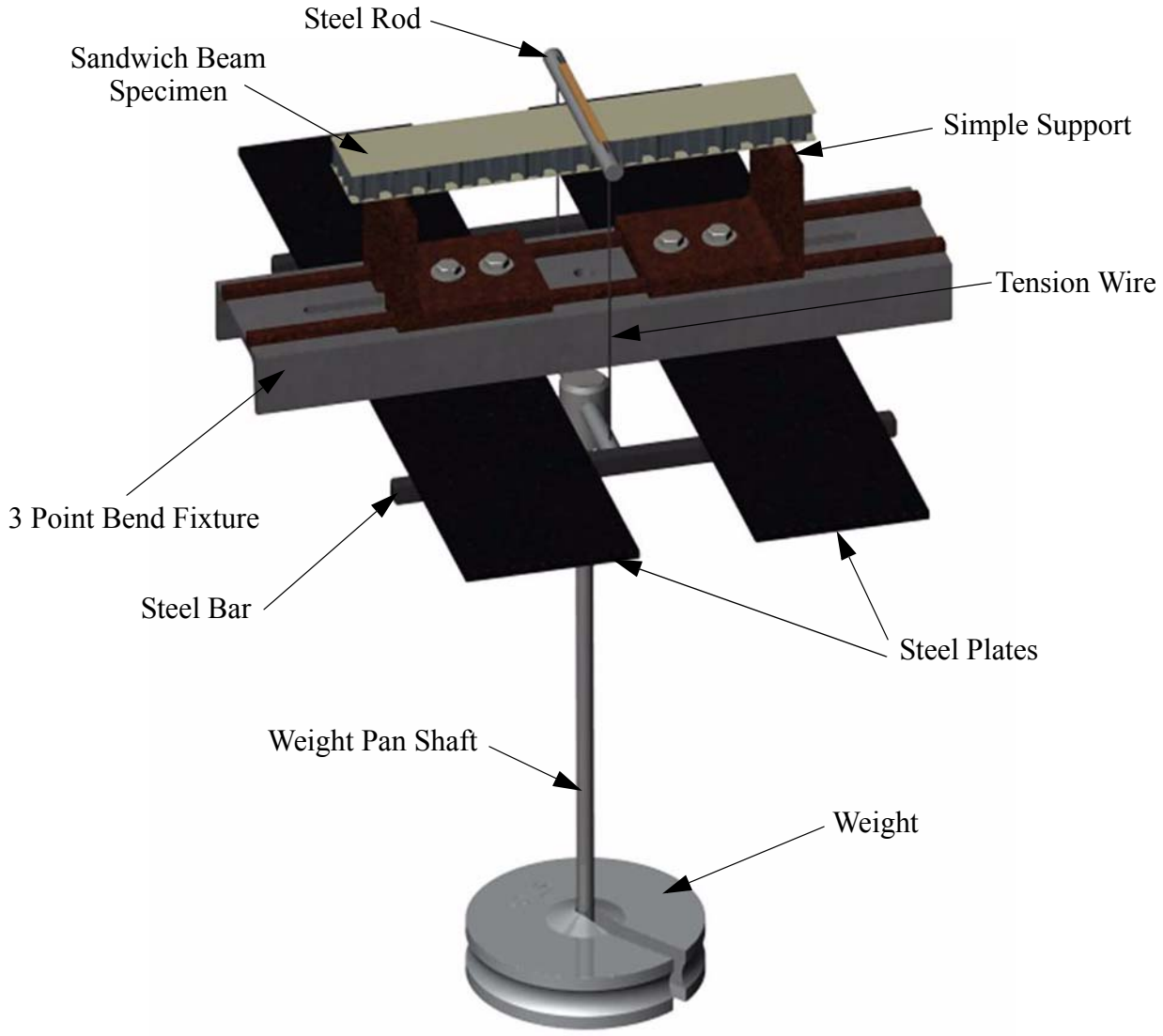

Figure 5.9: Beam test fixture model

The dial gauges were placed at the midspan and quarter-spans of the beam. Each gauge was initially zeroed with only the weight pan, which had a weight of 2.07 lb. The beam was loaded by carefully placing four 10-lb weights onto the weight pan. The displacement of the beam at each dial gauge location was recorded to the nearest 0.0001 in. after each weight was applied. The weights were then removed one at a time as the displacements were recorded to determine if the displacement returned to zero. After the initial test, the beam was rotated such that the quarter-span dial gauges were reversed. The loading and unloading procedure was then repeated. The third test was performed on the beam reoriented such that the facesheet initially on top and in contact with the dial gauges was on the bottom. The beam was rotated once more for a

fourth and final test. By rotating and reorienting the beam, it was possible to examine the effect of the non-uniformity of the facesheets.

As shown in Table 4.1, the facesheets of the beam made from random wetlay panels CG25.4 and CG25.5 had a large degree of non-uniformity. Therefore, the facesheet thickness was considered to vary along the length of the beam, as discussed in Section 2.8. Before the facesheets were bonded to the core, the thickness of each facesheet was measured along the length of the beam. Because the beam model is one-dimensional, it was assumed that the facesheet thickness did not vary significantly across the width of the beam. Figure 5.10 shows the measured facesheet thicknesses as a function of length and the best-fit quadratic polynomials to the data with the origin in the center of the beam. The thickness for the top, $t_T(x)$, and bottom, $t_B(x)$, facesheets can be approximated by

$$t_T(x) = -0.237x^2 + 0.551x + 29.7 \tag{5.2}$$

$$t_B(x) = -0.230x^2 + 0.230x + 29.8 \tag{5.3}$$

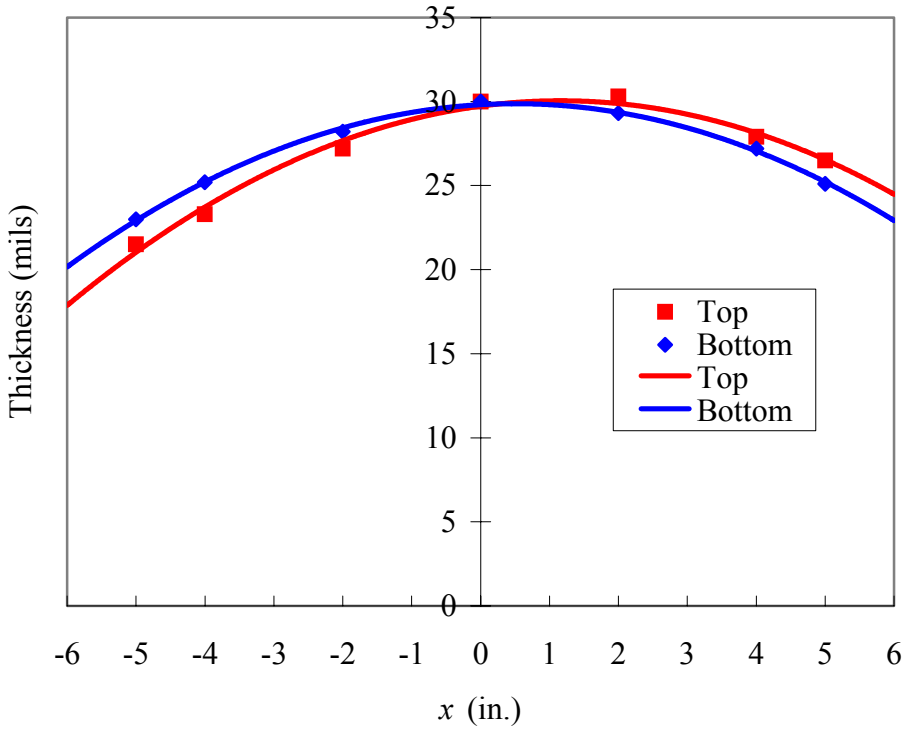

Figure 5.10: Facesheet thicknesses of beam specimen

The predicted compliance along the length of the sandwich beam is given in Figure 5.11. The facesheet elastic modulus is assumed to be 1.105 msi, the average value measured by Lu [21]. The displacement is found by multiplying the compliance by the applied load, in pounds. The non-uniform solution uses the facesheet thicknesses shown in Figure 5.10. The uniform solution assumes an average facesheet thickness of 26.8 mils. The difference between the two solutions at the center of the beam is only 4.77%. The non-uniform facesheet compliance appears almost symmetric despite the non-uniformity of the facesheets. The predicted compliance at $x = -L/4$ is 1.221 mils/lb and the predicted compliance at $x = L/4$ is 1.208 mils/lb. The predicted compliance for the non-uniform facesheets at the midspan of the beam is 2.03 mils/lb. No distinction is made in the model between which facesheet is on the top or bottom of the sandwich.

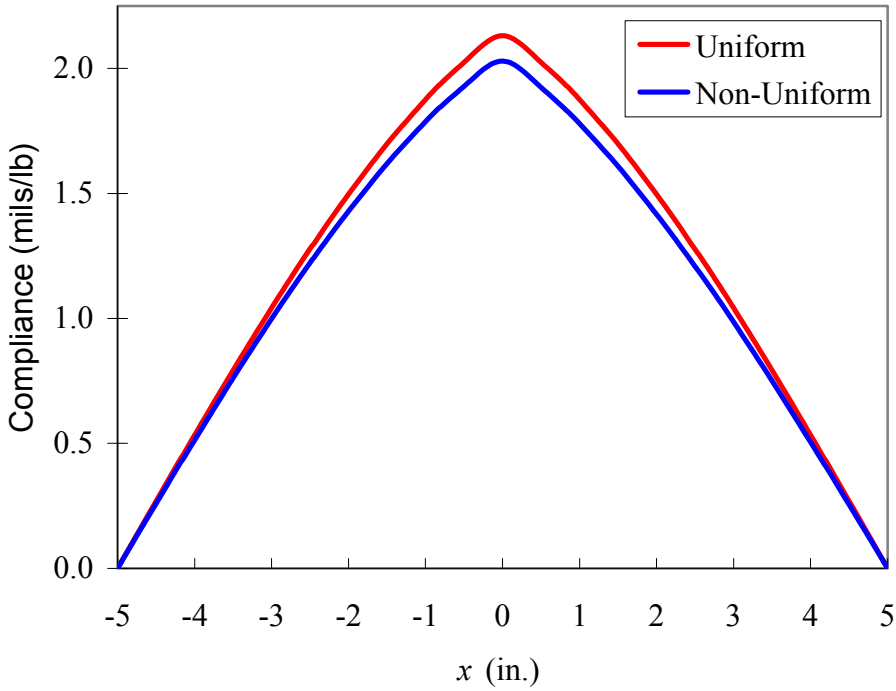

Figure 5.11: Predicted sandwich beam compliance

The measured displacements at the midspan and quarter-spans of the beam are shown in Figures 5.12 through 5.14 for applied loads of 10, 20, 30, and 40 lb. Four trials were performed at each load level, as described previously. Care was taken to measure at the same x-location on the beam as it was rotated and reoriented for the four different trials. For each trial, the displacement data were very linear with the applied load for all four all applied load levels. However, the

straight line fit to these four data points did not pass through the origin. The experimental displacement data and the least-squares straight line fit to the data for each trial are given in Appendix B. It was thought that non-perfect support conditions were responsible for the least-squares straight lines not passing through the origin. The slopes of the least-squares straight lines represent the measured compliance of the beam in mils/lb. At the midspan of the beam, the average compliance was 2.32 mils/lb. At $x = -L/4$, the average compliance was 1.375 mils/lb, and at $x = L/4$, the average compliance was 1.361 mils/lb.

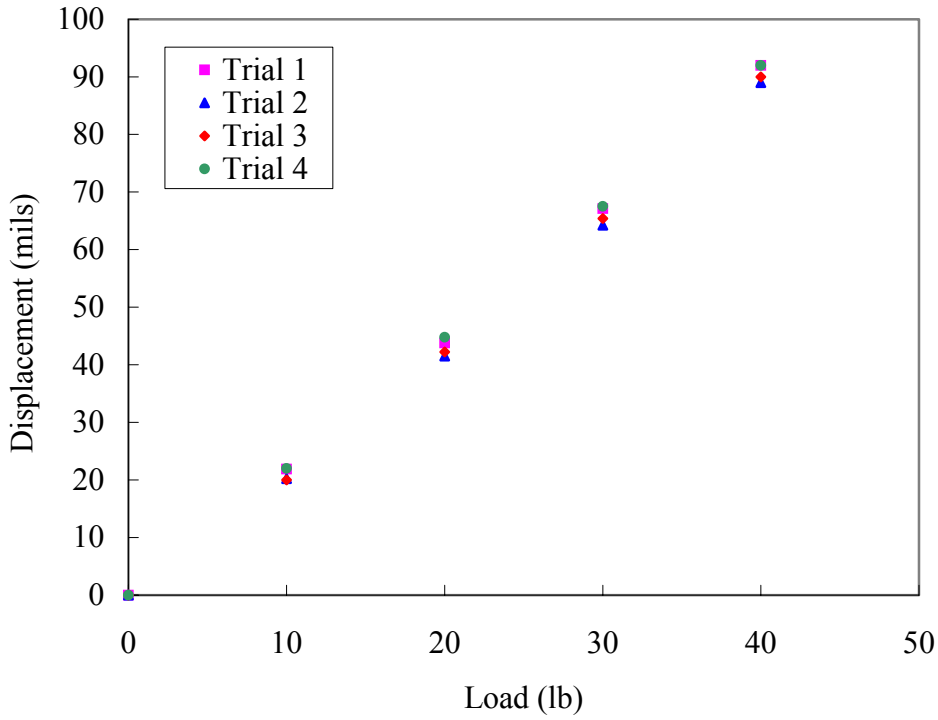

Figure 5.12: Measured midspan ($x = 0$) displacements of sandwich beam

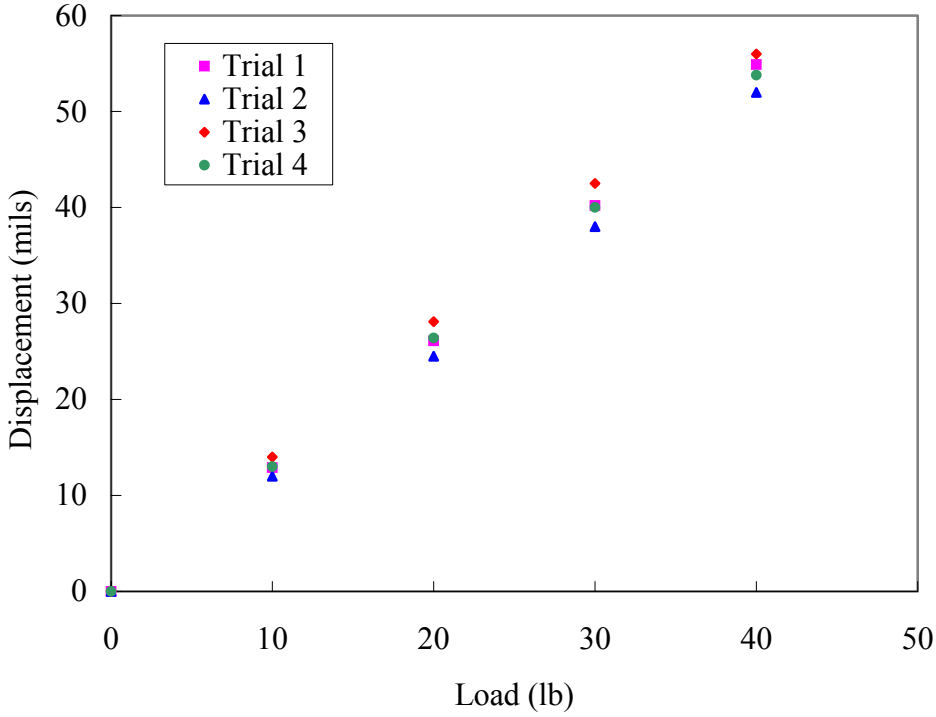

Figure 5.13: Measured quarter-span ($x = -L/4$) displacements of sandwich beam

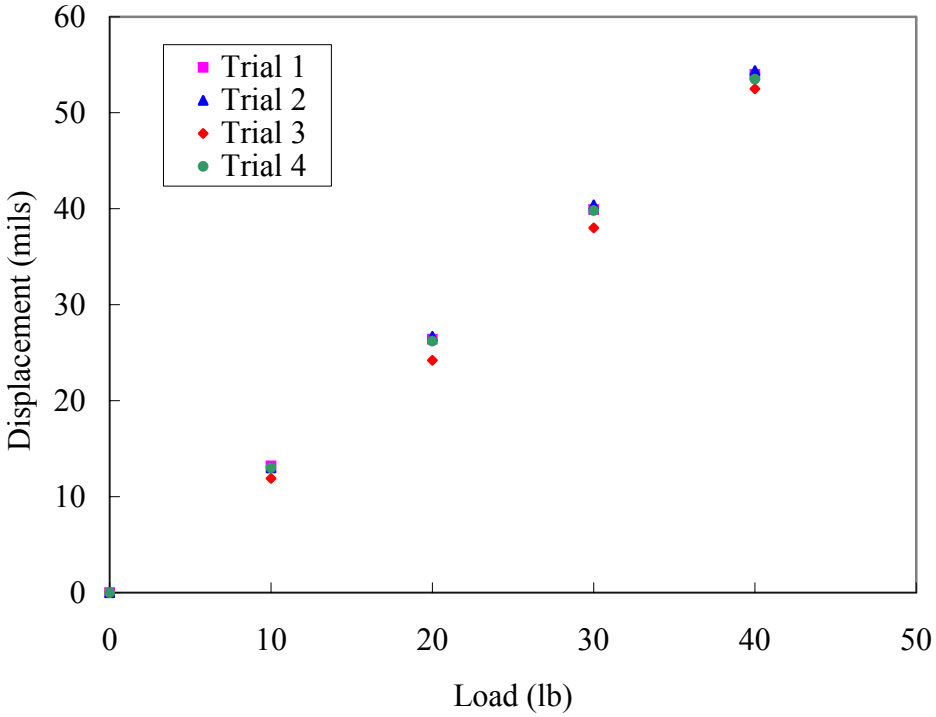

Figure 5.14: Measured quarter-span ($x = L/4$) displacements of sandwich beam

The predicted compliances at the midspan and quarter-spans of the beam given in Figure 5.11 were less than the measured compliances determined from the slopes of the straight line fits in Appendix B. The facesheet elastic modulus of 1.105 msi was adjusted in the sandwich beam theory until the predicted compliances matched the measured compliances. The smallest elastic modulus measured by Lu [21] was 1.063 msi, but the predicted compliances were still less than the measured compliances. It was found that an effective facesheet elastic modulus of 0.900 msi, 19% less than the average value reported by Lu, gave good agreement between the predicted displacements and the measured data, as shown in Figures 5.15 through 5.17. The measured data in the figure are shifted by an amount equal to the intercept of the least-squares line such that the least-squares line passes through the origin.

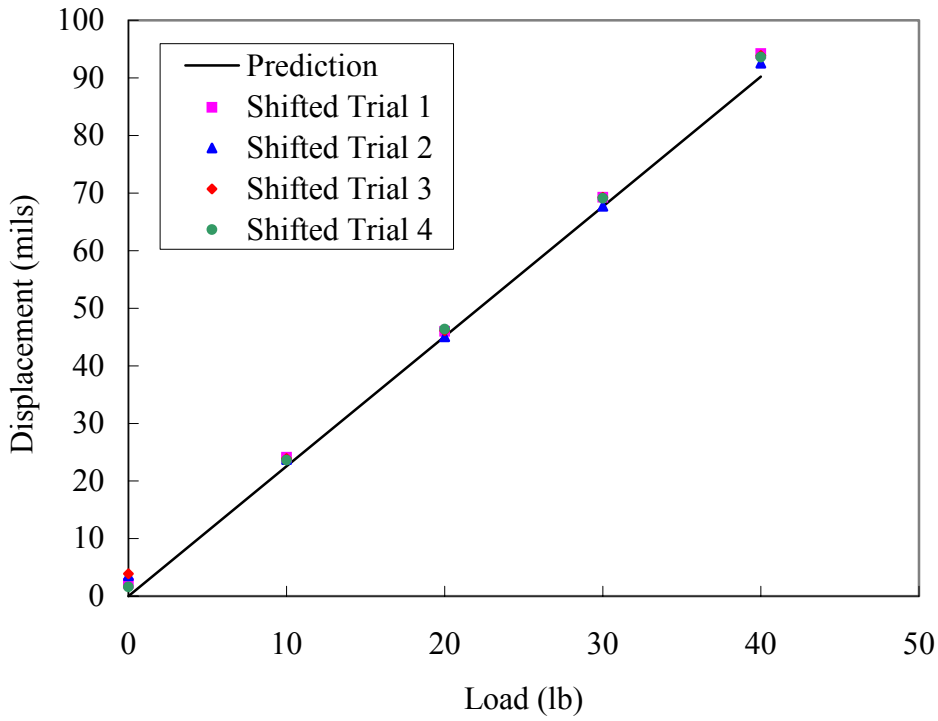

Figure 5.15: Predicted and shifted midspan ($x = 0$) displacements of sandwich beam

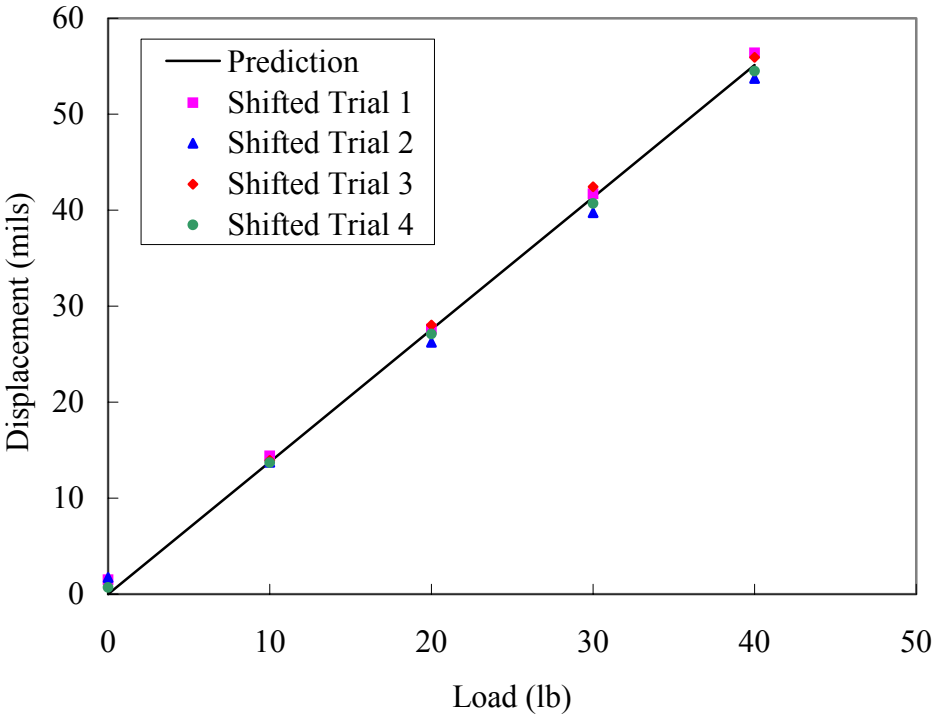

Figure 5.16: Predicted and shifted quarter-span ($x = -L/4$) displacements of sandwich beam

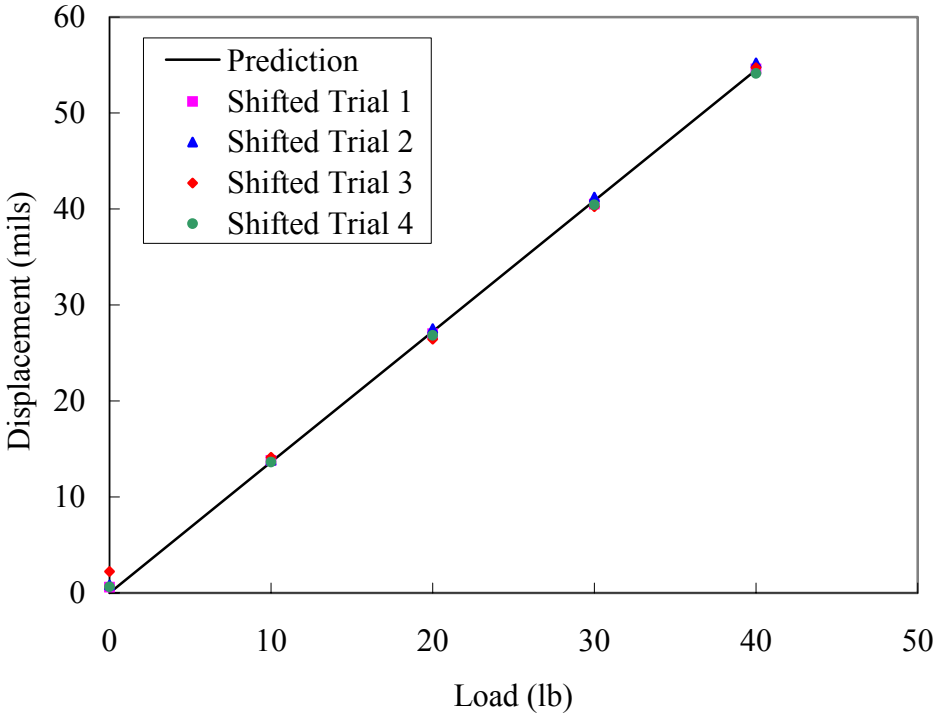

Figure 5.17: Predicted and shifted quarter-span ($x = L/4$) displacements of sandwich beam

5.3 Displacement Tests of Sandwich Plate

As discussed in Chapter 3, a uniform load would have been difficult to apply over the entire surface of a sandwich plate. Therefore, a representative line load was applied to a 12-in. x 12-in. sandwich plate that was simply supported along two opposite edges and free along the other two edges. This arrangement was illustrated in Figure 3.15. To simulate the line load, a wiffle tree was designed to distribute a single point load along the center-line of the plate, as shown in Figure 5.18. The wiffle tree was attached to the sandwich plate through eight 50-lb capacity 0.030 in. diameter monofilaments with a crimped aluminum fastener at each end. The diameter of the holes drilled through the plate was 0.040 in. The fastener was designed be crimped by hand with pliers. Using a load cell, it was determined that 29 lb of tension were required to pull the crimped fastener off the monofilament. Thus, the maximum load that could be supported by eight monofilaments was 232 lb. The eight monofilaments were attached to four horizontal aluminum bars using the crimped fasteners. Several more vertical and horizontal bars were used to reduce the wiffle tree down to a single weight pan shaft, similar to that of the three-point bend test for the sandwich beam. Steel pins were used to hold the wiffle tree together so that the aluminum bars could rotate independently to permit the anticlastic curvature of the plate to develop. The total weight of the wiffle tree fixture was 3.91 lb.

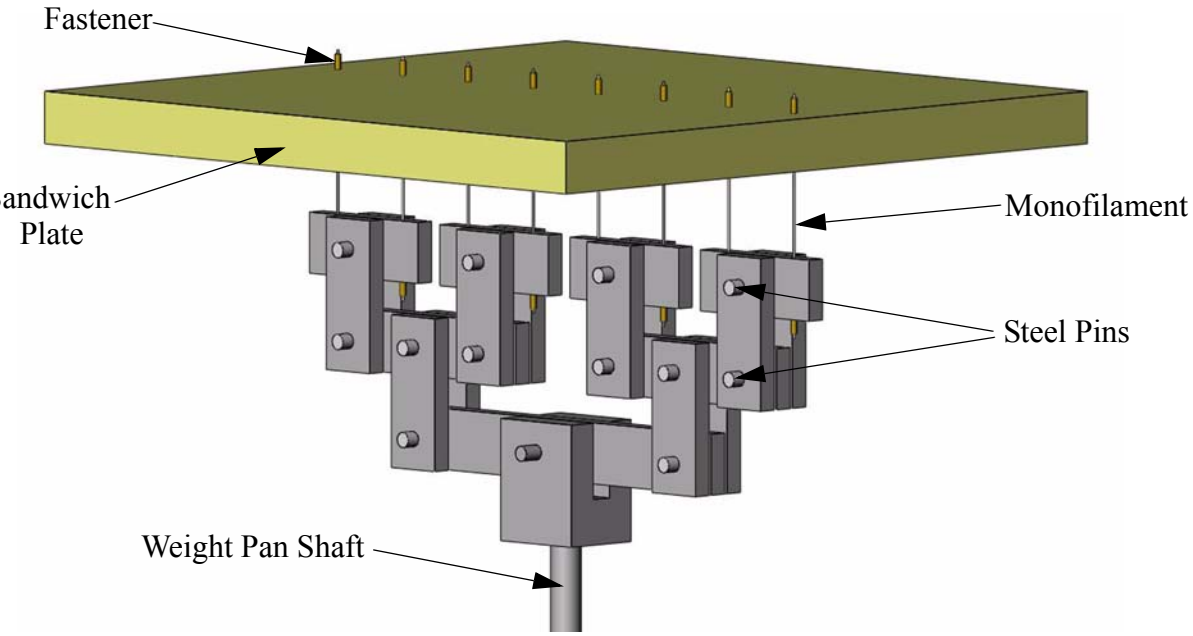

Figure 5.18: Wiffle tree fixture model

The experimental setup for measuring the displacements of the sandwich plate is shown in Figure 5.19. The facesheets used in the sandwich plate were CG25.14 and CG25.15. They were bonded to the core using the polyurethane glue with Cab-O-Sil. The plate was supported on the top surfaces of two tables. Extreme care was taken to assure that the two tables were rigid and level. Part of the wiffle tree can be seen hanging beneath the plate between the two tables. Round wooden dowels were used as the simple supports, and the bottom facesheet of the plate simply rested on the dowels. The span from one simple support to the other was 11 in. This approach was used because, as discussed in Chapter 3, no downward forces were required on the corners of the plate to enforce the zero displacement corner conditions. Wooden dowels were used as the simple supports because it was thought that the wood would conform slightly to account for the non-uniformity of the facesheets, but not significantly enough to cause an overall rigid body displacement of the plate. The analysis used to estimate the deformations of the round wooden dowels is given in Appendix C. Small strips of tape were used to keep the wooden dowels from rolling. Four dial gauges were used to measure the displacements of the plate at various positions.The dial gauges were held in place by magnetic bases attached to steel plates. Dial gauge #1 was placed at the free edge along the center-line of the plate. Dial gauge #2 was located at the center of the plate. Dial gauge #3 measured the displacement at the end of the support, and dial gauge #4 measured the displacement at the midlength of the support.

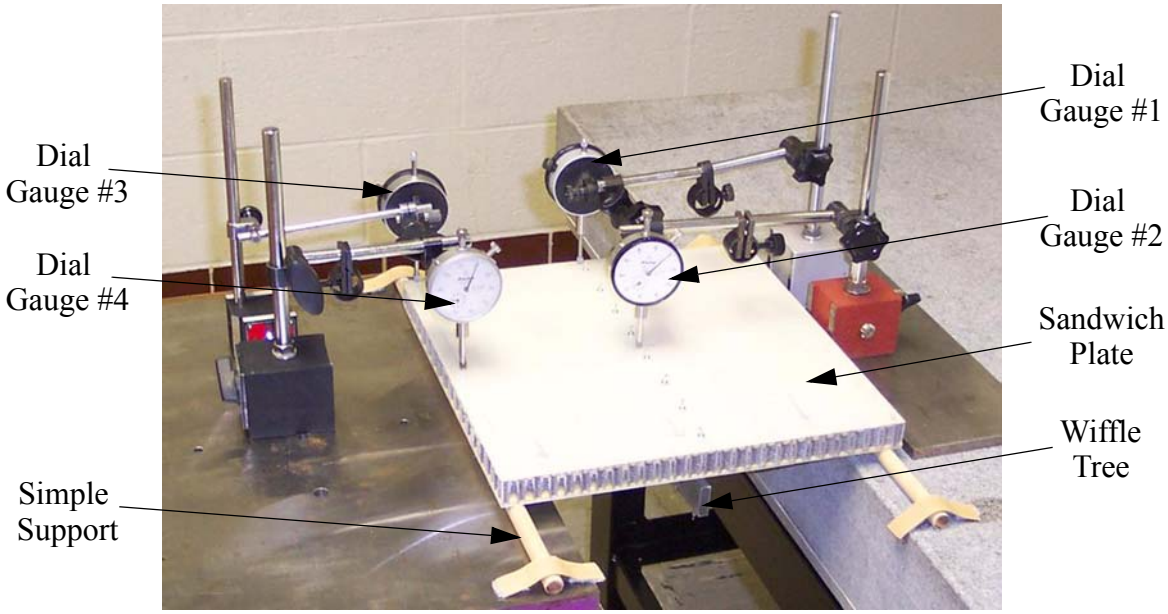

Figure 5.19: Displacement test of sandwich plate

Before the wiffle tree was attached, each of the dial gauges was set to zero. The wiffle tree was then carefully constructed and the displacements were recorded to the nearest 0.0001 in. The weight of the wiffle tree was found to cause measurable displacements at all four dial gauge locations. Twelve 10-lb weights were then added to the weight pan, for a maximum load of 123.9 lb, including the weight of the wiffle tree. The weights were applied as quickly as possible to reduce the effects of creep. The measured displacements at each dial gauge are shown in Figure 5.20. The anticlastic curvature of the plate is immediately obvious, because the displacement at the free edge is greater than the displacement at the center of the plate.

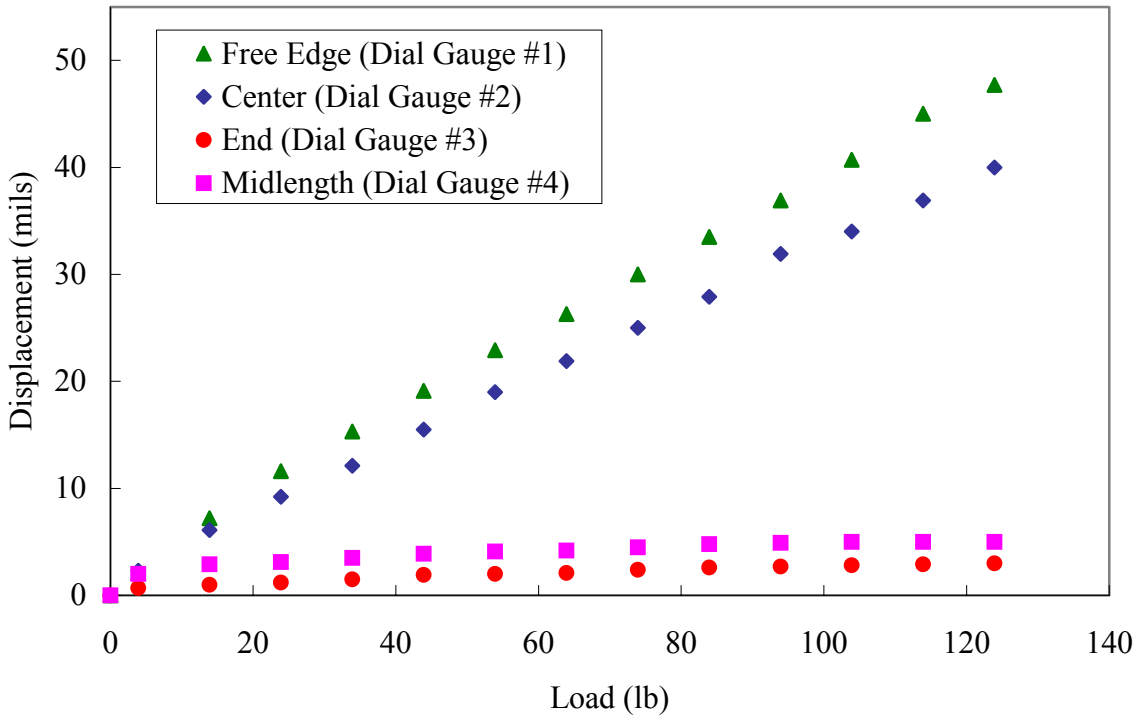

Figure 5.20: Measured displacements of line-loaded sandwich plate

As can be seen from Figure 5.20, the displacements along the loaded center-line of the plate (dial gauges #1 and #2) were not initially linear with the applied load. Also, the displacements at the simple supports (dial gauges #3 and #4) were not entirely negligible compared to the displacements along the center-line of the plate. It was thought that the displacements at the supports and the nonlinearity away from the supports resulted from the non-uniform thickness of the bottom facesheet. Before any load was applied, a small of amount of light was seen at various points between the bottom facesheet and round wooden dowel supports, indicating that some por-

tions of the facesheet were not in contact with the supports. At large loads, the displacements along the center-line of the plate kept increasing, while the displacements at the supports became stationary. It was theorized that the displacements at the supports became stationary because uniform contact along the length of the supports had occurred. As a result, the center-line displacement data for large loads were quite linear and were thought to reflect the actual stiffness of the plate. Figure 5.21 shows the best-fit straight line through the data in the region where the support displacements were stationary. The equations of the lines are

$$w_1 = 0.350F + 4.33 \tag{5.4}$$

$$w_2 = 0.300F + 2.79 \tag{5.5}$$

where F is the total applied load in lb, and w_1 and w_2 are the displacements of the free edge and center of the plate in mils, respectively. (The center data point was removed from the free edge data because it was clearly out of line with respect to the rest of the data.) The slopes of the lines represent the measured compliances of the plate in mils/lb.

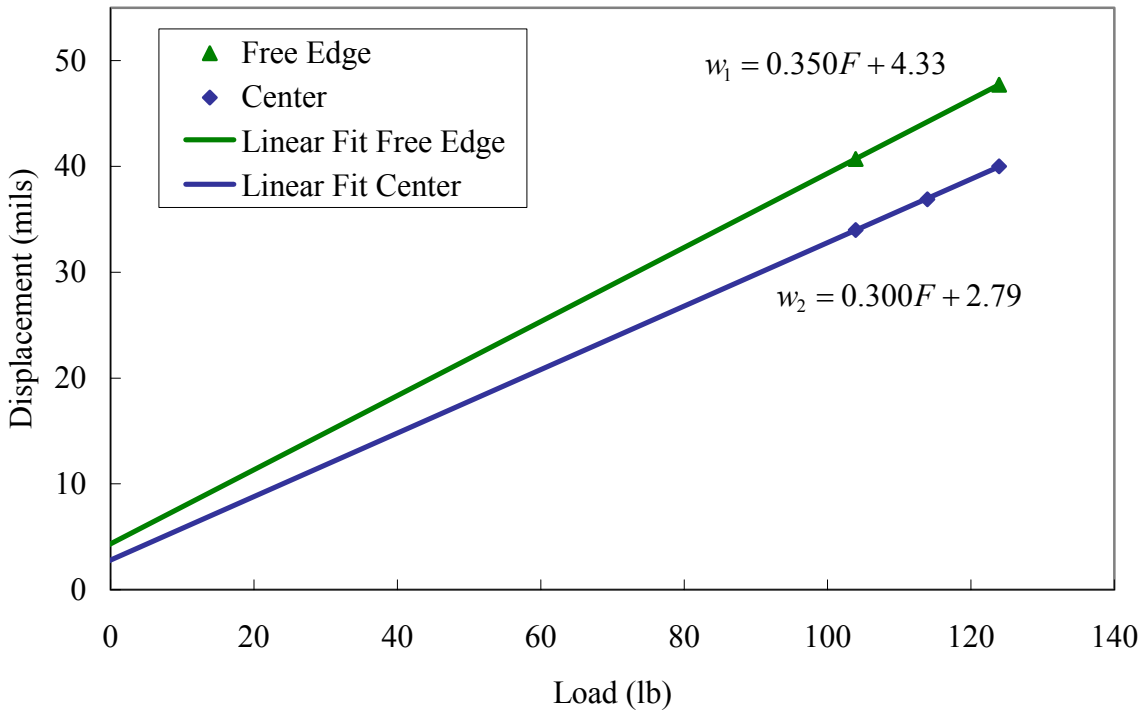

Figure 5.21: Linear fit of stationary data for line-loaded sandwich plate

To remove the influence of the displacements at the supports due to the lack of complete initial contact with the bottom facesheet, the measured data at the free edge and center of the plate (dial gauges #1 and #2) were shifted by an amount equal to the intercepts of the lines in Figure 5.21. The shifted data are shown in Figure 5.22, along with the shifted straight line fits. Although the shifted data were negative for low load levels, they were positive and appeared linear for loads above 50 lb. Thus, the effects of the displacements at the supports could be removed from the data to determine the true compliance of the plate. The compliance data were then used to estimate the effective material properties of the facesheets. This step was believed to be essential because it is important to know how closely using accepted values of material properties measured by other researchers in the idealized models matches with reality.

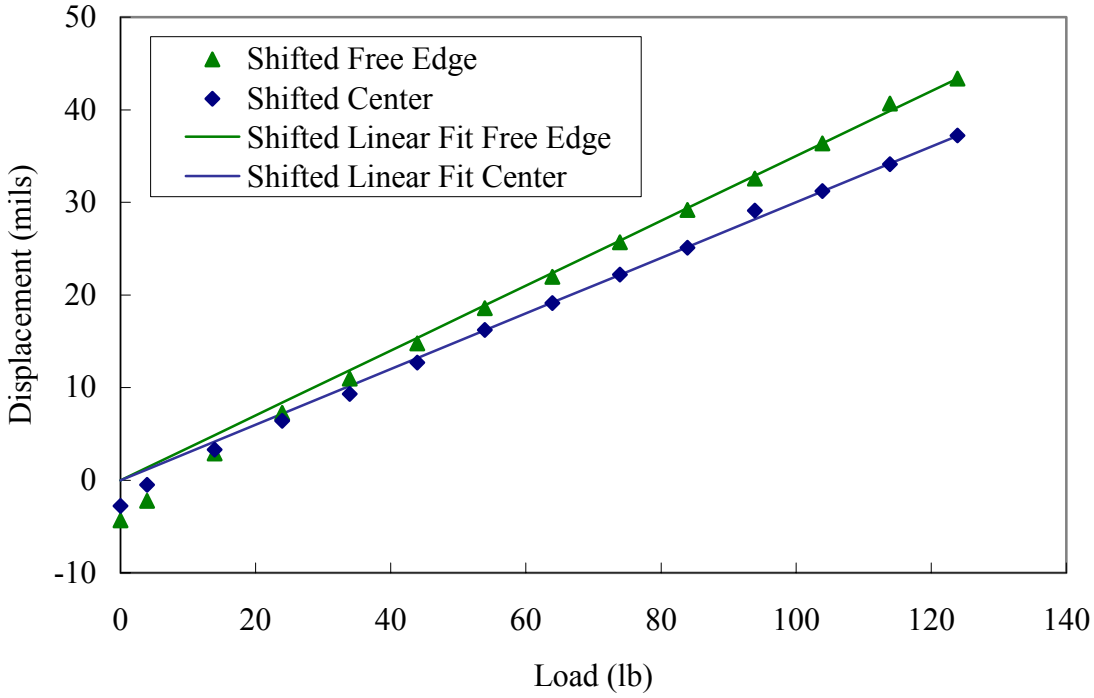

Figure 5.22: Shifted displacements of line-loaded sandwich plate

There were many factors that influenced the compliance of the sandwich plate that were not considered in the development of the sandwich plate theory in Chapter 3. The elastic modulus of the facesheets was not accurately known because it was never measured directly. The average facesheet elastic modulus measured by Lu [21] was 1.105 msi, but individual measurements ranged from 1.063 msi to 1.145 msi. Also, there were no data available for Poisson's ratio of the facesheet material. The facesheets of the sandwich panel used in the plate test (CG25.14 and

CG25.15) were much more uniform than the facesheets of the sandwich panel used in the beam test (CG25.4 and CG25.5). However, it was shown in Figure 5.11 that the predicted displacements for the uniform and non-uniform beam differed only by 4.77%. Therefore, it was assumed that the non-uniformity of the facesheets used for the plate would not significantly affect the geometric midplane location and the local bending stiffness. The thickness of the facesheets was assumed to be an average value of 0.0384 in., as given in Table 4.1. Lastly, the polyurethane glue with Cab-O-Sil was significantly thick in comparison to the thickness of the core, as shown in Figure 4.12. This adhesive layer was thought to increase the bending stiffness of the plate by preventing the transverse shear of the core, and by increasing slightly the in-plane extensional modulus of the core, which was originally assumed to be negligible. Here, these unknown factors, with the exception of Poisson's ratio, were grouped together to produce an effective elastic modulus of the facesheet, which was estimated using the measured compliances and the sandwich plate theory in Section 3.8.

Figure 5.23 shows the predicted compliance of the sandwich panel for various values of the effective facesheet modulus and Poisson's ratio. The two dashed lines are the measured compliances from the slopes of the lines in Figure 5.21. The effective elastic modulus and Poisson's ratio were adjusted until the predicted compliances at the free edge and center of the plate closely matched the measured compliances. The first effective modulus considered was the average value of 1.105 msi, as measured by Lu. The predicted compliances were larger than the measured values, so the effective modulus was actually larger than this value, leading to a reduced overall measured compliance. The next effective modulus examined was 1.145 msi, the maximum elastic modulus measured by Lu. Once again the predicted compliances were too large. The effective elastic modulus was continuously increased until it was found that 1.330 msi centered the predictions between the two measured values. The three values considered for Poisson's ratio were 0.30, 0.35, and 0.40 shown in Figure 5.23 by the square, diamond, and triangle shapes, respectively. A larger Poisson's ratio had the effect of increasing the compliance at the free edge while decreasing the compliance at the center. A Poisson's ratio of 0.40 gave good agreement with measured compliances. Thus, the values of the effective elastic modulus and Poisson's ratio of the facesheets were taken to be 1.330 msi and 0.40. This effective modulus was 20% larger than the average value measured by Lu. The predicted displacements using these values in the sand-

wich plate theory from Section 3.8 are shown with the shifted data in Figure 5.24. There is good agreement between predictions and measurements for loads greater than about 40 lb.

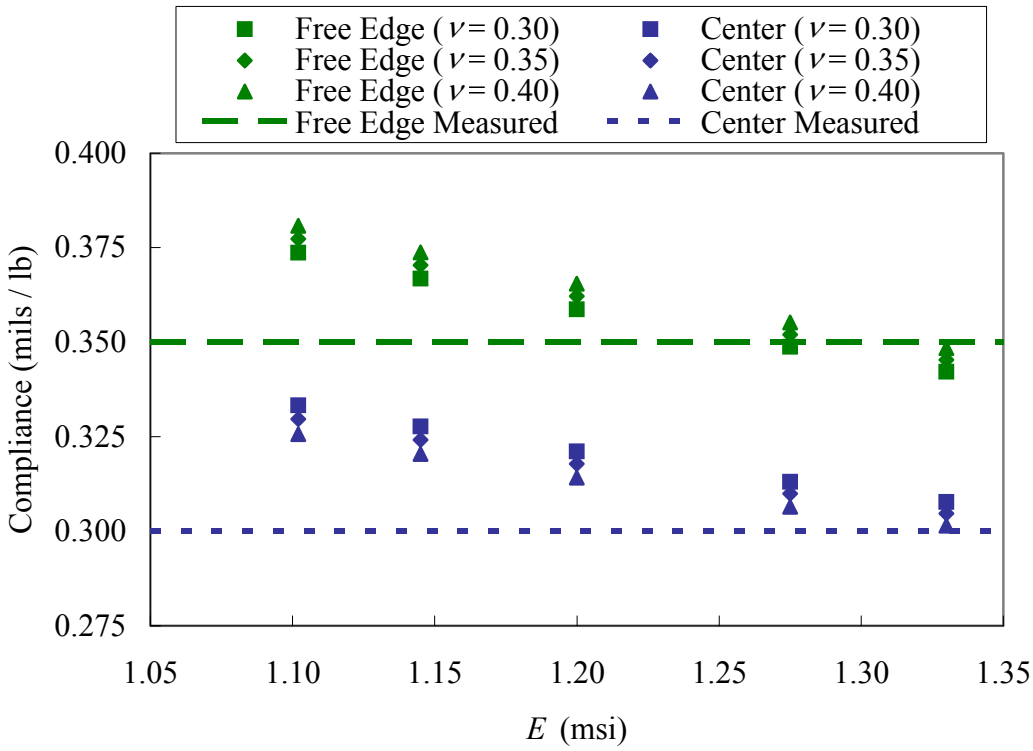

Figure 5.23: Effect of elastic modulus and Poisson's ratio on compliance of sandwich plate

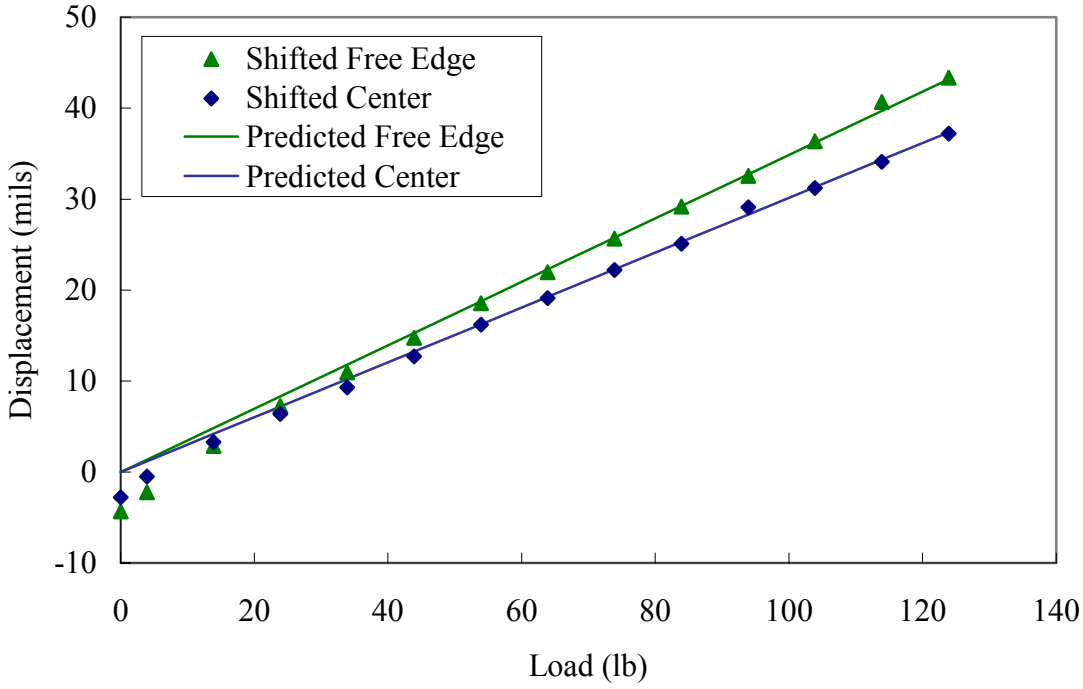

Figure 5.24: Predicted and shifted displacements of line-loaded sandwich plate

5.4 Shadow Moiré Tests of Sandwich Plate

Shadow moiré is a technique for visualizing the out-of-plane displacements of a plate by projecting beam of light through a reference grating of equally spaced parallel opaque and clear lines. A moiré fringe pattern is observed from the superposition of the reference grating and its shadow on the surface of the plate [35]. The displacements at every point of the plate can be determined. This technique was used to visualize the displacements of the line loaded sandwich plate discussed in Section 5.3.

The geometry associated with creating a shadow moiré is shown in Figure 5.25. The pitch of the reference grating, p, is the distance from the center of one clear line to the next. The beam of light strikes the reference grating at an angle of incidence α and projects a shadow from the opaque lines onto the specimen. For example, the dark line at a on the reference grating casts a shadow at a' on the specimen. It is assumed that the observer is at normal incidence, looking down on the specimen. A plot of the observed intensity of light is shown above the reference grating. At the locations where a clear line on the reference grating coincides exactly with a dark line (a shadow) on the specimen, a dark fringe of intensity 0 appears to the observer. At locations where a clear line on the reference grating coincides exactly with a space between shadows on the specimen, the maximum intensity appears to the observer. The distance between two adjacent fringes as seen by the observer is δ. The out-of-plane displacements from the reference grating to the specimen at these two fringe locations are d_1 and d_2. From simple geometry, it is found that

$$d_2 - d_1 = \frac{p}{\tan\alpha} \tag{5.6}$$

If the distance d_1 is known to be zero at some point on the specimen, the fringe order is considered to be zero at this location. Each successive visible fringe location increases the fringe order by one. The out-of-plane displacement, w, at an arbitrary fringe order n is then given by

$$w = \frac{np}{\tan\alpha} \tag{5.7}$$

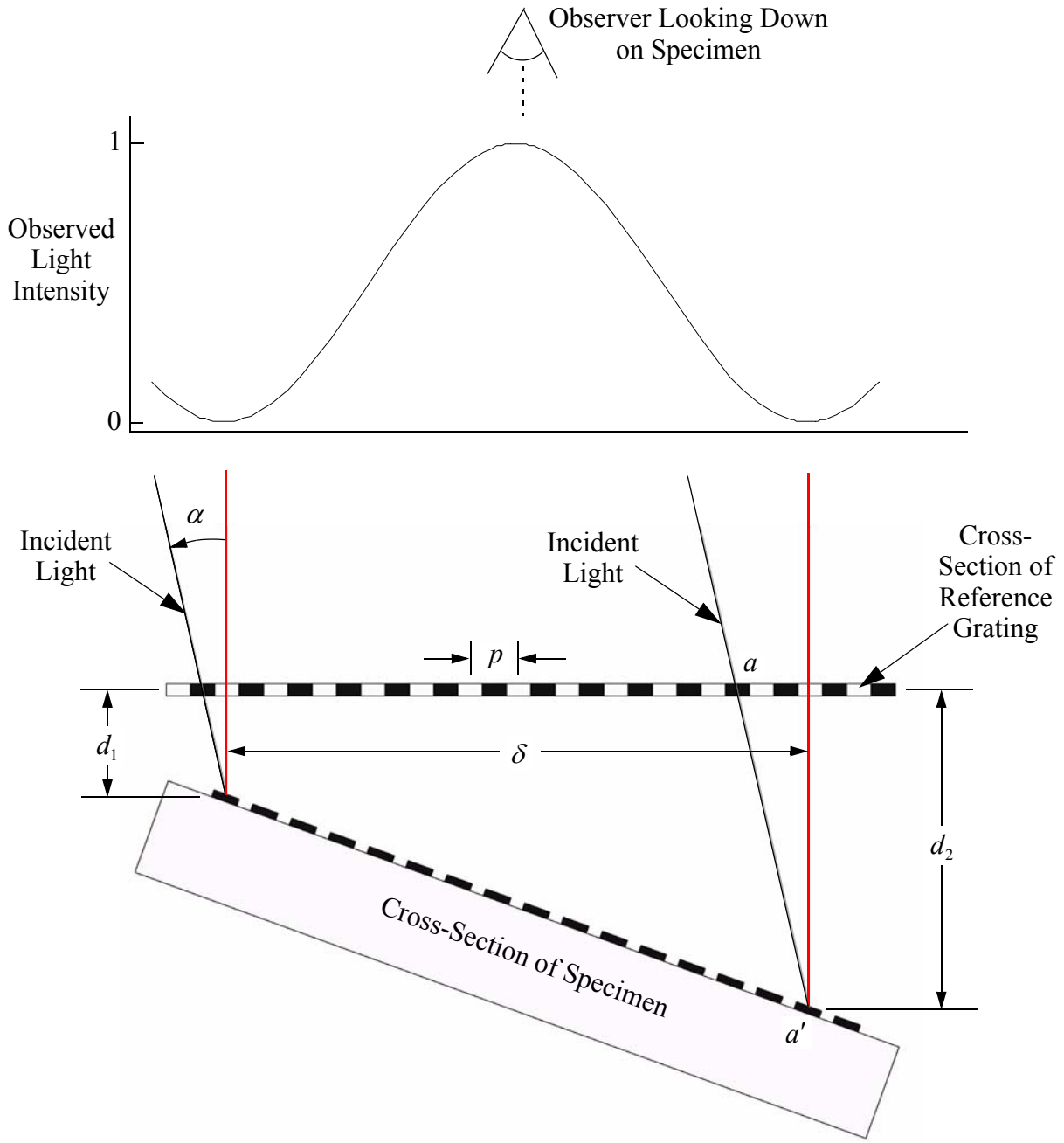

Figure 5.25: Shadow moiré geometry

There are many practical considerations that must be made when utilizing the shadow moiré technique. First, the surface of the specimen must be covered in a matte finish, such as white spray paint, to create distinct shadows. Placing the light source and the observer at the same distance above the plane of the specimen will assure that the out-of-plane displacements are directly proportional to the fringe order of the moiré pattern [35]. The light source used for

shadow moiré should be a small slit or point, but it does not have to be monochromatic. Any irregularities in the surface of the specimen or reference grating results in an initial fringe pattern and must be taken into consideration when determining the out-of-plane displacements [36]. This last fact is important because the facesheets of the sandwich panel were known to be of non-uniform thickness.

The shadow moiré setup for the line-loaded sandwich plate is shown in Figure 5.26. First, the top of the plate was spray painted flat white, then a 1-in. reference grid was drawn on the surface with a thin felt-tip marker to assist with counting the moiré fringes and locating particular fringe orders. Only one half of the sandwich plate could be observed with the shadow moiré technique because of the crimped fasteners on top of the plate used to attach the wiffle tree. The reference grating was a sheet of film attached to a piece of glass with a thin coat of oil. The glass was much larger than necessary (having been used in a previous research project) and extended beyond the edges of the plate. The extra size was an advantage because the reference grating could be held in place with two small weights. The pitch of the reference grating was 0.02 in., or alternatively, the frequency was 50 lines/in. The opaque lines in the reference grating were oriented perpendicular to the simple supports. The incident light was parallel to the simple supports at an angle of approximately 65.5° from the vertical. There was a very small initial gap between the reference grating and the top surface of the plate. A 0.040-in. shim was then placed under the reference grating at the free edge closest to the light source to ensure that the fringe order increased monotonically moving towards the light source, and to produce a so-called carrier pattern. Several different combinations of bulbs and lamps were tested to determine which gave the most contrast in the initial fringe pattern due to the shim and the non-uniform thickness of the top facesheet. It was found that a standard desk lamp with a 40 W flood bulb gave the best results. The inside of the lamp was spray painted black to cover the reflective metal surface. A digital camera was mounted on the tripod at the same height as the light source.

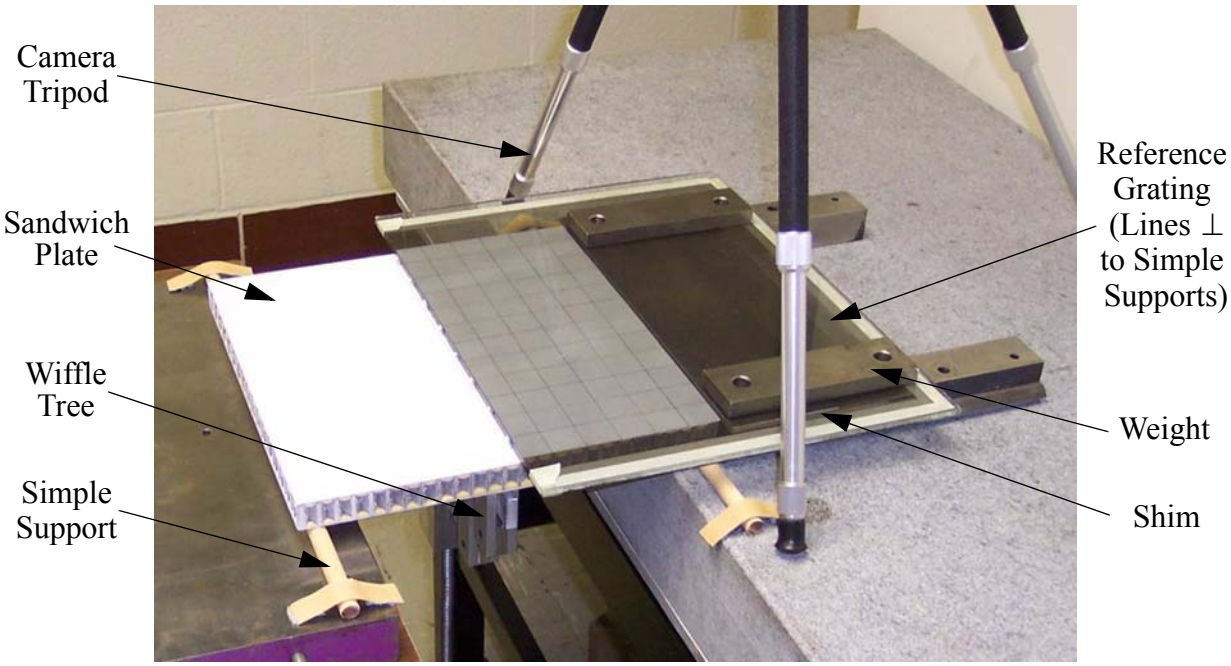

Figure 5.26: Shadow moiré test of sandwich plate

The initial fringe pattern shown in Figure 5.27 was observed with only the weight of the wiffle tree fixture attached. The digital camera can be seen in the reflection of the glass of the reference grating. The 1-in. x 1-in. reference grid drawn on the specimen is clearly visible. The center-line of the plate, and thus the locus of the line load, was at $x = 0$ in. and the plate was simply supported by the wooden dowel along $x = 5.5$ in. The 0.040-in. shim was located underneath the reference grating at $y = 6$ in. The fringe contrast was greater on the right because the reference grating was closer to the surface of the sandwich plate due to the shim on the left. The numbers along edges of the grid represent the fringe order, starting with zero in the lower right corner. From Eq. (5.6), each fringe order represented an out-of-plane distance of 9.12 mils from the zero order fringe. The fringe order at the intersection of the grid lines was approximated by linearly interpolating between fringes. Accuracy of visual inspection was limited to within ±1/5 of a fringe order [35].

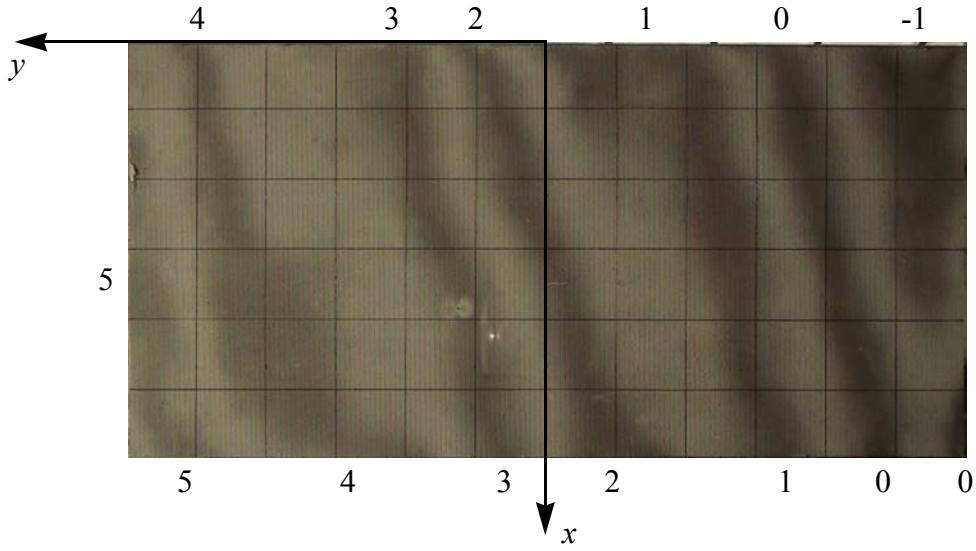

Figure 5.27: Initial fringe pattern

After the initial fringe pattern was recorded, the plate load was increased by 120 lb in increments of 10 lb. The fringes were observed to move to the right as more weight was added. Digital photographs were taken at each load step to follow the individual fringes. The final fringe pattern for a load of 120 lb is given in Figure 5.28. The total number of visible fringes increased from 7 to 10. Once again, the fringe order at the intersection of the grid lines was approximated by linearly interpolating between fringes. The relative change in displacement due to the 120-lb load increase was found by subtracting the initial fringe order from the final fringe order at each point on the 1-in. x 1-in. reference grid, and then applying Eq. (5.7). For comparison, Figure 5.20 is repeated in Figure 5.29 with the shadow moiré displacements included as stars. The displacements at the simple supports measured using shadow moiré were in very good agreement with the dial gauge measurements. The estimates of the fringe orders at the free edge and center of the plate for both the initial and final fringe patterns were less accurate because the fringes were wider and less distinct than at the simple supports, as can be seen in Figures 5.27 and 5.28. Therefore, the displacements at the free edge and center of the plate were still considered to be adequate.

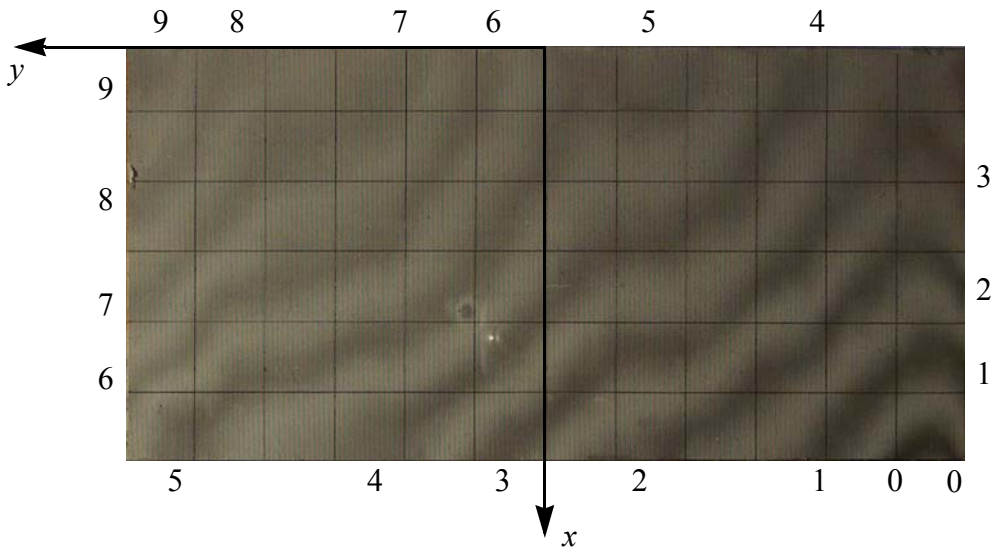

Figure 5.28: Final fringe pattern

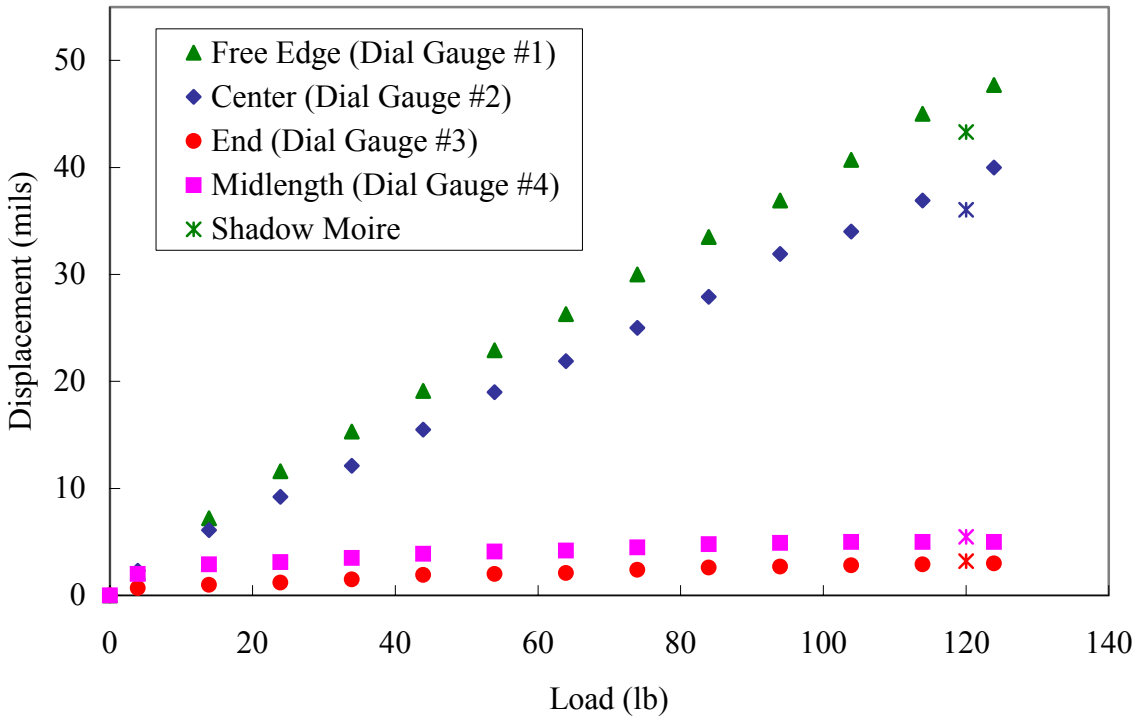

Figure 5.29: Measured displacements of line-loaded sandwich plate with shadow moiré

As mentioned earlier, unlike the dial gauge measurements which were made at distinct points, the shadow moiré method was used to determine the displacements at every point of the plate. The displacement profile for one-quarter of the plate was generated from the fringes on the

right half ($y < 0$) of Figures 5.27 and 5.28 because the fringes on the left half ($y > 0$) were not distinct enough to accurately measure the fringe order. The displacement of the rest of the plate was then assumed to be the same because of symmetry. Figure 5.30 shows the displacement profile for the entire sandwich plate. The shape is very similar to that predicted by Figure 3.16. As discussed previously, the displacements are not zero at the simple supports. The measured anticlastic curvature of the sandwich plate is quite obvious. The irregularities in the displacement profile are due to the uncertainty in resolving the fringe orders in Figures 5.27 and 5.28.

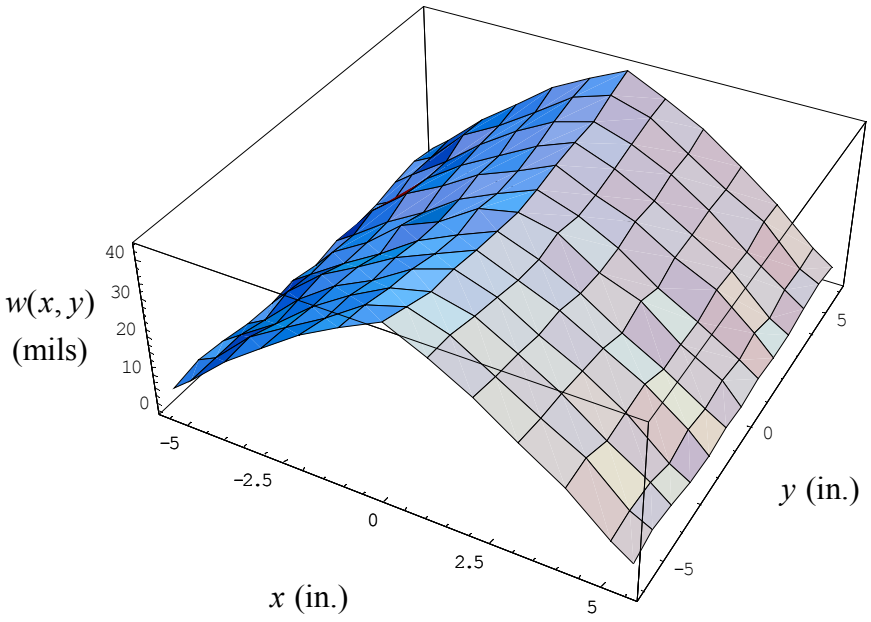

Figure 5.30: Displacement of line-loaded sandwich plate using shadow moiré

This concludes the discussion of the experiments and comparisons with the predictions. The next chapter summarizes the study with conclusions and recommendations for future work.

Chapter 6 Conclusions and Recommendations

6.1 Conclusions

Mathematical models were first developed to predict the static behavior of sandwich beams. The cantilever sandwich beam model presented by Dugundji [1] was used for a simply supported sandwich beam in three-point bend. This sandwich beam model compared very well to the shear plus bending theory given by Allen [13] and ASTM C 393 [11]. An approximate series solution was developed and shown to be in good agreement with the exact solution. The approximate solution was then extended to include beams with non-uniform facesheet thicknesses.

The sandwich beam theory was extended into a sandwich plate theory in which the facesheets behaved as isotropic plates that obeyed the Kirchhoff hypothesis. It was found that a uniformly-loaded sandwich plate simply supported on all four edges required external reaction forces at the corners to keep the corners at zero displacement. The solution for a uniformly-loaded sandwich plate simply supported along two opposite edges was adapted from Timoshenko's solution for an isotropic plate [16]. This set of boundary conditions did not require external reaction forces at the corners. The solution for a line-loaded sandwich plate simply supported along two opposite edges was developed to compare with experimental results.

Successful compression molding of the random wetlay composite mat was found to be very dependent upon the maximum temperature and the rate of cooling. It was impossible to fabricate a panel of completely uniform thickness with zero percent mass loss. Several different adhesives were studied to bond the composite facesheets to the honeycomb core. The polyurethane glue was absorbed into the honeycomb and did not create an adequate fillet at the base of the honeycomb walls. Adding Cab-O-Sil filler kept the polyurethane glue from absorbing into the honeycomb. Epoxy paste and 3M Scotch-Grip™ plastic adhesive were also used to bond the facesheets to the core. Both of these adhesives were more difficult to apply than the polyurethane glue.

Flatwise tension tests were performed on sandwich specimens in accordance with ASTM C 297 [33]. The flatwise tension tests of the polyurethane glue with Cab-O-Sil specimens were inconclusive because only one specimen did not disbond at the facesheet/aluminum block interface. It was assumed that the flatwise tensile strength was at least 182.7 psi. The average flatwise tensile strengths for the epoxy paste and Scotch-Grip™ plastic adhesive specimens were 113.3 psi and 80.3 psi, respectively. There was a great deal of variability in the flatwise tensile strength of the Scotch-Grip™ plastic adhesive specimens because of the difficulty in applying the adhesive.

Three-point bend tests were performed on a sandwich beam in accordance with ASTM C 393. The facesheets of the sandwich beam were found to be non-uniform in thickness. The data were very linear except near the origin of the load vs. displacement plots. The original predicted compliances were less than the measured compliances. An effective facesheet modulus of 0.900 msi used in the sandwich beam theory gave good agreement with the data shifted to account for the lack of linearity near the origin.

The displacements of a line-loaded sandwich plate simply supported along two opposite edges were measured using dial gauges. The displacement at the free edge was greater than the displacement at the center of the plate because of the anticlastic curvature. The non-uniformity of the bottom facesheet caused measurable displacements at the simple supports. At larger load levels, the displacements at the simple supports became stationary, so the true increase in plate displacements with increasing load could be determined. The result was to shift the data to account for the displacements measured at the supports. An effective facesheet modulus of 1.330 msi and Poisson's ratio of 0.40 in the sandwich plate model gave good agreement with the shifted data at larger load levels.

The shadow moiré technique was used to visualize the displacement of the entire plate. Estimates of the fringe order were limited to within ±1/5 of a fringe order. The displacements at the simple supports measured using shadow moiré were in good agreement with the dial gauge measurements. The displacements at the free edge and center of the plate were considered to be adequate because the fringes were wider and less distinct than at the simple supports. The overall

shape of the displacement was similar to the shape of the displacement predicted from the sandwich plate theory.

One troubling issue is as follows: For the sandwich beam, the modulus of the facesheets had to be decreased in order to obtain good agreement between the predicted and measured bending compliance of the beam. For the sandwich plate, the modulus of the facesheets had to be increased to obtain good agreement. There was a great deal of variability to the average thickness and uniformity for the facesheet material. It was expected that the modulus of the facesheets would increase as more matrix material was squeezed out from the mold during consolidation, thus causing a greater volume fiber fraction of glass. Why the adjustments for the beam and plate were in opposite directions is vexing.

6.2 Recommendations for Future Work

The random wetlay composite sandwich panels considered here might be used for interior aircraft structures, such as floor or light-duty bulkheads for separating classes of passengers. If the rigidity of the panels is high enough, they could conceivably be used for lightly loaded secondary structures. There are a number of other applications, including the transportation and building industries.

The compression molding of the facesheets took several hours to heat and cool back to room temperature. For low-cost industrial applications this time would have to be reduced considerably. To accurately determine the flatwise tensile strength of the sandwich panel bonded using polyurethane glue with Cab-O-Sil, a more suitable adhesive must be found for bonding the facesheets to the aluminum blocks. To investigate the effect of the thickness of the adhesive layer on the effective facesheet modulus, sandwich beams and plates with various amounts of adhesive could be tested. A material with well-known properties, such as aluminum, could be tested in the fixtures to determine if the experiments were accurately measuring the extensional modulus and Poisson's ratio. Different core materials such as closed-cell foam should be considered. Other methods for bonding the facesheets to the core include film adhesives and thermal bonding.

Additional test such as ASTM C 273 “Standard Test Method for Shear Properties of Sandwich Core Materials” [37] and ASTM D 6416 “Standard Test Method for Two-Dimensional Flexural Properties of Simply Supported Sandwich Composite Plates Subjected to a Distributed Load” [38] may also be performed. Finally, closer attention needs to be given to the experimental setups for measuring deflections. Unwanted compliance in the fixtures could be wrongly interpreted as compliance of the specimen, and lead to erroneous conclusions regarding the quality of the facesheet material.

References

1. Dugundji, J., "Cantilever Boundary Condition, Deflections, and Stresses of Sandwich Beams," *AIAA Journal*, Vol. 40, No. 5, May 2002, pp. 987-995.

2. Sokolinsky V., and Frostig Y., "Nonlinear Behavior of Sandwich Panels with a Transversely Flexible Core," *AIAA Journal*, Vol. 37, No. 11, November 1999, pp. 1474-1482.

3. Whitney, J. M., "A Local Model for Bending of Weak Core Sandwich Plates," *Journal of Sandwich Structures and Materials*, Vol. 3, No. 4, 2001, pp. 269-288.

4. Swanson, S. R., "An Examination of a Higher Order Theory for Sandwich Beams," *Composite Structures*, Vol. 44, No. 2-3, 1999, pp. 169-177.

5. Gdoutos, E. E., Daniel, I. M., Wang, K. A., and Abot J. L., "Nonlinear Behavior of Composite Sandwich Beams in Three-Point Bending," *Proceedings of the SEM IX International Congress on Experimental Mechanics*, June 5-8, 2000, pp. 155-158.

6.Satapathy, N. R., and Vinson J. R., "Sandwich Beams with Mid-Plane Asymmetry Subjected to Lateral Loads," *Journal of Sandwich Structures and Materials*, Vol. 2, No. 4, October 2000, pp. 379-390.

7. Thomsen, O. T., and Vinson J. R., "Modeling of Tapered Sandwich Panels Using a High-Order Sandwich Theory Formulation," *AIAA Journal*, Vol. 40, No. 9, September 2002, pp. 1867-1875.

8. Hohe, J. and Becker, W., "A Refined Analysis of the Effective Elasticity Tensor for General Cellular Sandwich Cores," *International Journal of Solids and Structures*, Vol. 38, 2001, pp. 3689-3717.

9. Librescu, L., Hause, T., and Camarda, C. J., "Geometrically Nonlinear Models of Initially Imperfect Sandwich Plates and Shells Incorporating Non-Classical Effects," *Proceedings of the AIAA/ASME/ASCE/AHS/ASC Structures, Structural Dynamics, and Materials Conference and Exhibit*, April 15-17, 1996, pp. 284-299.

10. Ebcioglu, I. K., "A General Nonlinear Theory of Sandwich Panels," *International Journal of Engineering Science*, Vol. 27, No. 8, 1989, pp. 865-878.

11. ASTM C 393-94, "Standard Test Method for Flexural Properties of Sandwich Constructions," *Annual Book of ASTM Standards*, Vol. 15.03, 1995, pp. 22-25.

12. Wolfram Research, Inc., 100 Trade Center Drive, Champaign, IL 61820, (217) 398-0700.

13. Allen, H. G., "Analysis and Design of Structural Sandwich Panels," Pergamon, Oxford, 1969, pp. 8-18.

14. Reddy, J. N. “An Introduction to the Finite Element Method,” McGraw Hill, Boston, 1993, pp. 177.

15. Timoshenko, S., and Woinowsky-Krieger, S., “Theory of Plates and Shells,” McGraw-Hill, New York, 1959, pp. 79-116.

16. Timoshenko, S., and Woinowsky-Krieger, S., “Theory of Plates and Shells,” McGraw-Hill, New York, 1959, pp. 214-218.

17. Hyer, M. W., “Stress Analysis of Fiber-Reinforced Composite Materials,” McGraw-Hill, Boston, 1998, pp. 154-155.

18. Reddy, J. N., “Mechanics of Laminated Composite Plates: Theory and Analysis,” CRC Press, Boca Raton, 1997, pp. 163.

19. Loos, A. C., “Moldable Thermoplastic Composite Sheet Technology,” *Proceedings of the Society of Manufacturing Engineers Composites Manufacturing and Tooling Conference*, February 21-23, 2001.

20. DuPont, 1007 Market Street, Wilmington, DE 19898, (800) 441-7515.

21. Lu, Y. “Mechanical Properties of Random Discontinuous Fiber Composites Manufactured from Wetlay Process,” *Virginia Tech Electronic Theses and Dissertations*, 2002, pp. 104.

22. Dowling, N. D., “Mechanical Behavior of Materials,” Prentice Hall, Upper Saddle River, New Jersey, 1993, pp. 51.

23. Hexcel Composites, 11711 Dublin Boulevard, Dublin, CA 94568, (925) 551-4900.

24. Owen, T., Hexcel Composites, Private communication, 2002.

25. Hexcel Composites, “HexWeb™ Honeycomb Sandwich Design Technology,” Publication No. AGU 075b, pp. 20.

26. Price-O’Brien, J. T., Virginia Tech Random Wetlay Composites Laboratory, Private communication, 2002.

27. Cagle, C. “Handbook of Adhesive Bonding,” McGraw-Hill, New York, 1973, pp. 19.4-19.12.

28. 3M Adhesives Division, 3M Center, Building 220-7E-05, St. Paul, MN 55144, (800) 364-3577.

29. Elmer’s Products, Inc., 1000 Kingsmill Parkway, Columbus, OH 43215, (800) 848-9400.

30. Fiberglass Supply, Inc., P.O. Box 345, 314 West Depot, Bingen, WA 98605, (509) 493-3464.

31. Eager Plastics, Inc., 3350 W. 48th Pl., Chicago, IL 60632, (773) 927-3484, http://www.eager-plastics.com/cab.htm.

32. PC-Products, 221 South Third Street, Allentown, PA 18102, (610) 432-3543.

33. ASTM C 297-94, "Standard Test Method for Flatwise Tensile Strength of Sandwich Constructions," *Annual Book of ASTM Standards*, Vol. 15.03, 1995, pp. 10-11.

34. SolidWorks Corporation, 300 Baker Avenue, Concord, MA 01742, (800) 693-9000.

35. Post, D., Han, B., and Ifju, P., "High Sensitivity Moiré: Experimental Analysis for Mechanics and Materials," Springer-Verlag, New York, 1994, pp. 118-122.

36. Dally, J. W. and Riley, W. F., "Experimental Stress Analysis," McGraw-Hill, New York, 1978, pp. 394-396.

37. ASTM C 273-94, "Standard Test Method for Shear Properties of Sandwich Core Materials," *Annual Book of ASTM Standards*, Vol. 15.03, 1995, pp. 10-11.

38. ASTM D 6416-94, "Standard Test Method for Two-Dimensional Flexural Properties of Simply Supported Sandwich Composite Plates Subjected to a Distributed Load," *Annual Book of ASTM Standards*, Vol. 15.03, 1995, pp. 10-11.

Appendix A Compression molded facesheet thickness profiles

Shown here are the thickness profiles for all compression molded facesheets. The thicknesses were measured using a long-arm sheet metal micrometer. Panels CG25.8, CG25.9, and CG25.10 were 6 in. x 6 in. with thickness measurements taken every 1 in. All other panels were 12 in. x 12 in. with thickness measurements taken every 2 in. The thickness of panel CG25.7 was not recorded because there was a severe error in the manufacturing process.

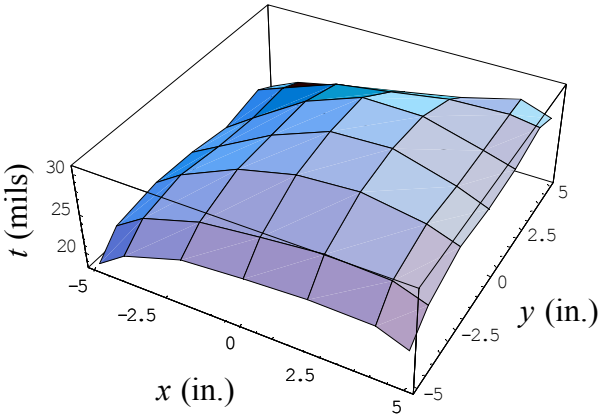

Figure A.1: Thickness of panel CG25.4

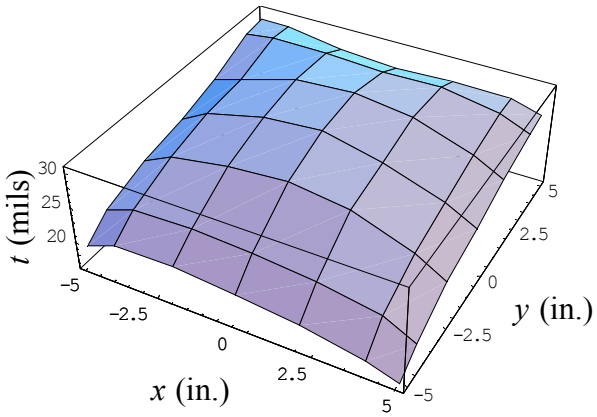

Figure A.2: Thickness of panel CG25.5

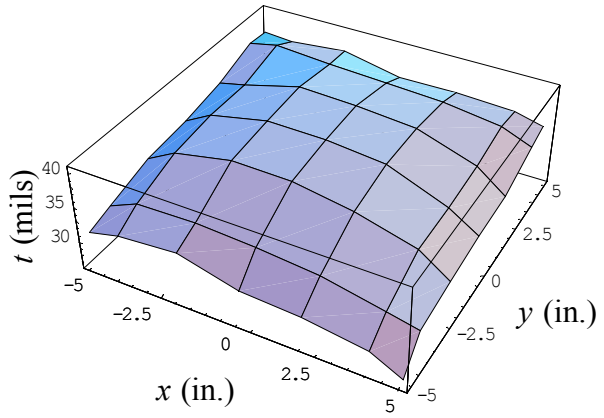

Figure A.3: Thickness of panel CG25.6

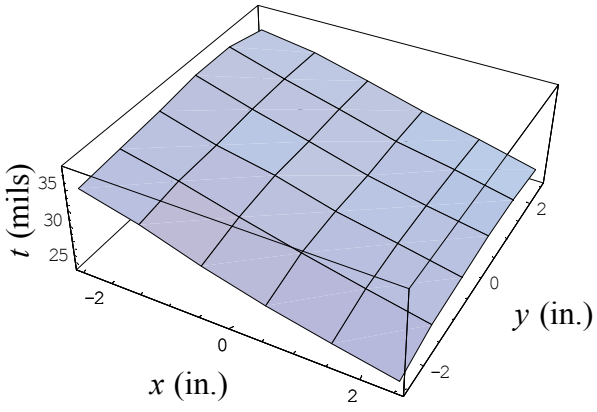

Figure A.4: Thickness of panel CG25.8

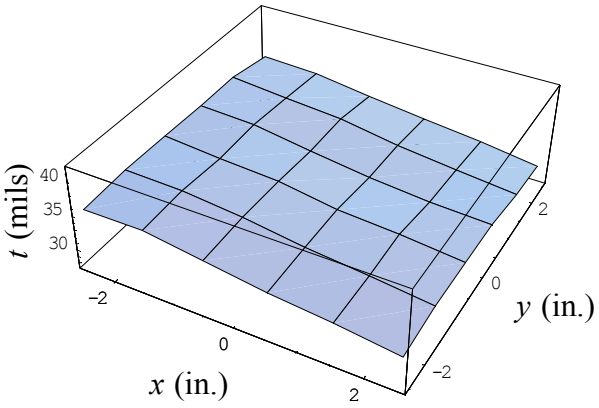

Figure A.5: Thickness of panel CG25.9

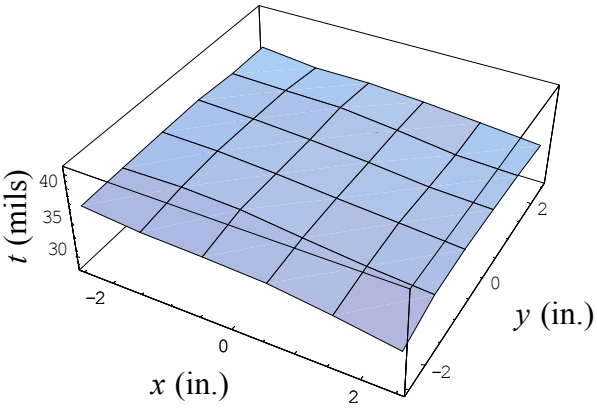

Figure A.6: Thickness of panel CG25.10

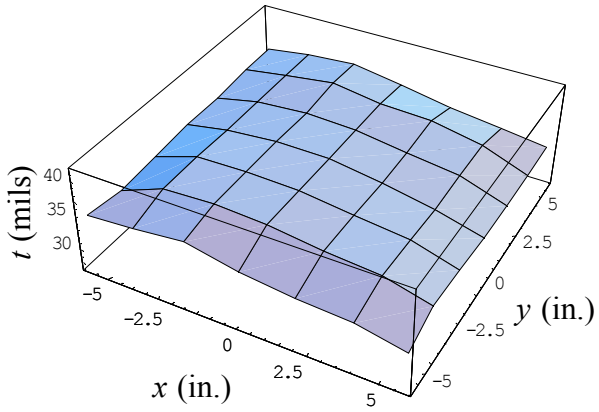

Figure A.7: Thickness of panel CG25.11

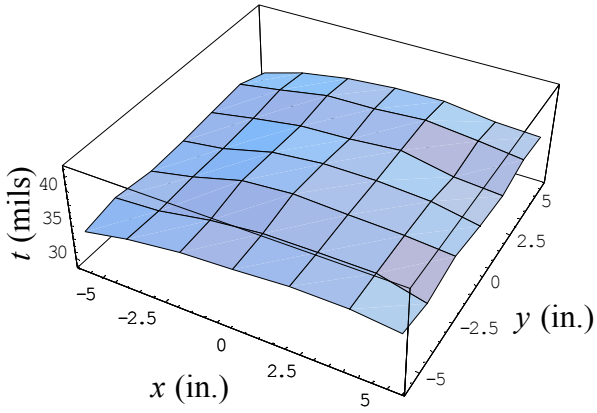

Figure A.8: Thickness of panel CG25.12

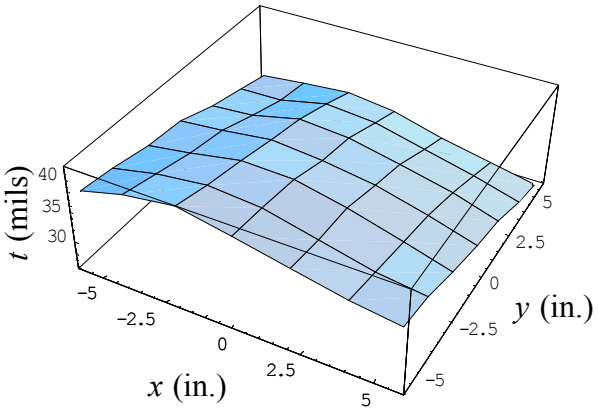

Figure A.9: Thickness of panel CG25.13

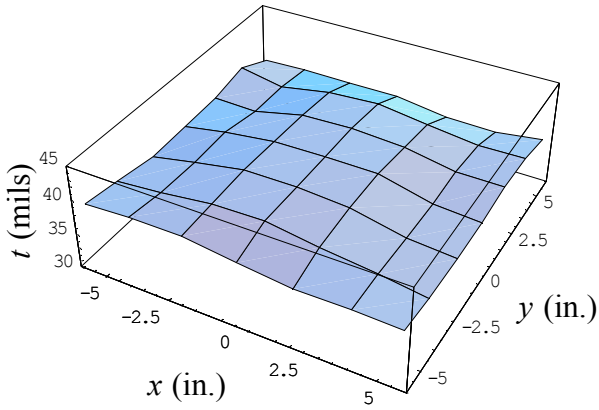

Figure A.10: Thickness of panel CG25.14

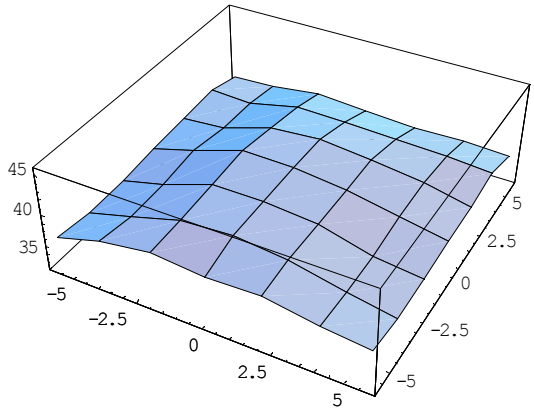

Figure A.11: Thickness of panel CG25.15

Appendix B Sandwich beam displacement data

Figures B.1 through B.12 show the least-squares straight lines through the displacement data from the three-point bend test for each trial at the three locations on the beam. The measured data were very linear for applied loads of 10, 20, 30, and 40 lb. The equations of the lines are given in terms of the displacement, w, in mils and the load, P, in lb. All of the intercepts were negative with the exception of Trial 3 at $x = -L/4$. The R^2 value used to determine the adequacy of fit was always at least 0.999.

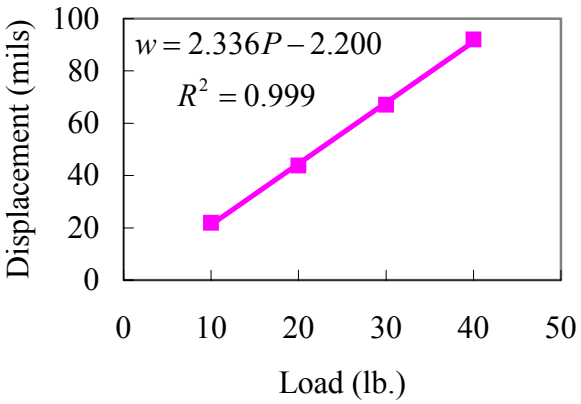

Figure B.1: Midspan ($x = 0$) Trial 1

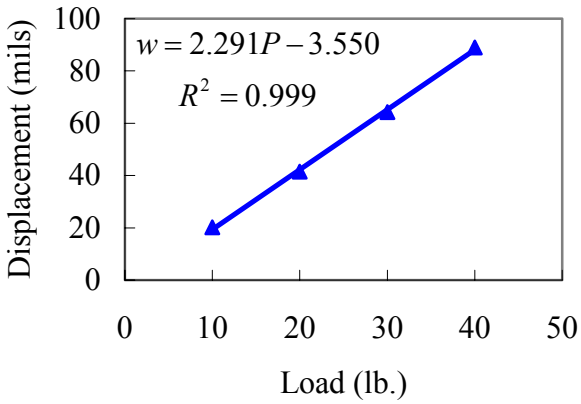

Figure B.2: Midspan ($x = 0$) Trial 2

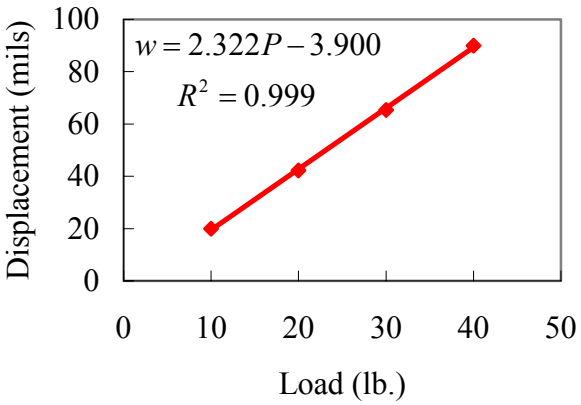

Figure B.3: Midspan ($x = 0$) Trial 3

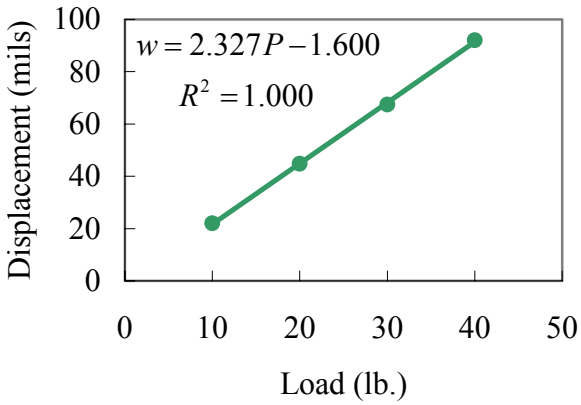

Figure B.4: Midspan ($x = 0$) Trial 4

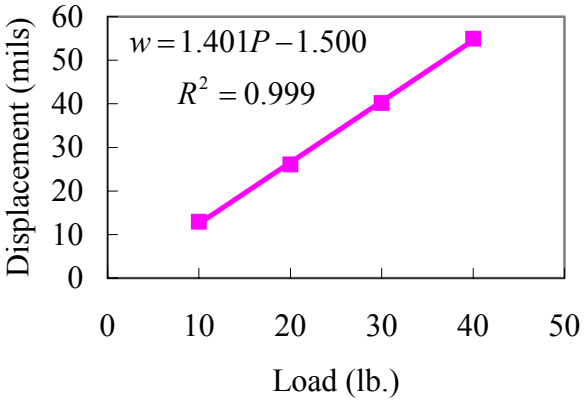

Figure B.5: Quarter-span ($x = -L/4$) Trial 1

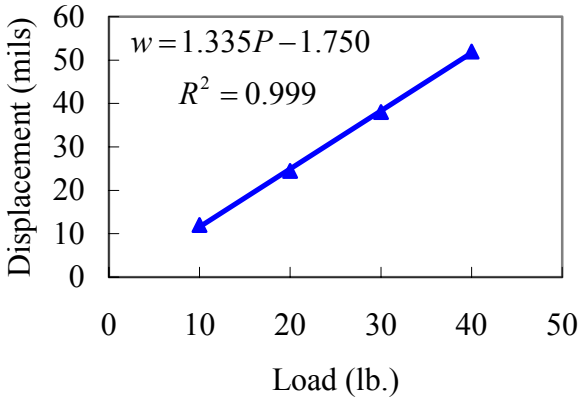

Figure B.6: Quarter-span ($x = -L/4$) Trial 2

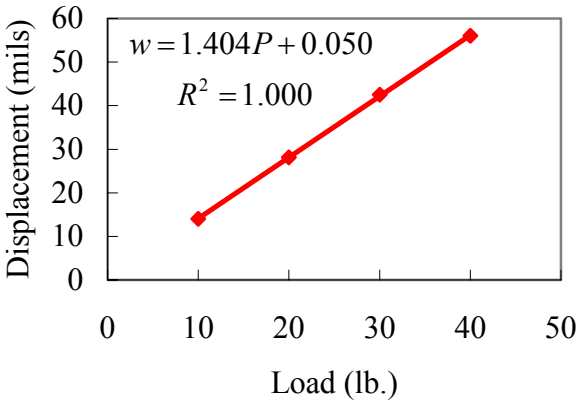

Figure B.7: Quarter-span ($x = -L/4$) Trial 3

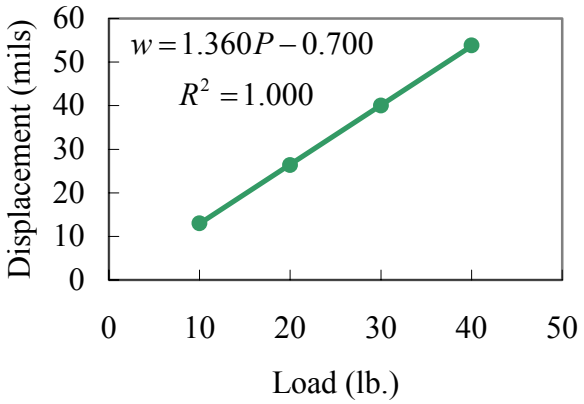

Figure B.8: Quarter-span ($x = -L/4$) Trial 4

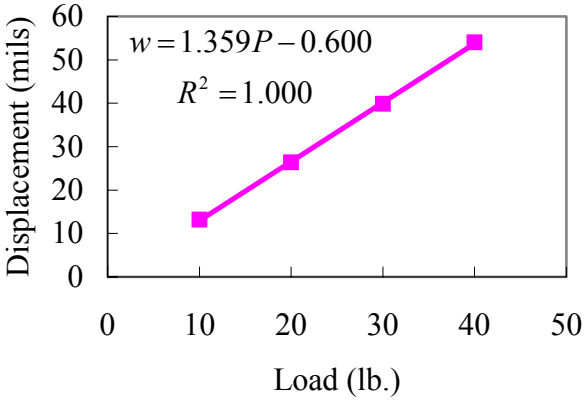

Figure B.9: Quarter-span ($x = L/4$) Trial 1

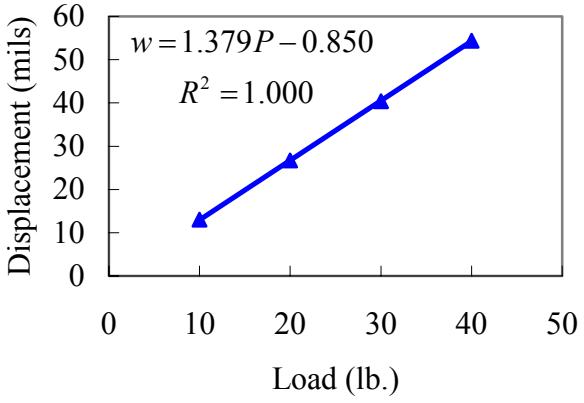

Figure B.10: Quarter-span ($x = L/4$) Trial 2

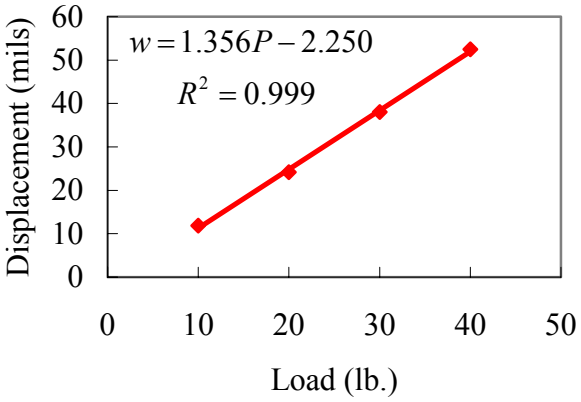

Figure B.11: Quarter-span ($x = L/4$) Trial 3

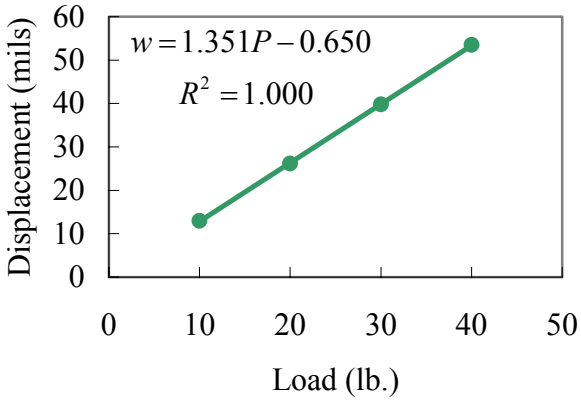

Figure B.12: Quarter-span ($x = L/4$) Trial 4

Appendix C Deflection of simple support

The line-loaded sandwich plate was simply supported on two opposite edges using round wooden dowels. As the load was increased, a significant amount of deflection was measured above the supports. In an ideal environment, all of this deflection could be considered rigid body motion of the plate due to the compression of the wooden dowels. To estimate the amount of compression expected, an elasticity solution was developed for an infinitely long cylinder subjected to a line load P along the top and bottom. The cross-section of such a cylinder is shown in Figure C.1.

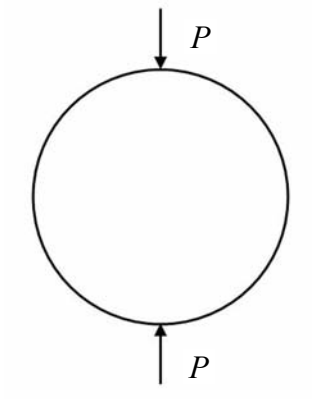

Figure C.1: Cross-section of simple support

This problem is well suited to be solved in polar coordinates with the r–θ coordinates shown in Figure C.2 and the x-axis going into the page. The outer radius of the cylinder is R. To avoid a singularity in the stress at $\theta = 0$ and $\theta = \pi$, the line load P is considered to be distributed over a small angle $\Delta\theta$ such that the average radial stress at the boundary is $-\frac{P}{R\Delta\theta}$. The negative sign is used to indicate that the stress acts in the negative r-direction. The stress at the bottom is the same because the cylinder is in static equilibrium. It is convenient to write this applied stress in a Fourier series with period π as

$$\sigma_r\left(R,\theta\right) = \frac{a_0}{2} + \sum_{n=1}^{\infty}\left[a_n \cos\left(\frac{n\pi\theta}{L}\right) + b_n \sin\left(\frac{n\pi\theta}{L}\right)\right] \tag{C.1}$$

where $L = \frac{\pi}{2}$ is half the period. The constants a_n and b_n are given by

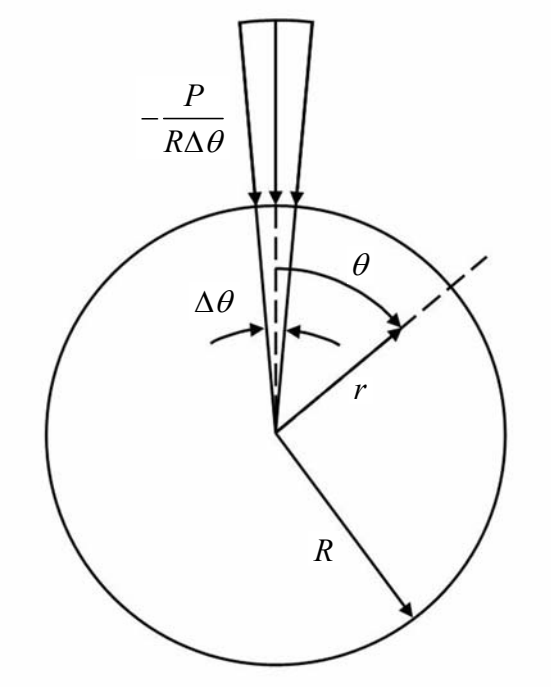

Figure C.2: Polar coordinate system of cross-section

$$a_n = \frac{1}{L}\int_{-L}^{L}\left[f(\theta)\cos\left(\frac{n\pi\theta}{L}\right)\right]d\theta = -\frac{2P\sin(n\Delta\theta)}{n\pi R\Delta\theta} \tag{C.2}$$

$$b_n = \frac{1}{L}\int_{-L}^{L}\left[f(\theta)\sin\left(\frac{n\pi\theta}{L}\right)\right]d\theta = 0 \tag{C.3}$$

where $f(\theta)$ is the applied stress of

$$f(\theta) = \begin{cases} 0 & -\frac{\pi}{2} < \theta < -\frac{\Delta\theta}{2} \\ -\frac{P}{R\Delta\theta} & -\frac{\Delta\theta}{2} < \theta < \frac{\Delta\theta}{2} \\ 0 & \frac{\Delta\theta}{2} < \theta < \frac{\pi}{2} \end{cases} \tag{C.4}$$

Because the cylinder is infinitely long in the *x*-direction, it is assumed that the *x*-displacement, *u*, is zero at every point. Also, it is assumed that there is no variation of any variable with the *x*-coordinate. This assumption makes the dowel stiffer than in the experiment, but makes the

problem easier to solve. It is not expected to have a large impact on the estimated compression of the dowel. Thus,

$$\frac{\partial(\ )}{\partial x} = 0 \tag{C.5}$$

This assumption requires that the θ-displacement v and the r-displacement w be functions of r and θ only. Thus, the six strain components in polar coordinates are given by

$$\varepsilon_x = \frac{\partial u}{\partial x} = 0 \tag{C.6}$$

$$\varepsilon_\theta = \frac{1}{r}\left(w + \frac{\partial v}{\partial \theta} \right) \tag{C.7}$$

$$\varepsilon_r = \frac{\partial w}{\partial r} \tag{C.8}$$

$$\gamma_{\theta r} = \frac{1}{r}\left(\frac{\partial w}{\partial \theta} - v + r\frac{\partial v}{\partial r} \right) \tag{C.9}$$

$$\gamma_{xr} = \frac{\partial u}{\partial r} + \frac{\partial w}{\partial x} = 0 \tag{C.10}$$

$$\gamma_{x\theta} = \frac{\partial v}{\partial x} + \frac{1}{r}\frac{\partial u}{\partial \theta} = 0 \tag{C.11}$$

The stress-strain relationships are assumed to be linearly elastic with isotropic material properties. Therefore, the six stress components are given by

$$\begin{Bmatrix} \sigma_x \\ \sigma_\theta \\ \sigma_r \\ \tau_{\theta r} \\ \tau_{xr} \\ \tau_{x\theta} \end{Bmatrix} = \begin{bmatrix} C_{11} & C_{12} & C_{12} & 0 & 0 & 0 \\ C_{12} & C_{11} & C_{12} & 0 & 0 & 0 \\ C_{12} & C_{12} & C_{11} & 0 & 0 & 0 \\ 0 & 0 & 0 & C_{44} & 0 & 0 \\ 0 & 0 & 0 & 0 & C_{44} & 0 \\ 0 & 0 & 0 & 0 & 0 & C_{44} \end{bmatrix} \begin{Bmatrix} \varepsilon_x \\ \varepsilon_\theta \\ \varepsilon_r \\ \gamma_{\theta r} \\ \gamma_{xr} \\ \gamma_{x\theta} \end{Bmatrix} \tag{C.12}$$

where

$$C_{11} = \frac{E(1-\nu)}{(1+\nu)(1-2\nu)} \tag{C.13}$$

$$C_{12} = \frac{E\nu}{(1+\nu)(1-2\nu)} \tag{C.14}$$

$$C_{44} = \frac{E}{2(1+\nu)} \tag{C.15}$$

The stresses are related to each other through the three polar equilibrium equations as

$$\frac{\partial \sigma_x}{\partial x} + \frac{1}{r}\frac{\partial \tau_{x\theta}}{\partial \theta} + \frac{\partial \tau_{xr}}{\partial r} + \frac{1}{r}\tau_{xr} = 0 \tag{C.16}$$

$$\frac{\partial \tau_{x\theta}}{\partial x} + \frac{1}{r}\frac{\partial \sigma_\theta}{\partial \theta} + \frac{\partial \tau_{\theta r}}{\partial r} + \frac{2}{r}\tau_{\theta r} = 0 \tag{C.17}$$

$$\frac{\partial \tau_{xr}}{\partial x} + \frac{1}{r}\frac{\partial \tau_{\theta r}}{\partial \theta} + \frac{\partial \sigma_r}{\partial r} + \frac{\sigma_r - \sigma_\theta}{r} = 0 \tag{C.18}$$

Upon substitution of the strains into Eq. (C.12) and the stresses into the equilibrium equations, it is found that the first equilibrium equation, Eq. (C.16), is identically satisfied. The remaining two equations are coupled partial differential equations in $v(r,\theta)$ and $w(r,\theta)$ given by

$$\frac{1}{r^2}\left[C_{44} r^2 \frac{\partial^2 v}{\partial r^2} + C_{44} r \frac{\partial v}{\partial r} + C_{11}\frac{\partial^2 v}{\partial \theta^2} - C_{44} v + (C_{12} + C_{44}) r \frac{\partial^2 w}{\partial r \partial \theta} + (C_{11} + C_{44})\frac{\partial w}{\partial \theta} \right] = 0 \tag{C.19}$$

$$\frac{1}{r^2}\left[(C_{12} + C_{44}) r \frac{\partial^2 v}{\partial r \partial \theta} - (C_{11} + C_{44})\frac{\partial v}{\partial \theta} + C_{11} r^2 \frac{\partial^2 w}{\partial r^2} + C_{11} r \frac{\partial w}{\partial r} + C_{44}\frac{\partial^2 w}{\partial \theta^2} - C_{11} w \right] = 0 \tag{C.20}$$

Due to symmetry considerations, the displacement $v(r,\theta)$ must be an odd function of θ, and the displacement $w(r,\theta)$ must be an even function of θ. Separation of variables assumes the displacements have the following forms:

$$v(r,\theta)=\sum_{n=1}^{\infty}V_n(r)\sin(2n\theta) \tag{C.21}$$

$$w(r,\theta)=\sum_{n=0}^{\infty}W_n(r)\cos(2n\theta) \tag{C.22}$$

The trigonometric terms $\sin(2n\theta)$ and $\cos(2n\theta)$ are used because they result in stresses at the boundary that are known to match the applied traction $\sigma_r(R,\theta)$ given by Eqs. (C.1) through (C.3). Substitution of the assumed solutions into Eqs. (C.19) and (C.20) results in the following two equations:

$$\sum_{n=1}^{\infty}\sin(2n\theta)\left[C_{44}V_n''(r)+\frac{C_{44}V_n'(r)}{r}-\frac{(4n^2C_{11}+C_{44})V_n(r)}{r^2}-\frac{2n(C_{12}+C_{44})W_n'(r)}{r}-\frac{2n(C_{11}+C_{44})W_n(r)}{r^2}\right]=0 \tag{C.23}$$

$$\sum_{n=1}^{\infty}\cos(2n\theta)\left[\frac{2n(C_{12}+C_{44})V_n'(r)}{r}-\frac{2n(C_{11}+C_{44})V_n(r)}{r^2}+C_{11}W_n''(r)+\frac{C_{11}W_n'(r)}{r}-\frac{(C_{11}+4n^2C_{44})W_n(r)}{r^2}\right]+C_{11}W_0''(r)+\frac{C_{11}W_0'(r)}{r}-\frac{C_{11}W_0(r)}{r^2}=0 \tag{C.24}$$

For this solution to be valid for all values of θ, the coefficients of the trigonometric functions must be zero for each n. The coefficients are coupled ordinary homogeneous differential equations for $V_n(r)$ and $W_n(r)$. The last three terms of Eq. (C.24) also represent an ordinary differential equation for $W_0(r)$ with a solution given by

$$W_0(r)=\Omega_0^1 r+\frac{\Omega_0^2}{r} \tag{C.25}$$

where Ω_0^1 and Ω_0^2 are unknown constants to be determined later from the boundary conditions.

The solutions for $V_n(r)$ and $W_n(r)$ are found by assuming

$$V_n(r)=\Phi_n r^{\lambda_n} \tag{C.26}$$

$$W_n(r) = \Omega_n r^{\lambda_n} \tag{C.27}$$

where Φ_n, Ω_n, and λ_n are constants. Substituting into Eqs. (C.23) and (C.24) and factoring r^{λ_n} yields two homogeneous linear equations for Φ_n and Ω_n. For this set of equations to have a solution other than $\Phi_n = 0$ and $\Omega_n = 0$, the determinant of the coefficient matrix must be zero. The determinant is a fourth-order polynomial in λ_n with four unique real roots given by

$$\lambda_n^1 = -(2n+1) \tag{C.28}$$

$$\lambda_n^2 = -(2n-1) \tag{C.29}$$

$$\lambda_n^3 = 2n-1 \tag{C.30}$$

$$\lambda_n^4 = 2n+1 \tag{C.31}$$

The total solution for $V_n(r)$ and $W_n(r)$ is therefore

$$V_n(r) = \sum_{i=1}^{4} \Phi_n^i r^{\lambda_n^i} \tag{C.32}$$

$$W_n(r) = \sum_{i=1}^{4} \Omega_n^i r^{\lambda_n^i} \tag{C.33}$$

The constants Φ_n^i and Ω_n^i are not independent of one another. Substituting into Eqs. (C.23) or (C.24) and collecting coefficients of $r^{\lambda_n^i}$ yields

$$\Phi_n^1 = \Omega_n^1 \tag{C.34}$$

$$\Phi_n^2 = \frac{n-2+2\nu}{n+1-2\nu}\Omega_n^2 \tag{C.35}$$

$$\Phi_n^3 = -\Omega_n^3 \tag{C.36}$$

$$\Phi_n^4 = -\frac{n+2-2\nu}{n-1+2\nu}\Omega_n^4 \tag{C.37}$$

Thus, there are four unknown constants for each term in the series of Eqs. (C.21) and (C.22).

Two of the constants are found by applying the fact that the displacements at the center of the cylinder must be bounded. Mathematically, the displacements cannot be a function of r raised to a negative exponent or the displacements will go to infinity at $r = 0$. It is seen by Eqs. (C.28) and (C.29) that λ_n^1 and λ_n^2 are always negative for any $n = 1, 2, 3\ldots$ Thus,

$$\Omega_n^1 = 0 \text{ and } \Omega_n^2 = 0 \tag{C.38}$$

The displacement $W_o(r)$ given in Eq. (C.25) must also be bounded in the center by requiring that

$$\Omega_0^2 = 0 \tag{C.39}$$

The remaining constants are found by applying the boundary conditions at the outer radius of the cylinder. There is no shear stress $\tau_{\theta r}$ along the outer boundary. After much algebra, this boundary condition reduces to

$$\tau_{\theta r}\left(R,\theta\right) = \sum_{n=1}^{\infty}\left\{-\frac{ER^{2n-2}}{1+\nu}\left[\left(2n-1\right)\Omega_n^3 + \frac{\left(2n^2+n\right)R^2}{n-1+2\nu}\Omega_n^4\right]\sin\left(2n\theta\right)\right\} = 0 \tag{C.40}$$

The radial stress at $r = R$ is equal to the applied traction given in Eqs. (C.1) through (C.3) as

$$\begin{aligned}\sigma_r\left(R,\theta\right) &= \frac{E}{\left(1+\nu\right)\left(1-2\nu\right)}\Omega_0^1 + \sum_{n=1}^{\infty}\left\{\frac{ER^{2n-2}}{1+\nu}\left[\left(2n-1\right)\Omega_n^3 + \frac{\left(2n^2-n-1\right)R^2}{n-1+2\nu}\Omega_n^4\right]\cos\left(2n\theta\right)\right\} \\ &= -\frac{P}{\pi R} + \sum_{n=1}^{\infty}\left[-\frac{2P\sin\left(n\Delta\theta\right)}{n\pi R\Delta\theta}\cos\left(2n\theta\right)\right]\end{aligned} \tag{C.41}$$

The constant terms outside of the summation in Eq. (C.41) give

$$\Omega_0^1 = -\frac{P\left(1+\nu\right)\left(1-2\nu\right)}{\pi ER} \tag{C.42}$$

Equating coefficients of the trigonometric functions results in two linear equations which can be solved for Ω_n^3 and Ω_n^4. After much algebra, the constants are found to be

$$\Omega_n^3 = -\frac{2P\left(1+\nu\right)\sin\left(n\Delta\theta\right)}{\pi E\Delta\theta R^{2n-1}\left(2n-1\right)} \tag{C.43}$$

$$\Omega_n^4 = \frac{2P(1+\nu)(n-1+2\nu)\sin(n\Delta\theta)}{n\pi E\Delta\theta R^{2n+1}(2n+1)} \tag{C.44}$$

The total displacements are therefore

$$w(r,\theta) = -\frac{P(1+\nu)(1-2\nu)}{\pi ER}r + \sum_{n=1}^{\infty}\left\{\left[-\frac{2P(1+\nu)\sin(n\Delta\theta)}{\pi E\Delta\theta R^{2n-1}(2n-1)}r^{2n-1} + \frac{2P(1+\nu)(n-1+2\nu)\sin(n\Delta\theta)}{n\pi E\Delta\theta R^{2n+1}(2n+1)}r^{2n+1}\right]\cos(2n\theta)\right\} \tag{C.45}$$

$$v(r,\theta) = \sum_{n=1}^{\infty}\left\{\left[\frac{2P(1+\nu)\sin(n\Delta\theta)}{\pi E\Delta\theta R^{2n-1}(2n-1)}r^{2n-1} - \frac{2P(1+\nu)(n+2-2\nu)\sin(n\Delta\theta)}{n\pi E\Delta\theta R^{2n+1}(2n+1)}r^{2n+1}\right]\sin(2n\theta)\right\} \tag{C.46}$$

The round wooden dowels used in the experiment had a radius of 0.25 in. The slash pine material was not truly isotropic, so the elastic modulus in the radial direction of 0.01193 msi was used. Poisson's ratio was assumed to be 0.447[1]. The length of plate supported by each dowel was 12 in. Thus, a total load of 120 lb applied to the plate produced a line load P = 5 lb/in. on each dowel. The contact angle of the plate, $\Delta\theta$, was assumed to be somewhere between 2° and 10°. The nondimensionalized radial displacement at the top of the dowel, $-\frac{w(R,0)}{R}$, is plotted in Figure C.3 as a function of the contact angle. Each curve represents a different number of terms in the series of the displacement given by Eq. (C.45). It is found that the solution converges over the entire range of θ using approximately 200 terms. To visualize the effect of the number of terms in the series, Figure C.4 shows the Fourier series approximation of the applied radial stress for $\Delta\theta$ = 2°. The maximum normalized displacement of 4.05 x 10^{-4} occurs at the smallest contact angle of 2°. This displacement corresponds to a change in diameter of the dowel of -2.02 x 10^{-4} in. which is insignificant in comparison to the overall deflections of the plate. Therefore, it can be concluded that the rigid body motion due to the compression of the wooden dowels can be neglected.

1. Forest Products Laboratory, "Wood handbook - Wood as an Engineering Material," Gen. Tech. Rep. FPL–GTR–113, U.S. Department of Agriculture, Forest Service, Forest Products Laboratory, Madison, WI, 1999, pp. 4.1-4.8.

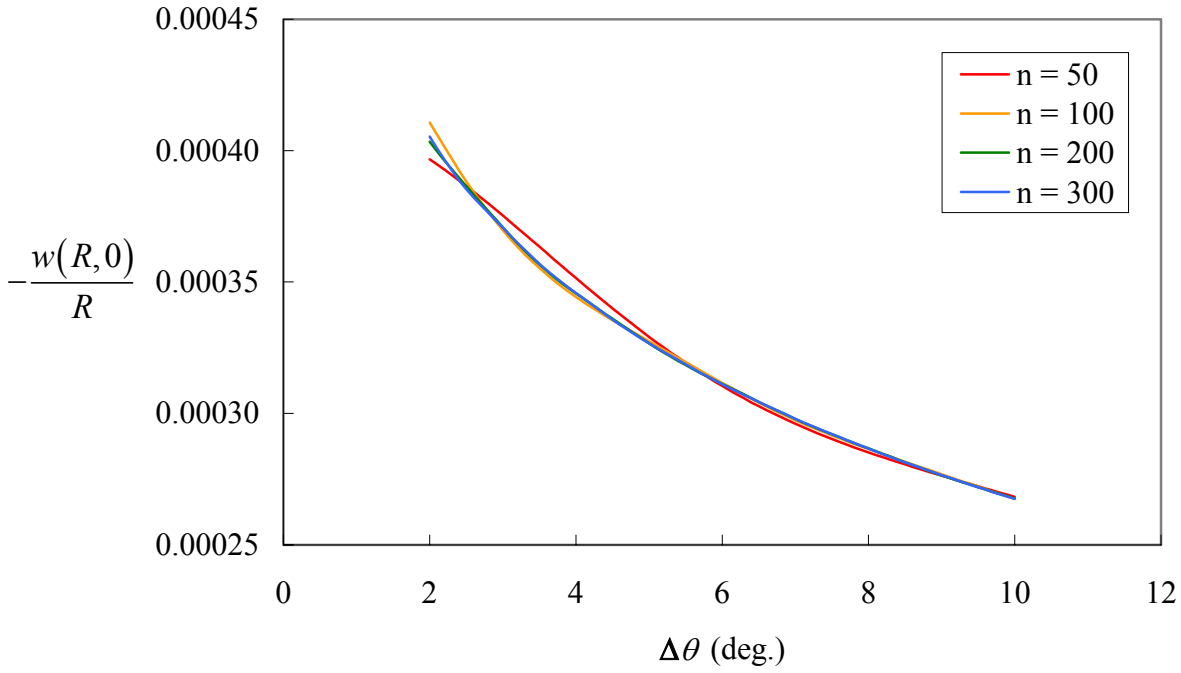

Figure C.3: Radial displacement at top of wooden dowel

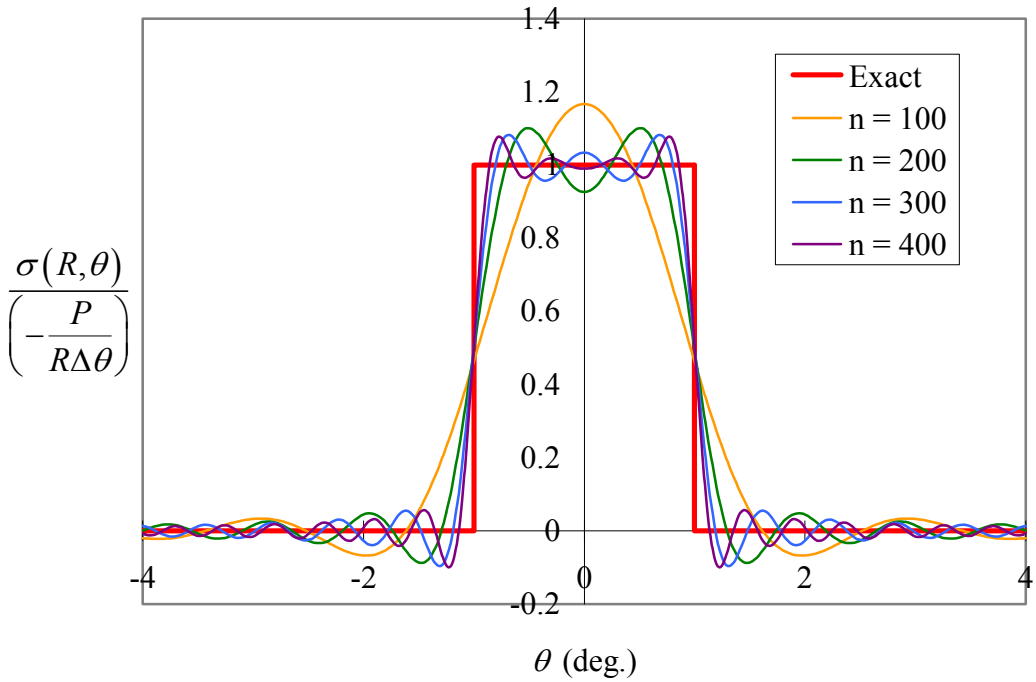

Figure C.4: Fourier series approximation of applied radial stress

Vita

Christopher Edward Glenn

Christopher Glenn was born on October 9, 1978 in Newport News, Virginia. He spent all of his childhood growing up in Hampton, Virginia. While in high school, he participated in the George Washington University Engineering Apprentice Program and the New Horizons Governor's School Mentorship Program, both at NASA Langley Research Center. In 1996, he graduated as valedictorian of Kecoughtan High School and enrolled at Virginia Tech. He spent his summers as an undergraduate working on internships with Gateway Computers, IBM, and Lexmark. He took time off of school in 1999 to participate in a co-op with Lockheed Martin Michoud Space Systems in New Orleans, Louisiana. He served as a Graduate Teaching Assistant for Mechanics of Deformable Bodies in the spring of 2001. In May 2001, he graduated summa cum laude from Virginia Tech with a Bachelor of Science in Engineering Science and Mechanics. He remained at Virginia Tech and completed his Master of Science in Engineering Mechanics in June 2003.